NOVEL MODE-LOCKING TECHNIQUES FOR COLOUR-CENTRE LASERS.

Gordon T. Kennedy

A Thesis Submitted for the Degree of PhD
at the
University of St Andrews

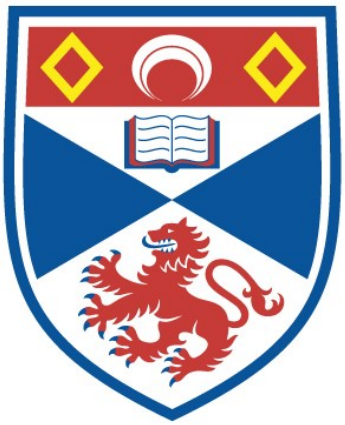

1994

Novel Mode-Locking Techniques for Colour-Centre Lasers

Thesis submitted for the degree of Doctor of Philosophy
to the University of St. Andrews
by
Gordon T. Kennedy, B.Sc.

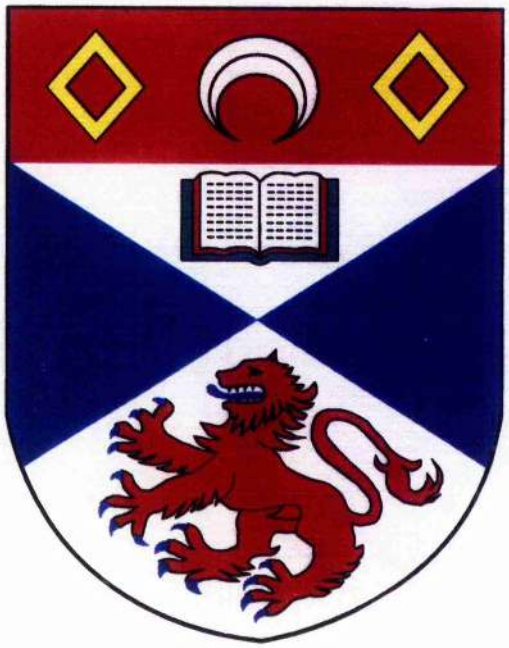

J. F. Allen Physics Research Laboratories
Department of Physics and Astronomy
University of St. Andrews
North Haugh
St. Andrews
Scotland KY16 9SS

September 1993

ProQuest LLC.
789 East Eisenhower Parkway
P.O. Box 1346
Ann Arbor, MI 48106 – 1346

Declaration

I Gordon Thomas Kennedy certify that this thesis has been composed by myself, that it is a record of my own work, and that it has not been accepted in partial or complete fulfilment of any other degree or qualification.

I was admitted to the Faculty of Science of the University of St. Andrews under Ordinance General No 12 on 1st October 1989.

Signed Date 7/9/93

I hereby certify that the candidate has fulfilled the conditions of the Resolution and Regulations appropriate to the Degree of Ph.D.

Signature of Supervisor Date

Copyright

Mum and Dad

Abstract

The work reported in this thesis is primarily concerned with the generation of ultrashort pulses from a NaCl:OH^- colour-centre laser. Active mode locking of the NaCl:OH^- laser by synchronous pumping and acousto-optic loss modulation was characterised in detail. Synchronously mode-locked pulses of 8 ps duration were compressed to 250 fs in an anomalously-dispersive optical fibre and a novel soliton-effect pulse compressor was constructed from a nonlinear fibre-loop mirror. Using this device, the synchronously mode-locked pulses were compressed to 300 fs with no discernible background radiation.

The NaCl:OH^- laser was coupled-cavity-mode locked using both nonlinear Fabry-Perot and Michelson cavity configurations, and pulses of 110 fs duration were obtained. A sawtooth amplitude modulation of the laser output was observed. This modulation, which arose from the beating of the mode-locked Nd:YAG pump laser and NaCl:OH^- laser pulse trains, was avoided by frequency-referencing the colour-centre laser to the pump laser. A characterisation of the phase noise of the frequency-referenced, coupled-cavity mode-locked laser was performed. By replacing the frequency synthesiser for the pump laser mode locker with a crystal oscillator, the phase noise of both the Nd:YAG pump laser and the NaCl:OH^- colour-centre laser were reduced by two orders of magnitude.

The technique of self-mode locking was successfully applied to the NaCl:OH^- laser. For this laser, it was necessary to include a rod of high-nonlinearity lead-silicate glass in the laser cavity to achieve sufficient self focusing for self-mode locking. Stable mode-locking was initiated by a regenerative acousto-optic modulation and pulses of 95 fs were obtained.

The thesis concludes with descriptions of some experiments performed using a mode-locked NaCl:OH^- laser and a KCl:$Tl^0(1)$ colour-centre laser. Efficient pulsed Raman amplification in an optical fibre was achieved by using an optical fibre thats group-velocity dispersion was the same for both the pump and signal wavelengths. By co-propagating pulse trains from the KCl:$Tl^0(1)$ and NaCl:OH^- lasers through a semiconductor optical amplifier cross phase modulation was observed. Ultrafast all-optical switching using the nonlinearity at half the bandgap was demonstrated for an GaAlAs integrated interferometer. This nonlinearity was subsequently used to coupled-cavity mode lock the KCl:$Tl^0(1)$ colour-centre laser.

Contents

Chapter 1

Introduction

1.1 Background

Broadly-tunable mode-locked lasers have found widespread applications in many areas of scientific research. In the past decade, considerable research effort has been directed towards new solid-state laser materials and to novel mode-locking techniques for lasers based on such gain media. As a result, it is now possible to obtain sub-100 fs duration pulses across the entire visible and near-infrared spectral region from solid-state laser systems.

The wavelength region around 1.5 μm is of particular significance because it corresponds to the lowest-loss window for silica-based optical fibres. In recent years, there has been significant research in the fields of fibre-based and semiconductor-based semiconductor lasers, amplifiers and switching devices for telecommunication systems. Versatile mode-locked lasers are therefore required to characterise these devices, and the KCl:Tl^0(1) colour-centre laser has proved to be a valuable research tool in this wavelength region. It is capable of producing sub-100 fs duration pulses, and average powers of several hundred milliwatts . Unfortunately, the laser suffers from a gradual reduction of the output power over a period of approximately six months and it is also necessary to cool the laser crystal to liquid-nitrogen temperatures.

In this thesis, the development and characterisation of mode-locking schemes for an alternative NaCl:OH^- colour-centre laser are presented. This laser has a broader tuning range than the KCl:Tl^0(1) counterpart and it is capable of producing several watts of average output power in continuous-wave operation. Although the laser still requires cryogenic cooling, compact cryostats having storage times of several days can readily be constructed.

Within this introductory chapter, an overview of mode-locking techniques is presented followed by a brief review of colour-centre lasers. Techniques for measuring ultrashort pulses are described, and the chapter ends with a discussion of pulse propagation in dispersive and nonlinear media.

1.2 Mode locking

There are several comprehensive reviews of mode locking in the literature.[1-12] In this section, a brief outline of the pertinent concepts behind the different techniques of active and passive mode-locking are presented.

The output of a free-running laser consists of axial cavity modes separated in frequency by $\Delta\nu = c/2L$, where L is the optical path length of the laser resonator. The electric field may be written as

$$E(t) = \sum_{k=1}^{N} A_k \exp(i\omega_k t + \varphi_k) \tag{1.1}$$

where A_k is the amplitude of the k^{th} mode, ω_k is its angular frequency (=$2\pi\Delta\nu$) and φ_k is its phase. In general, the phases of the modes will be random and the output from the laser will consist of noise, whose shortest fluctuations have durations of the order of the inverse oscillating bandwidth. However, if the modes are forced to have a fixed phase relationship, the laser will emit a train of pulses having a period equal to the round-trip transit time of the laser cavity. The pulse duration will be close to the reciprocal of the bandwidth (hence the number of modes). In this condition the laser is said to be mode locked.

A number of different techniques have been used to generate mode-locked pulse trains. These techniques can be classified into two general categories: active mode locking and passive mode locking

1.2.1 Active mode locking

In this scheme, the phases of the modes are coupled by actively modulating the laser field at a frequency which corresponds to the mode separation of the laser cavity. Active mode locking can be sub-divided into three techniques: loss modulation, frequency modulation and synchronous pumping.

Loss modulation

This is the most commonly used technique for active mode locking. A loss modulator is placed close to a cavity end mirror and is driven electrically by a sinusoidal signal. In the time domain, a pulse will form in the region of maximum transmission of the modulator. Outwith this region, the light experiences loss on each cavity round trip and is progressively suppressed. This is shown schematically in Figure 1.1.

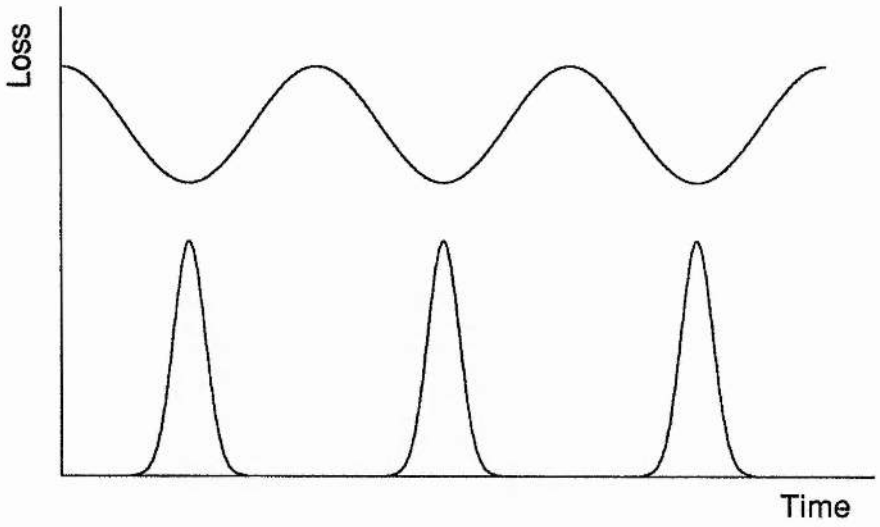

Figure 1.1. Schematic representation of mode locking by loss modulation.

Kuizenga and Siegman[2] developed a theory for AM mode locking based on the self-consistency of a Gaussian pulse as it propagates around the laser cavity. They predicted mode-locked pulse durations of

$$\Delta\tau_p = \frac{\left(\sqrt{2}\ln 2\right)^{\frac{1}{2}}}{\pi}\left(\frac{g_o}{\delta_m}\right)^{\frac{1}{4}}\left(\frac{1}{f_m \Delta\nu}\right)^{\frac{1}{2}} \tag{1.2}$$

where g_o is the round trip saturated gain, δ_m and f_m are the modulation index and frequency of the modulator and $\Delta\nu$ is the gain-bandwidth of the laser.

In the frequency domain, the modulation generates sidebands at the mode separation frequency about each oscillating mode. For an inhomogenously broadened laser operated far above threshold, a substantial fraction of the gain-bandwidth will be oscillating. The sidebands will therefore overlap with adjacent modes, and will injection-lock their relative phases. In the case of a strongly homogenously broadened gain medium, where only a few axial modes oscillate in cw operation, the modulation generates new modes at the modulation frequency. These new modes are hence in phase with the drive signal. Since it is necessary to generate new optical frequencies, a greater modulation depth is required to mode lock a homogenously broadened laser than one which is inhomogenously broadened. (Details of an actively mode-locked NaCl:OH^- laser using loss modulation are presented in Chapter 2.)

Frequency modulation

In practice, this technique is similar to mode-locking using loss modulation, except that an electro-optic material is located at one end of the cavity. The refractive

index of the material is sinusoidally modulated which frequency-shifts the intracavity light, except at the turning points of the modulation. The light is progressively shifted in frequency on each round trip until it is pushed outwith the gain bandwidth of the laser. Since there is no direct amplitude modulation of the laser field, this technique has a weaker effect than loss modulation.

Gain modulation by synchronous pumping

This technique can be applied to lasers which are pumped using a second laser or to semiconductor lasers which are electrically pumped. To achieve mode locking, the pump laser is mode locked and the optical path length of the slave laser is carefully adjusted to match that of the pump. After the pump pulse has excited the gain medium, the population inversion will decay slowly due to spontaneous emission which results in a long gain window. Mode locking can only be achieved if there is some degree of dynamic gain saturation to pull the gain below threshold and shorten the trailing edge of the pulse. This technique is therefore only suitable for gain media which have relatively short lifetimes and large gain cross sections such as dye lasers and colour-centre lasers. Unlike the methods described previously, where the pulse shaping is the same for both sides of the pulse, the pulse shortening mechanisms are different for the leading and the trailing edges of the pulse and asymmetric pulse profiles may result. The technique of synchronous mode locking has been assessed experimentally for a NaCl:OH^- laser and is discussed in Chapter 2.

1.2.2 Passive mode locking

In this technique, mode locking is achieved by including a nonlinear element whose loss is high for low light intensities but saturates, becoming low, for high intensities. The maximum emission principle[13] states that a laser will tend to operate in a condition which maximises its output power. Therefore, given the correct operating conditions, the laser will favour mode-locked operation because the high intensity pulses will reduce the intracavity loss.

Because the mode locking is driven by the laser field itself, the modulation frequency f_m in equation 1.2 can be replaced by $\Delta\nu$, the bandwidth of the gain medium. For some vibronically broadened gain media, this extends for tens of terahertz compared with modulation frequencies of ~ 100 MHz for active mode locking. For this case, equation 1.2 predicts a reduction in pulse duration of two to three orders of magnitude in comparison to active mode locking. Indeed, the shortest mode-locked pulses have been produced from passively mode-locked laser systems.

Passive mode locking can be sub-divided into three main categories: Passive mode locking using fast saturable absorbers, mode locking using synthetic fast

saturable absorbers and mode locking using slow saturable absorbers. These are considered in turn.

Passive mode locking using fast saturable absorbers

This is the simplest form of passive mode locking. In this scheme an absorbing element, which saturates on instantaneous intensity, is included at one end or at the centre of the laser resonator. The absorber is usually an organic dye or a semiconductor. When the laser is turned on, the gain increases until it reaches the cavity loss, including that of the saturable absorber, and the laser will begin to oscillate. At first the output from the laser will be noisy, however, the saturable loss will be less for the most intense noise features which will grow at the expense of less intense fluctuations. For specific pumping conditions, a single noise feature can be selected and a mode-locked pulse train will result. Since only the saturable absorber provides the pulse shaping, the pulse duration is limited to approximately the recovery time of the absorbing medium, which is typically several tens of picoseconds.

Passive mode locking using synthetic fast saturable absorbers

Recently, mode locking has been achieved using, essentially instantaneous, reactive nonlinearities. By configuring the lasers in such a way that the effects of the nonlinearity are converted into amplitude modulation, it is possible to mimic the response of a fast saturable absorber having an instantaneous recovery time. This mode-locking technique has proven to be extremely powerful. In most cases non-resonant nonlinearities are used. These are only weakly dependent on wavelength and therefore do not impose any tuning restrictions on the laser. Also, the rate at which the pulse duration is reduced increases monotonically with increasing peak power. For the other mode-locking schemes described in this section, the pulse shortening velocity decreases with increasing intensities.

To date, four methods of generating fast saturable absorbers have been reported. These are coupled-cavity mode locking, self mode locking (Kerr lens mode locking), polarisation rotation mode locking[14,15] and mode locking using second harmonic generation[16]. The first two methods have received considerable attention and have been widely applied. For these methods, the basic mechanisms for conversion of nonlinearity into amplitude modulation are outlined below.

Coupled-cavity mode locking

It is possible to exploit the third-order nonlinear effect of self-phase modulation to generate a mode-locked pulse train by constructing the laser as an interferometer.[17-19] Fabry-Perot[17] and Michelson[20,21] interferometer type cavity configurations are generally employed although mode locking has been observed for

nonlinear Sagnac interferometers[22-24]. A nonlinear element is included in one arm of the interferometer so that an intense feature propagating in this arm experiences a phase shift across it. By selecting a suitable static phase difference between the interferometer arms, it can be arranged for constructive interference to occur at the pulse centre, while the intensity of the wings of the pulse is reduced due to destructive interference. Usually an optical fibre is used as the nonlinear element since large phase shifts can be achieved for relatively low peak powers, while the waveguide geometry eliminates the effects of self focusing. However, mode locking has also been achieved for bulk nonlinearities[21,22] and active[18,25] and passive[26] semiconductor waveguides. Coupled-cavity mode locking of a NaCl:OH^- colour centre laser is presented in detail in Chapter 3

Self-mode locking[27,28]

In this technique self focusing arising from the optical Kerr effect is converted into amplitude modulation by placing an aperture or slit close to a beam waist. The laser is configured such that an intense, self-focused beam experiences less loss at the aperture than low intensity cw radiation. Although this technique was first reported in 1990, it has already been successfully applied to a variety of solid-state lasers and has resulted in pulse durations as short as 11 fs[29] being produced. The first application of this technique to a NaCl:OH^- laser is described in Chapter 4.

Passive mode locking using slow saturable absorbers

For some lasers, it was observed that, under specific operating conditions, mode-locked pulses having durations significantly less than the absorber recovery time could be produced[30]. It was realised that this was a result of dynamic gain saturation in the laser gain medium[31]. The absorber saturates on the pulse energy, shortening the leading edge of the pulse and transmits the rest of the pulse unchanged, while gain saturation serves to sharpen the trailing edge of the pulse.

To achieve stable mode locking using a slow saturable absorber several conditions must be fulfilled: the saturation energy of the absorber must be less than that of the gain to create a gain window and the absorber must recover faster than the gain to ensure overall loss for the rest of the cavity round-trip period. The creation of a stable gain window using the combined effects of slow saturable absorption and gain saturation is illustrated in Figure 1.2.

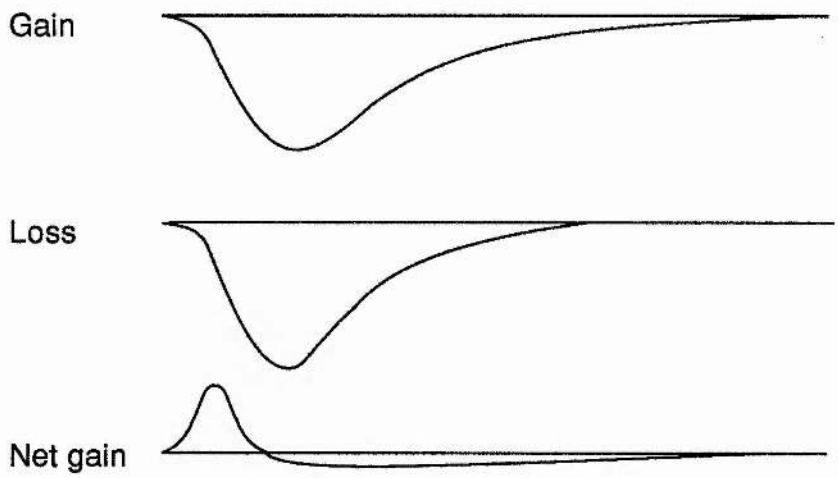

Figure 1.2. Schematic showing the creation of a short gain window arising from saturable absorption and gain saturation.

1.3 Colour-centre lasers[32,33]

The first colour centre-laser was reported by Fritze and Menke in 1965[34]. They obtained pulsed laser action around 2.7 μm in a flashlamp-pumped rod of KCl:Li^+. In their experiments, optical feedback was provided by depositing reflective coatings directly onto the ends of the crystal rod. By using a three-mirror resonator to achieve high intensities within the gain medium and by utilising efficient optical pumping from a krypton ion laser (techniques that had been successfully applied to dye lasers) Mollenauer and Olson[35] were able to obtain tunable, continuous-wave laser operation from the same colour-centre system. Since then, about twelve colour-centre systems have been successfully developed, spanning the 0.8 to 4 μm spectral region.

Colour-centre gain media are homogenously broadened. This enables the construction of high-power single-mode lasers[36] and, due to their large gain-bandwidth, colour-centre lasers can be mode locked to produce pulses of sub-picosecond durations[17]. These properties make colour-centre lasers versatile tools for studies in spectroscopy and nonlinear optics.

Colour centres are electron (or hole) traps at point defects in insulating crystals. They may be created either by radiation damage or chemically by additive colouration.[37] The simplest colour centre, the F-centre, consists of an electron bound to an anion (halogen ion) vacancy. The potential of the trapped electron is dominated by the surrounding lattice which, in the case of the F-centre, resembles a three dimensional square potential well. A simplified energy level diagram of the centre is presented as Figure 1.3.

Optical excitation of the centre from the 1s to the 2p energy level causes a reduction in the electron density of the centre. The neighbouring centres relax outwards due to mutual Coulomb repulsion. This causes the bottom of the potential well to be raised, making the electron density of the excited state even more diffuse and shifting its energy levels upwards towards the conduction band. This relaxation process continues until balanced by restoring forces from the crystal lattice. The final energy levels are termed the relaxed excited state (RES).

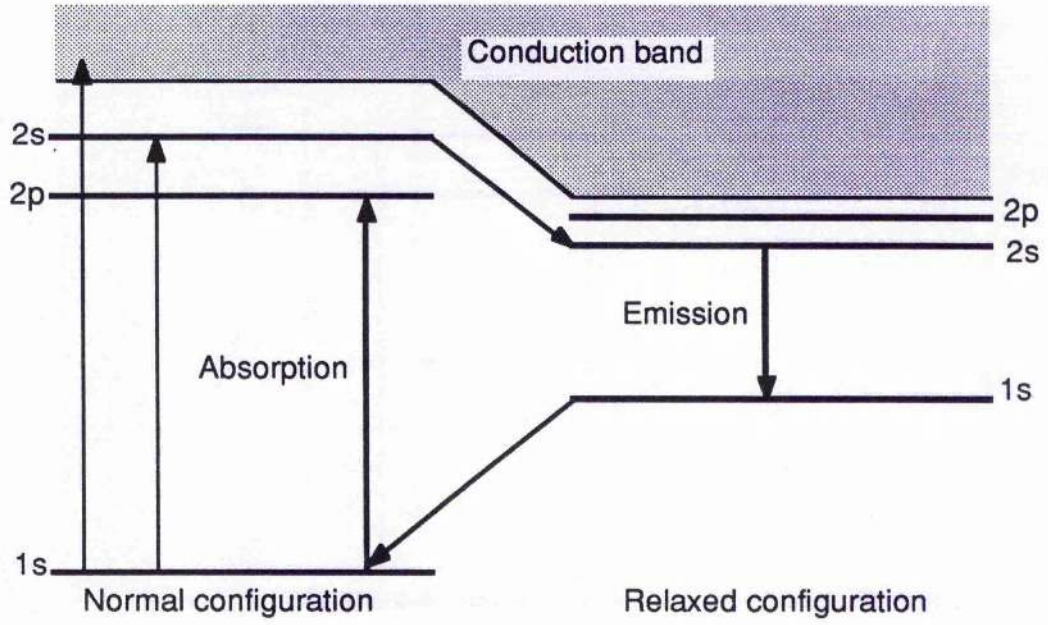

Figure 1.3. Energy level diagram for the F centre.

Since the potential of the colour centre is influenced by the surrounding lattice, its energy levels are strongly broadened by lattice vibrations or phonons. This vibronic broadening is conventionally illustrated using a configurational coordinate diagram[38] as shown in Figure 1.4. The diagram shows the electronic levels of the ground and excited states, represented by parabolas, plotted against the distance from the lattice vacancy to its nearest neighbouring ions (the configurational coordinate). Within the parabolas are phonon states which are represented by horizontal lines. For harmonic oscillators, these vibronic levels are equally spaced. Optical excitation from the ground state causes a vertical transition to the excited state at a fixed configurational coordinate (Franck-Condon principle). The probability of the transition depends on the overlap of the wavefunctions of the two states. The excited state is not in equilibrium with the surrounding lattice, and so the ions rapidly relax outwards by emitting phonons, to achieve equilibrium (relaxed excited state). The excited electron, now at the bottom level of the excited state, can then spontaneously

decay to the ground state, where further phonon emission ensues until it reaches the bottom level of the ground state.

The interaction between the colour-centre and crystal lattice vibrations causes a Stokes shift in the energy levels which results in an effective four-level system. Since the time taken to decay into the relaxed excited state is much less than the RES lifetime[39], quantum efficiencies approaching unity can be achieved.

For the F-centre, the relaxed excited state is situated close (~ 0.1 eV) to the conduction band and the centre is easily thermally ionised. The overlap integral between the relaxed excited state wavefunction and the ground state is small, resulting in a small emission cross section ($\sigma < 10^{-17}$ cm^2). Therefore, the F-centre itself is not laser active. However, its properties are common to the, more complex, aggregate centres and it is used as a building block for these centres.

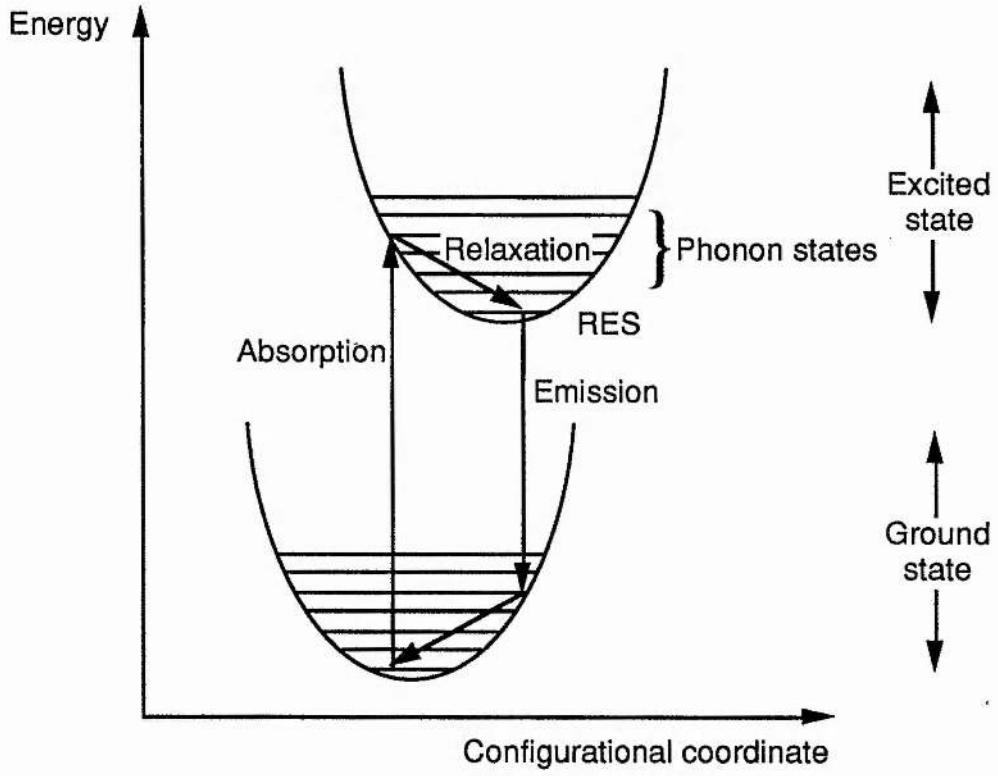

Figure 1.4. Configurational coordinate diagram.

The simplest laser-active colour centre is the F_A centre[40,41]. It consists of an F centre adjacent to a substitutional alkali impurity. This colour centre exists in two forms depending on the configuration of the relaxed excited state. Laser action can only be obtained from centres which relax into a symmetric double well configuration - the type II F_A centre (written as F_A(II)). These centres emit in the 2.3 – 3.6 μm wavelength range and their absorption bands are from 600 to 700 nm, enabling

pumping using a krypton-ion laser. The large Stokes shift of the transitions limits the output power of these lasers since approximately 80% of the pump energy must be dissipated as heat. Furthermore, the quantum efficiency is less than 50% at 1.6 K and decreases with increasing temperature which indicates a non-radiative decay route to the ground state. Laser action in the 2.5 - 2.9 μm wavelength range has also been reported for F centres adjacent to two substitutional impurities - the F_B(II) centre[42,43] but these lasers possess small slope efficiencies of the order of 2%. This has been attributed to absorption in the laser emission band due to F_A(I) and F_B(I) centres in the crystal.[44]

A KCl:Tl^0(1) colour-centre laser[45,46] was used for the experiments described in Chapter 5 of this thesis. The centre consists of a neutral thallium atom perturbed by an adjacent anion vacancy. In contrast to the F_A colour centre, the electron resides predominantly on the impurity atom, and so its energy level diagram is similar to that of the thallium atom. Changing the crystal host thus only results in small changes to the laser characteristics. The absorption band of the centre is centred at 1.06 μm and the laser is tunable from 1.4 - 1.63 μm. This encompasses the lowest loss window for silica-based optical fibres around 1.55 μm and the laser has been used to characterise materials and devices for telecommunications systems.[47,48] The synchronously mode-locked KCl:Tl^0(1) laser also formed the basis of the soliton laser[17] which was later demonstrated to be a particular case of the coupled-cavity mode-locked laser[18,19] (see Chapter 3).

Output powers in excess of 1 W have been reported for the KCl:Tl^0(1) laser when it was pumped by 6 W of 1064 nm light from a Nd:YAG laser. However, the output suffers from a gradual fading which is pump power dependent. The laser is typically operated at a pump power of 2 W which yields 150 - 300 mW of output power and results in a crystal lifetime of 6 - 12 months. For this reason, the KCl:Tl^0(1) laser has largely been superceded by the more powerful, NaCl:OH^- laser which has an unlimited operational lifetime.

The F_2^+ aggregate colour centre is formed by two anion vacancies in the <110> crystal direction sharing a trapped electron. The centres show small Stokes shifts and have quantum efficiencies close to unity. These properties have resulted in efficient, relatively high average power (> 1 W) cw laser action from F_2^+ centres in several different crystal hosts spanning the 0.8 - 1.9 μm spectral region[49]. Unfortunately, these lasers suffer from a severe fading of their output power on a timescale of several minutes. This occurs because the colour centres do not have a fixed location in the crystal lattice. Under optical excitation, the centres can flip their orientation causing them to 'walk through' the lattice where they may combine to form more complex aggregate F centres. Also, the F_2^+ centre is not electrically neutral and is easily converted into the more stable F_2 centre through electron capture. It is

therefore necessary to dope the crystal with divalent metal transition ions or OH^- ions to trap the free electrons generated by the formation of the F_2^+ centres.

It is possible to stabilise the F_2^+ centre by associating it with defects or impurities in the crystal lattice. This fixes the location of the centre, thus preventing the fading in power caused by aggregate centre formation. If the defect is a substitutional ion which replaces an alkali or halogen ion, it is described as a $(F_2^+)_A$ or a $(F_2^+)_H$ centre. Some centres can be stabilised through defects created by radiation damage and these are termed as $(F_2^+)^*$ and $(F_2^+)^{**}$ centres.

1.3.1 The $(F_2^+)_H$ centre in NaCl

The (F_2^+) colour centre in a NaCl host lattice was used for most of the work reported in this thesis. It was first reported by Pinto et al.[50] in 1985. In the original report, the K^+ ion was thought to be the stabilising defect. However, subsequent spectral analysis[51] revealed that laser crystal had been contaminated by OH^- ions and the O^{2-} ion was identified as the stabilising defect. As a result the laser has been designated as the NaCl:OH^- colour-centre laser and has proven to be a reliable, tunable source in the 1.5 μm spectral region. It exhibits a high-power non-fading output extending over the 1.37 - 1.85 μm wavelength range, and cw output powers of 3 W have been obtained when pumped by a 10 W Nd:YAG laser[36]. Single-mode operation with a linewidth of less than 2 MHz at output powers in excess of 2 W have been obtained. Active mode locking has produced pulses having 2.7 ps duration[52] and the laser has been passively mode locked using semiconductor saturable absorbers[53] and coupled-cavity techniques[54] to produce pulses having durations as short as 275 fs and 75 fs respectively.

The structure of the $(F_2^+)_H$ centre is illustrated in Figure 1.5. It consists of a F_2^+ centre formed by two adjacent anion (Cl^-) vacancies in the <110> crystal direction and a neighbouring O^{2-} ion occupying a halide ion site. The centre has been successfully modelled as a singly ionised hydrogen molecule embedded in a dielectric medium perturbed by the O^{2-} ion[55]. The O^{2-} ion acts as a spatial trap preventing the centre from migrating through the crystal and forming aggregate centres. It is also electronegative and acts as an electron trap. The centre is electrically neutral which minimises the probability of centre transformation through electron capture. The energy level diagram of the centre is presented in Figure 1.6 and some optical properties of the laser crystal are included in Table 1.1.

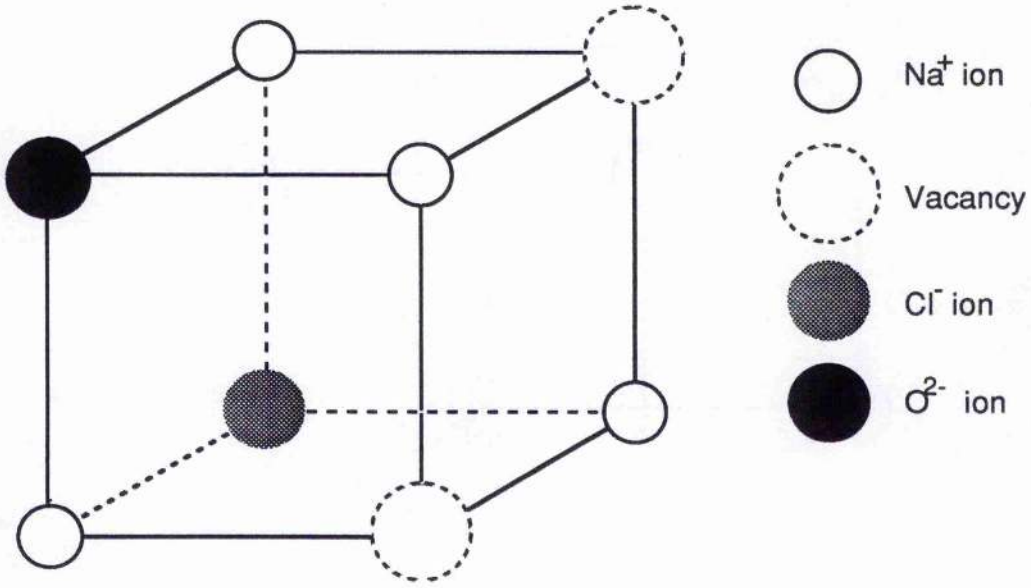

Figure 1.5. Structure of the $(F_2^+)_H$ centre in NaCl.

Property	Value	Reference
Absorption peak, λ_{abs}	1090 nm	56
Emission peak, λ_{em}	1550, 1590 nm	56,57
Emission FWHM	33, 30 THz	56,57
Stokes shift	0.34 ev	56
Dipole direction	<110>	56
Emission cross section, σ_{em}	8.5×10^{-17} cm^2	51
Quantum efficiency, η	1	56
Upperstate lifetime, τ_{rad}	150 ns	56

Table 1.1. Some properties of the $(F_2^+)_H$ colour centre in NaCl.

Under intense optical pumping, the output power of the laser is reduced due to reorientational bleaching. This occurs as the centres may flip their orientation such that their dipole moments are perpendicular to the polarisation of the pump laser, thus causing a reduction in the pump absorption and resulting in a gradual fading of the output power until laser action ceases. This is a characteristic of many laser systems based on F_2^+ colour centres. However, the centres may be reorientated by pumping the crystal with an auxiliary light source.

There are two possible routes for centre reorientation. The crystal can be illuminated with F-band light (400- 500 nm) which causes an excitation from the ground state of the $(F_2^+)_H$ centre ($1s\sigma_g$) to the second excited state ($2p\pi_u$). Reorientation then occurs during radiationless decay to the first excited state ($2p\sigma_u$)[56] Alternatively, the centres may be reoriented by two-photon pumping using 1064 nm light from a Nd:YAG laser and radiation from a HeNe, argon ion or frequency-doubled Nd:YAG laser. In this case, the 1064 nm illumination causes excitation from the ground state ($1s\sigma_g$) to the first excited state ($2p\pi_u$) and the secondary pump light excites this state to a higher energy level. Reorientation occurs during the non-radiative transitions to the $2p\sigma_u$ state via the $2p\pi_u$ state.

This latter approach, requiring two pump sources, may appear cumbersome but, in practice, it is more convenient than F-band pumping because both the 1064 nm and 532 nm light may be derived from the Nd:YAG laser used as the primary pump source for the colour centres. This scheme was used to pump the NaCl:OH^- laser used in this project. The Nd:YAG pump beam was circularly polarised so that there was a vertically polarised pump component that could interact with the misaligned centres, promoting them to the $2p\sigma_u$ state and the 532 nm light was horizontally polarised to excite the misaligned centres from this state to the $3d\pi_g$ level.[58]

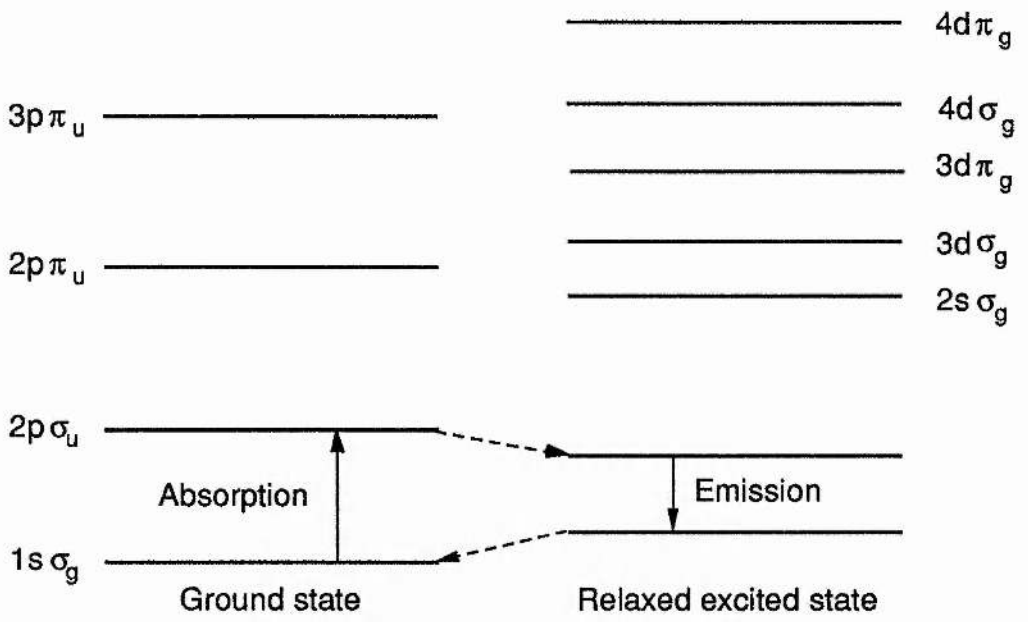

Figure 1.6. Energy level diagram of the $(F_2^+)_H$ colour centre in NaCl.

1.3.2 Preparation of NaCl:OH^- laser crystals

A brief description of the crystal preparation procedure is given here (For a more detailed description, the reader should consult References **56** and **36**.). OH^- ions

are incorporated in the sodium chloride crystal by adding 5 x 10^{-4} mol% NaOH to the crystal melt. The crystal is cleaved into (10x10x2) mm^3 slabs and polished using a diamond-based polishing compound. It is then additively coloured in a Na heat pipe[37] at a temperature of 650 ^{o}C and a pressure of around 30 mbar to create F-centres. Following this process, the crystal is annealed at 650 ^{o}C for several minutes to remove any strongly-scattering colloids, which may restrict the tuning range of the laser. By exposing the crystal to F-band light (400-500 nm) at room temperature, the F-centres are aggregated to form F_2 colour centres. The crystal is then cooled to liquid nitrogen temperature (77 K) and illuminated with F-band light, or 1064 nm radiation from a Nd:YAG laser and HeNe, argon ion or frequency-doubled Nd:YAG laser light. This ionises the F_2 centres to F_2^+ centres and causes them to migrate through the crystal lattice until they are trapped by O^{2-} substitutional ions, forming the laser-active $(F_2^+)_H$ colour centres. When this second photoaggregation process is performed using F-band light, F_2^- colour centres are also formed. These centres absorb in the emission band of the $(F_2^+)_H$ centres, but they are destroyed by the 1064 nm pump light and so do not adversely affect the performance of the laser[59].

1.4 The laser cryostat

To obtain cw laser action from colour-centre gain media, it is necessary to maintain the laser crystal at cryogenic temperatures. A laser cryostat, shown schematically in Figure 1.7, was designed at the University of St. Andrews for this purpose.

The colour-centre crystal is held at Brewster's angle in an mount which is attached to a copper cold finger contained within an evacuated chamber. To achieve good thermal contact between the crystal and the cold finger, the crystal mount is covered with indium foil, and crycon compound is used to contact the mount to the cold finger. Two Brewster-angled windows provide optical access to the crystal. The position of the crystal relative to the Dewar windows can be adjusted using a micrometer and its height above the optical table is varied by adjusting the threaded legs attached to the base-plate of the cryostat. Liquid nitrogen from a five-litre-capacity Dewar is supplied to the cold finger using a concentric tube arrangement. The liquid nitrogen flows down the centre tube directly onto the back of the cold finger while the evaporated nitrogen gas returns to the Dewar through the outer tube where it is released to the atmosphere though a valve.

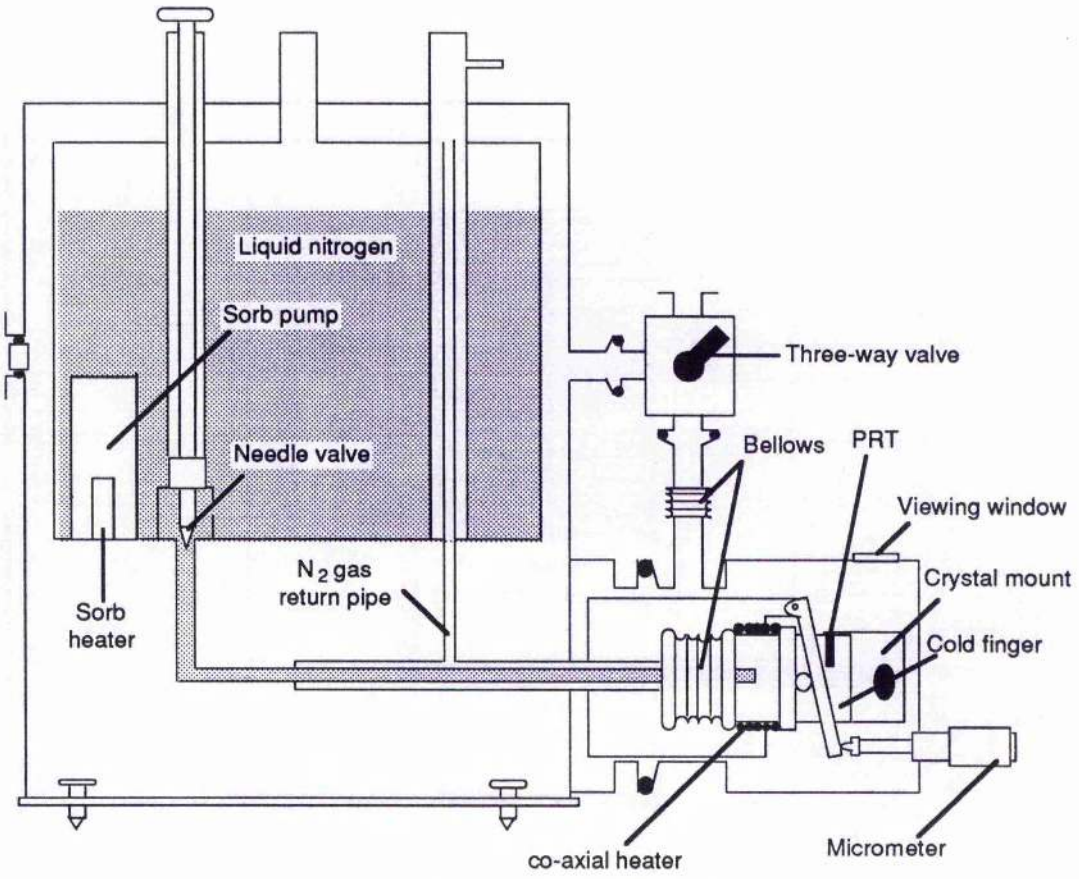

Figure 1.7. Schematic of the laser cryostat.

An absorption pump, located in the liquid nitrogen chamber, helps to maintain a high vacuum within the cryostat after it is evacuated. The pump consists of activated alumina or charcoal which, at low temperatures, traps atoms or molecules. A heater is incorporated into the pump so that the 'sorb' could be heated above room temperature to drive out the trapped gas while the cryostat is pumped down using a diffusion pump. When freshly evacuated, the hold time of the nitrogen Dewar is approximately 36 hours, and decreases to about 20 hours after six months.

The flow of liquid nitrogen to the cold finger is regulated using a needle valve which enables the temperature of the crystal (measured using a platinum resistance thermometer (PRT)) to be adjusted. The vacuum chamber containing the crystal mount can also be hermetically isolated from the main vacuum chamber using a three-way valve. These last two features permit removal of the colour-centre crystal while the main chamber is evacuated and at cryogenic temperatures. A 24 V co-axial heater is wrapped around the cold finger so that the crystal temperature can be quickly raised to room temperature after the needle valve is closed. Typically, it takes 20 - 30 minutes to warm the crystal chamber from 77 K to 290 K. The crystal mount takes approximately 10 minutes to cool to 77 K once the chamber is reconnected to the

main vacuum chamber and the needle valve is opened. Thus, a crystal may be changed in less than 45 minutes. This is a considerable advantage over other colour-centre laser cryostat designs[60, 32, 33], which have a crystal change-over period of 16 hours. A further advantage of this cryostat is that all the resonator optics are external to the vacuum chamber, enabling easy adjustment and a large degree of flexibility in the resonator design.

1.5 Measurement of ultrashort pulses

1.5.1 Linear detection

The most convenient means to measure mode-locked laser pulses is direct detection using a photodiode and a fast oscilloscope. Photodiodes having bandwidths in excess of 100 GHz (a temporal resolution of < 5 ps) have been reported[61] and diodes having bandwidths of 20 GHz are commercially available. The resolvable pulse duration is in fact limited by the bandwidth of the oscilloscope which is typically 0.5 GHz. Although these oscilloscopes have insufficient bandwidth to enable measurement of pulses of less than 1 ns duration, they are capable of resolving the individual pulses in a mode-locked pulse sequence A germanium photodiode having a bandwidth of 300 MHz (Germanium Power Devices GM4) was used in conjunction with a Tektronix 2834 storage oscilloscope equipped with a model 7B92A 500 MHz bandwidth timebase, to monitor the mode-locked pulse trains from the NaCl:OH^- laser.

If the laser signal is repetitive sampling oscilloscopes, having effective bandwidths as large as 50 GHz[62] may be used to obtain temporal resolutions of approximately 10 ps. A PIN photodiode and a Tektronix 7603 sampling oscilloscope, having a combined temporal resolution of 50 ps, were used to measure the duration of the acousto-optically mode-locked laser pulses as described in Chapter 2.

The streak camera[63,64] is an attractive measurement instrument, offering high sensitivity, a linear response and temporal resolutions of approximately 2 ps at 1.5 μm (in synchroscan operation). However, in comparison to the other measurement techniques described in this section, they are relatively cumbersome and were not used in this project.

1.5.2 Second-harmonic generation autocorrelation

For pulse durations of less than one picosecond, it is necessary to use nonlinear correlation measurement techniques. The most commonly used technique is that of second harmonic generation (SHG) autocorrelation[65-67]. The pulse to be measured is divided into two intensity components. One pulse is delayed with respect to the other using an optical delay line and the two pulses are then recombined in an

optically nonlinear crystal. Since the second harmonic generation in the crystal depends quadratically on the input intensity, the second-order autocorrelation function $G_2(\tau)$ of the pulse can be generated by varying the temporal overlap of the two pulses in the crystal using the delay line. The duration of the pulse can then be inferred by measuring the displacement of the delay stage. Thus a time measurement of 10^{-13} s is converted into a length measurement of 10^{-5} m, which may be easily performed by using a micrometer to adjust the delay line.

Unfortunately, since the autocorrelation function is symmetric, the information relating to the temporal profile of the pulse is lost. This makes the exact duration of the pulse ambiguous since it depends upon the pulse shape. Cross-correlation techniques[68,69] provide information of the pulse profile but are considerably more involved and require intensive computation.

Three types of SHG autocorrelator can be constructed, depending on the type of phase matching used in the nonlinear crystal and whether the two beams are collinear. In early autocorrelators type II phase matching was used, requiring orthogonally polarised input beams. In this configuration, the second harmonic is only generated when the pulses have some degree of temporal overlap in the crystal. Nowadays type I phase matching (where the input beams are similarly polarised) is more common. If the two beams input to the crystal are collinear, the autocorrelation function will have a background level. This occurs because each beam independently generates second harmonic light, the SHG being enhanced when the pulses have some coincidence. Background-free autocorrelations can be generated using a non-collinear alignment. In this case, the frequency-doubled light arising from the coincidence of the two pulses is generated at the angle bisecting the SHG generated by the individual pulses. The background free autocorrelation is then simply obtained by placing an aperture before the detector to select this SHG contribution.

A schematic of the type I phase-matched, collinear autocorrelator used throughout this project is presented as Figure 1.8. The light is input to a Michelson delay line constructed from a 50/50 beamsplitter and two gold-coated, air-spaced retroreflectors. An aperture, placed at the input to the delay line, prevents any reflected light being fed back into the laser cavity. One of the retroreflectors is attached to the cone of an 8-inch diameter loudspeaker having a 15 mm travel. The speaker is driven at 22 Hz by a rounded sawtooth waveform which enables 'real-time' monitoring of the autocorrelation using an oscilloscope[70]. In the other arm of the delay line, the corner cube is mounted on a three-axis translation stage so that the two beams input to the correlator could be overlapped. Also, by adjusting the length of this arm by a known distance, the autocorrelation could be accurately calibrated. The second-harmonic generation unit comprises a 250 μm thick $LiNbO_3$ crystal, a focusing lens and two filters. The filters prevent any ambient light or light at the

fundamental laser frequency entering the detector, which is a photomultiplier tube. The material and thickness of the frequency-doubling crystal was selected after consideration of its nonlinear coefficient and phase-matching bandwidth[71]. At 1.5 μm wavelength, the 250 μm thick $LiNbO_3$ crystal can phase match 74 nm resulting in a minimum resolvable pulse duration of 32 fs (for a $sech^2$ pulse shape).

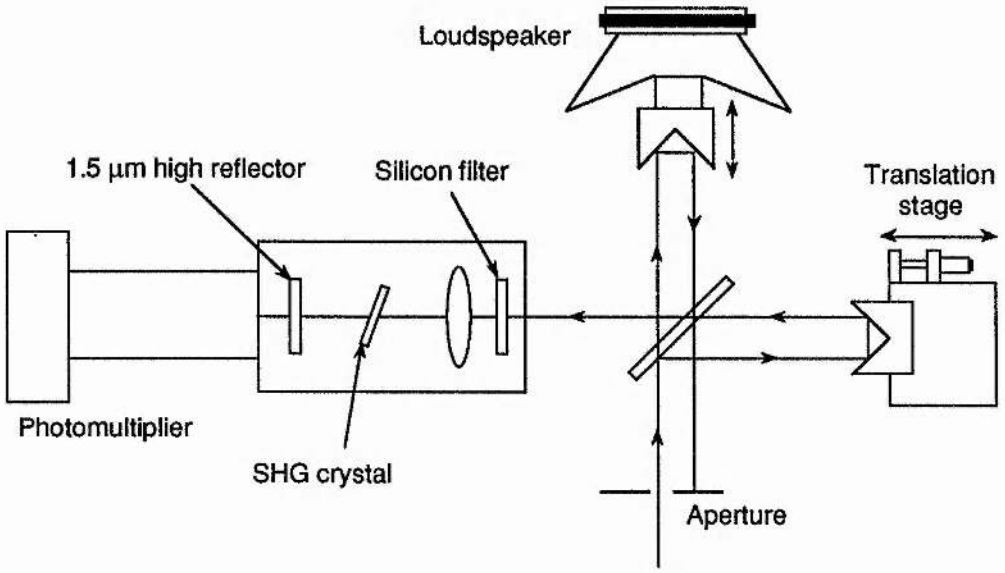

Figure 1.8. Schematic of the SHG autocorrelator.

It was observed by Grant[71] that the silicon filter possessed significant group-velocity dispersion. For this reason it was removed whenever the pulse duration approached 100 fs.

For collinear autocorrelation, the second-order intensity autocorrelation function is given by

$$G_2(\tau) = 1 + 2\frac{\int_{-\infty}^{\infty} I(t)I(t-\tau)dt}{\int_{-\infty}^{\infty} I^2(t)dt} \tag{1.3}$$

where $I(t)$ is the intensity of the pulse and τ is the delay. By inspection of this equation, it can be seen that the minimum possible background intensity is 1 unit and the maximum intensity for the autocorrelation is 3 units. The shape and contrast ratio of the autocorrelation signal yields information regarding the quality of the mode-locked pulse train. Three important examples are presented in Figure 1.9.

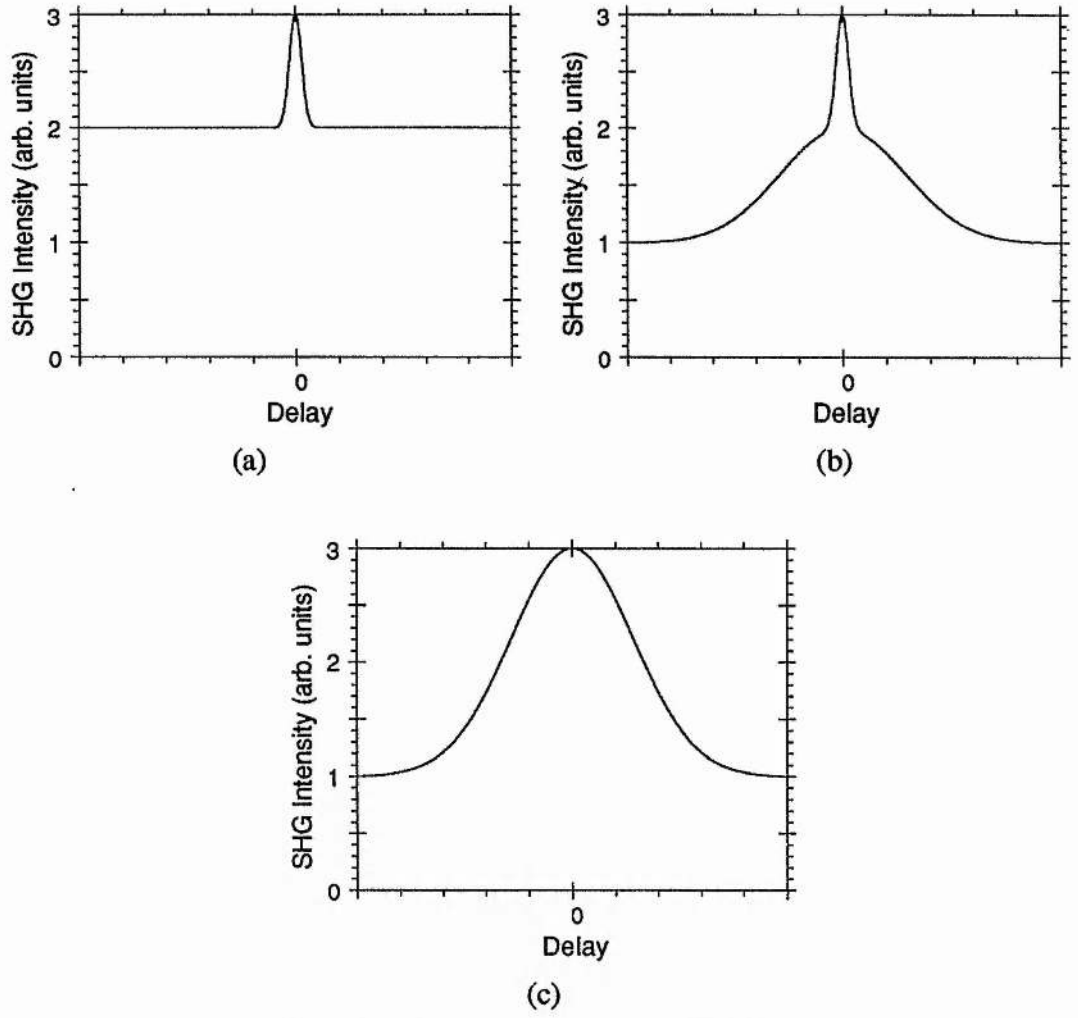

Figure 1..9. Calculated collinear intensity autocorrelation traces for: (a) cw radiation, (b) a noise burst and (c) mode-locked pulses.

Figure 1.9(a) shows the autocorrelation for cw light. The contrast ratio between the maximum intensity and the background level is 2:1. The spike at the centre of the autocorrelation occurs when the two arms of the delay line are exactly matched and is due to the coherent addition of the two fields. If a noise burst having a 100% modulation depth is input to the autocorrelator, the autocorrelation shown in Figure 1.9(b) is obtained. The broad pulse, having a contrast ratio of 2:1, relates to the duration of the noise burst and the duration of the coherence spike, with a peak intensity of 3 units, is a measure of the oscillating bandwidth. An autocorrelation of a perfectly mode-locked Gaussian pulse is shown in Figure 1.9(c). The 3:1 contrast ratio indicates that the entire oscillating bandwidth is phase locked and that there is no inter-pulse radiation. The duration of the pulse is obtained by measuring the duration of the autocorrelation function at an intensity of 2 units and dividing it by a factor, k, which depends on the assumed pulse shape. The validity of this assumed pulse shape

can be checked by measuring the bandwidth of the pulse spectrum and comparing the duration-bandwidth product with the calculated value for the chosen pulse profile. This comparison is only valid for pulses having no frequency chirp. Calculated values for the Fourier transform-limited duration-bandwidth product $\Delta\tau_p\Delta\nu$, and the factor k for some common pulse shapes are presented in Table 1.2.

Pulse profile	I(t)	$\Delta\tau_p\Delta\nu$	k
$sech^2$	$\text{sech}^2\left(\frac{t}{T}\right)$	0.315	1.543
Gaussian	$\exp\left(-\frac{t^2}{T^2}\right)$	0.441	1.414
Single-sided exponential	$\begin{cases}\exp\left(-\frac{t}{T}\right) & ;t \geq 0 \\ 0 & ;t < 0\end{cases}$	0.110	2.00

Table 1.2. Transform-limited duration-bandwidth products and correction factors for some common pulse shapes.

If the detection system used to measure the second harmonic generation has sufficient bandwidth, it is possible to resolve the fringes which result from the interference of two beams in the nonlinear crystal. In this case the second-order interferometric autocorrelation function is given by[70]

$$G_2(\tau) = \frac{\int_{-\infty}^{\infty}\left|\left\{E(t)e^{i(\omega t+\phi)} + E(t-\tau)e^{i[\omega(t-\tau)+\phi(t-\tau)]}\right\}^2\right|^2 dt}{2^4\int_{-\infty}^{\infty}E^4(t)dt} \tag{1.4}$$

The quartic dependence of the autocorrelation on the electric field results in an increased contrast ratio of 8:1. Since this autocorrelation resolves individual optical cycles, it is sensitive to frequency chirp. Interferometric autocorrelations of a 75 fs duration pulse having a Gaussian temporal profile are presented in Figure 1.10. Figure 1.10(a) shows a transform-limited pulse and Figures 1.10(b) and 1.10(c) show the autocorrelations of the pulse with increasing linear chirp. The chirp causes a reduction in the fringe visibility since the wings of the pulse cannot fully interfere. For large degrees of frequency chirp, as shown in Figure 1.10(c) the autocorrelation tends towards the intensity autocorrelation.

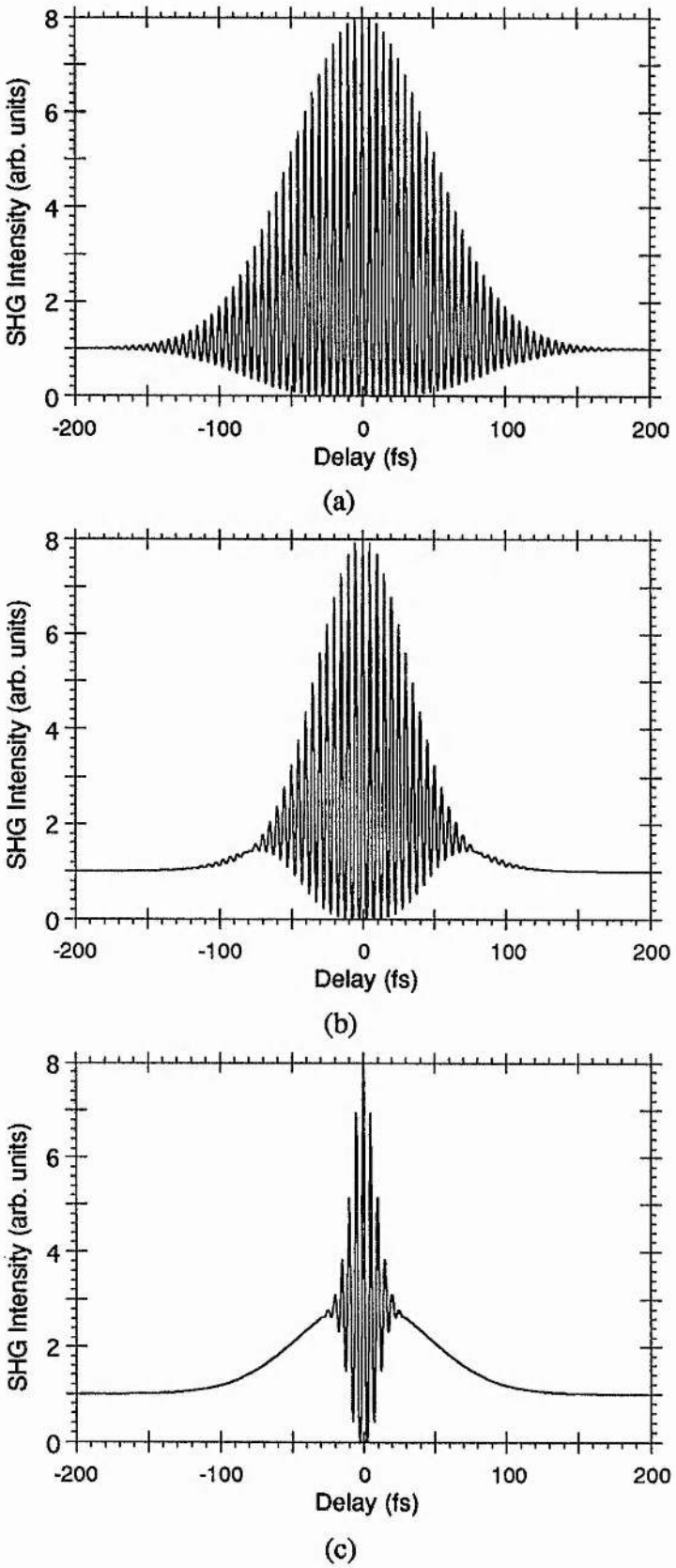

Figure 1.10. Calculated interferometric autocorrelations for Gaussian pulses having: (a) no frequency chirp, (b) a frequency chirp parameter of 2 and (c) a chirp parameter of 20.

1.5.3 Spectral Analysis

In addition to temporal measurements, the optical spectrum of the laser output provides useful information of the pulse quality. As mentioned in the previous section, measurement of the spectral bandwidth can assist in the determination of the pulse profile. Furthermore, a small cw component on a pulse train, which would cause a minimal increase in the background level of the autocorrelation, would appear as a clearly visible spike on the spectrum.

A 1 m Monospek monochromator having a resolution of 0.1 nm and a, home-built, scanning Fabry-Perot interferometer were used throughout this project. The Fabry-Perot interferometer was constructed from two plane 95% reflecting dielectric mirrors; one mounted on a precision translation stage and the other on a Photon Control piezoelectric mirror mount. It was calibrated by moving the mirrors together until they touched and then winding the translation stage back a known distance. A correction factor of 14 μm was added to the mirror separation to compensate for the thickness of the dielectric mirror coatings.

1.6 Chromatic dispersion

The response of a dielectric medium to electromagnetic radiation depends on the wavelength of the incident light. This manifests itself as a variation of the refractive index with wavelength and is termed chromatic dispersion. Since the bandwidth of mode-locked laser pulses may extend for several tens of nanometres, the effects of chromatic dispersion are extremely important. The variation of the refractive index with wavelength is described by the empirical Sellmeier expansion

$$n^2(\lambda)-1=\sum_{i=1}^{k}\frac{A_i\lambda^2}{\lambda^2-B_i^2} \tag{1.5}$$

where n is the refractive index, λ is the wavelength in microns, B_i are the wavelengths of the i^{th} optical resonance of the material and A_i are constants relating to the strength of the i^{th} resonance. Usually a three-term expansion, having two resonances in the ultraviolet and one resonance in the infrared, is sufficient to describe the refractive index of transparent materials in the visible and near-infrared wavelength region. The chromatic dispersion of a material can be mathematically represented by expanding the propagation constant β in a Taylor series about wavelength ω_0. That is

$$\beta(\omega)=n(\omega)\frac{\omega}{c}=\beta_0+\beta_1(\omega-\omega_0)+\frac{1}{2}\beta_2(\omega-\omega_0)^2+..... \tag{1.6}$$

where $$\beta_m = \left.\frac{d^m \beta}{d\omega^m}\right|_{\omega=\omega_0} \tag{1.7}$$

For waveguides, the propagation constant depends on their geometry as well as the constituent materials. Care must be taken to include both these contributions when calculating β_m. The first term in this series is related to the phase velocity of light whilst the group velocity, which represents the velocity at which a pulse will travel through the medium, is given by $v_g = 1/\beta_1$. The third term is related to group-velocity dispersion and is largely responsible for pulse broadening. For media transparent in the visible, the sign of β_2 is positive (normal dispersion) in the visible and changes sign in the near infrared (anomalous dispersion). For fused silica β_2 is zero at a wavelength of 1.27 μm.

In the normally dispersive regime ($\beta_2 > 0$) group-velocity dispersion causes a pulse to become up-chirped in frequency. That is, the short wavelength components of the pulse travel more slowly than the centre wavelength and are pushed to the trailing edge of the pulse, whilst the long wavelength components travel faster and move to the leading edge of the pulse. For anomalous group-velocity dispersion ($\beta_2 < 0$) the longer wavelength components are retarded with respect to the centre wavelength and the shorter wavelength components are advanced. This redistribution of energy results in a broadening of the pulse for either sign of group-velocity dispersion. At wavelengths close to zero group velocity dispersion, and for pulse durations less than 100 fs, higher order terms in β become significant.

A useful parameter for indicating the length scale at which the effects of group-velocity dispersion become important is the dispersion length, given by

$$L_D = \frac{T_0^2}{|\beta_2|} \tag{1.8}$$

where T_0 is the 1/e duration of the pulse which is related to the full-width at half-maximum duration by $T_{fwhm} = 1.665\ T_0$ for a Gaussian pulse shape and $T_{fwhm} = 1.763\ T_0$ for a sech^2 pulse profile. For example, if a Gaussian pulse is propagated through a medium of length z, it retains its shape but is broadened to

$$T_{out} = T_{in}\left[1+\left(\frac{z}{L_D}\right)^2\right]^{\frac{1}{2}} \tag{1.9}$$

Thus, for pulse propagation in a dispersion length, its duration is increased by a factor of $\sqrt{2}$.

1.7 Nonresonant optical nonlinearities

When light is propagated through a dielectric medium, the time varying electric field drives the valence electrons into oscillation. For low light levels, the frequency and amplitude of oscillation follows that of the incident light. However, if the amplitude of the propagating field is sufficiently strong, the response of the medium will not follow the incident light and a nonlinear response will occur. If the wavelength of the input light does not correspond to an optical resonance of the material, the nonlinear response will be almost instantaneous since the electron cloud has a very low mass. The polarisation (dipole moment per unit volume) may be written as

$$p = \varepsilon_o\left(\chi_{(1)}E + \chi_{(2)}E^2 + \chi_{(3)}E^3 + \ldots\right) \tag{1.10}$$

where $\chi_{(1)}$ represents the linear susceptibility of the medium and is related to its refractive index by

$$n^2 = \mathrm{Re}\left\{1 + \chi_{(1)}\right\} \tag{1.11}$$

The second term in this series, $\varepsilon_0\chi_{(2)}E^2$, represents a second-order nonlinearity. This is responsible for second-harmonic generation, optical rectification and optical parametric generation. As a result of its E^2 dependence, second-order nonlinearities only exist for materials which are non-centrosymmetric.

The third-order susceptibility is non-zero for all materials. This term is responsible for frequency tripling, Raman and Brillouin scattering and the Kerr effect. This latter effect causes self-phase modulation[72] and, its spatial analogue, self focusing[73] which are of particular relevance to the subject matter of this thesis.

When the third-order susceptibility is included in the expansion for the polarisation, the refractive index of the medium becomes intensity dependent and is given by

$$n = n_o + n_2 I \tag{1.12}$$

where n_0 is the linear refractive index, I is the intensity of the incident light and n_2 is the Kerr coefficient. For fused silica, n_2 has a value of 3.2×10^{-20} m^2W^{-1}.

In a similar manner to group-velocity dispersion, a characteristic nonlinear length, L_{NL}, may be defined as

$$L_{NL} = \frac{1}{\gamma P_o} \tag{1.13}$$

where $\gamma = \frac{cA}{n_2 \omega_o}$ and P_o is the peak power of the pulse. (1.14)

1.7.1 Self focusing

Generally laser beams do not have 'top hat' cross sections, but have a smooth intensity profile having a maximum at the centre of the beam. If such a beam is propagated through a material having a positive n_2, it will experience a higher refractive index at its centre than in its wings and the medium will act as an intensity dependent converging lens. This self focusing causes a reduction in the spot size of the beam which, in turn, results in an increase in the intensity of the beam. If the power of the beam exceeds a critical value, then the self focusing can run away until the intensity of the field causes optical damage to the material. Furthermore, if there are any intensity fluctuations across the laser beam, the effects of self focusing will cause the magnitude of these fluctuations to increase and may result in break-up of the beam.

1.7.2 Self-phase modulation

If a pulse is propagated through a material having a positive Kerr coefficient, the refractive index will vary with time through the pulse, reaching a maximum at its peak. This results in a nonlinear modulation of the phase across the pulse which is given by

$$\phi_{NL} = \frac{2\pi n_2}{\lambda} IL \tag{1.15}$$

where L is the length of the medium and λ is the wavelength. For a positive n_2, the self-phase modulation causes the leading edge of the pulse to be down-shifted in frequency (red shift) and the trailing edge is frequency up-shifted (blue shift). For a negative value of n_2 the frequency shifts are reversed.

1.8 Pulse propagation in nonlinear media

So far the effects of self-phase modulation and group-velocity dispersion have been considered in isolation. For many situations L_{NL} and L_D are of similar magnitudes and both effects must be considered simultaneously. The propagation of pulses in nonlinear dispersive material can be described using the nonlinear Schrodinger

equation[74]. In general, this equation cannot be solved analytically and appropriate numerical methods must be used.

In the normal group-velocity dispersion regime, self-phase modulation enhances the temporal broadening of a pulse, because the frequency chirps arising from both effects have the same sign throughout the pulse. The output pulse is almost rectangular in profile and has a near linear frequency chirp over most of its duration[75]. By compensating for this chirp using prisms or gratings, the pulse can be substantially temporally compressed.

For the anomalous group-velocity dispersion regime, the frequency chirp due to self-phase modulation is of opposite sign to that caused by the group velocity dispersion and the effects may cancel one another. In optical fibres, this leads to the formation of bright optical solitons[76,47]. These are pulses having a sech^2 intensity profile which can propagate for arbitrarily long distances (assuming no loss) with no change to their temporal or spectral profile. The fundamental, or first order, soliton occurs when $L_{NL} = L_D$. Since the soliton is a stable solution of the nonlinear Schrodinger equation, the input pulse will change its profile and shed energy so that it will evolve into a soliton. For large input peak powers $L_{NL} >> L_D$ and higher-order solitons, which follow a periodic evolution will result. The soliton order is given by

$$N = \sqrt{\frac{L_D}{L_{NL}}} \tag{1.16}$$

and its period is

$$z_o = \frac{\pi}{2} L_D \tag{1.17}$$

1.9 Summary

In this chapter, the motivation for tunable mode-locked laser sources in the 1.5 μm spectral region has been briefly outlined, and background material relevant to the rest of this thesis has been presented. A basic overview of active and passive mode-locking techniques has been given, and common methods for the characterisation of ultrashort pulses were discussed. A review of colour-centre lasers was given with particular emphasis on the NaCl:OH^- laser. The characterisation and development of mode-locking techniques for this laser form the backbone of this thesis. The chapter ends with a discussion of the effects of chromatic dispersion and nonlinearity on pulse propagation. For the pulse durations and intensities obtained from many mode-locked lasers, these effects become significant and are indeed fundamental to the passive mode-locking schemes implemented in this thesis.

References

1. A. E. Siegman in *Lasers,* (University Science Books, Mill Valley, California, 1986).
2. D. J. Kuizenga and A. E. Siegman, IEEE J. Quantum Electron. **QE-6,** 694 (1970).
3. A. E. Siegman and D. J. Kuizenga Appl. Phys. Lett. **14,** 181 (1969).
4. G. C. H. New, IEEE J. Quantum Electron. **QE-10,** 115 (1974).
5. H. A. Haus, J. Appl. Phys **46,** 3049 (1975).
6. H, A. Haus, IEEE J. Quantum Electron. **QE-11,** 736 (1975).
7. H. A. Haus, IEEE J. Quantum Electron. **QE-12,** 169 (1976).
8. P. W. Smith, Proc IEEE **58,** 1342 (1970).
9. D. von der Linde, Appl. Phys. **2,** 281 (1973).
10. A. Miller and W. Sibbett, J. Mod. Opt. **35,** 1879 (1988).
11. H. A. Haus, IEEE J. Quantum Electron. **QE-11,** 323 (1975).
12. G. C. H. New, Rep. Prog. Phys **46,** 877 (1983).
13. H. Statz and C. L. Tang J. Appl. Phys **36,** 3923 (1965).
14. L. Dahlstrom, Opt. Commun. **5,** 157 (1972).
15. G. Gabetta, D. Huang, J. Jacobson, M. Ramaswammy, H. A. Haus, E. P. Ippen and J. Fujimoto, in *Tichnical Digest Conference on Lasers and Electro-Optics* (Optical Society of America, Washington D.C. 1991) Paper CPDP8.
16. K. A. Stankov and J. Jethwa Opt. Commun. **66,** 41 (1988).
17. L. F. Mollenauer and R. H. Stolen, Opt. Lett. **9,** 13 (1984).
18. P. N. Kean, X. Zhu, D. W. Crust, R. S. Grant, N. Langford and W Sibbett, Opt. Lett. **14,** 39 (1989).
19. K. J. Blow and B. P. Nelson, Opt. Lett. **13,** 1026 (1988).
20. R. S. Grant and W. Sibbett, Opt. Commun. **86,** 177 (1991).
21. F. Ouelette and M. Pichet, Opt. Commun. **60,** 99 (1986).
22. T. F. Carruthers and I. N. Dulling III, Opt. Lett. **15,** 804 (1990).
23. I. N. Dulling III, Electron. Lett. **27,** 544 (1991).
24. D. J. Richardson, R. I. Lamming, D. N. Payne, V. Matsas and W. W. Phillips, Electron. Lett. **27,** 542 (1991).
25. R. S. Grant, P. N. Kean, D. Burns and W. Sibbett, Opt. Lett. **16,** 384 (1991).
26. R. S. Grant, G. K. Kennedy, W. Sibbett and J. S. Aitchison, Opt. Lett. **18,** (1993) To be published
27. D. E. Spence, P. N. Kean and W. Sibbett, Opt. Lett. **16,** 42 (1991).
28. D. K. Negus, L. Spinelli, N. Goldblatt and G. Feugnet, in *Advanced Solid-State Lasers,* vol. 10, OSA Proceedings Series (Optical Society of America, Washington D.C.,1991) p. 120.
29. M. T. Asaki, C. P. Huang, D. G. Harvey, Z, Zhou, H. C. Kapteyn and M. Murnane, Opt. Lett. **18,** 977 (1993).

30. E. P. Ippen, C. V. Shank and A. Dienes, Appl. Phys. Lett. **21,** 348 (1972).
31. G. H. C. New, Opt. Commun. **6,** 188 (1972).
32. L. F. Mollenauer, in *Tunable Lasers* (Springer, Berlin, Heidelberg, 1987)
33. W. Gellermann, J. Phys. Chem. Solids **52,** 249 (1991).
34. B. Fritz and E. Menke, Solid St. Commun **3,** 61 (1965).
35. L. F. Mollenauer and D. H. Olson, Appl. Phys. Lett. **24,** 386 (1974).
36. R. Beigang, K. Klameth. B. Becker, Z. Yoon and H. Welling, Opt. Commun. **65,** 383 (1988).
37. L. F. Mollenauer, Rev. Sci. Intr. **49,** 809 (1978).
38. W. B. Fowler and D. L. Dexter, Chem. Phys **43,** 768, (1965).
39. J. Wiesenfeld, L. F. Mollenauer and E. P. Ippen, Phys. Rev. Lett. **47,** 1668 (1981).
40. B. Fritz, F. Luty, G. Rausch, Phys. Stat. Sol. **11,** 635 (1965).
41. F. Luty, in Physics of Color Centers, ed. W. B. Fowler (Academic, New York 1968), Chapter 3.
42. K. German, J. Opt. Soc. Am. B **3,** 149 (1986).
43. G. Liftin, R. Beigang and H. Welling, Appl. Phys. Lett. **31,** 381 (1977).
44. K. Park and W. L. Faust, Phys. Rev. Let **17,** 137 (1966).
45. W. Gellermann, F. Luty and C. R. Pollock, Opt. Commun. **39,** 391 (1981).
46. L. F. Mollenauer, N. D. Vieira and L. Szeto, Phys. Rev. B **27,** 5332 (1983).
47. L. F. Mollenauer, R. H. Stolen and J. P. Gordon, Phys. Rev. Lett. **45,** 1095 (1980).
48. K. L. Hall, J. Mark, E. P. Ippen and G. Eisenstein, Appl. Phys. Lett. **56,** 1740 (1990).
49. C. R. Pollock J. Luminesc. **35,** 65 (1986).
50. J. F. Pinto, L. W. Stratton and C. R. Pollock, Opt. Lett. **10,** 384 (1985).
51. J. F. Pinto, E. Georgiou and C. R. Pollock, Opt. Lett. **11,** 519 (1986).
52. T. Kurobori, A. Nebel, R. Beigang and H. Welling, Opt. Commun. **73,** 365 (1989).
53. M. N. Islam, E. R. sunderman, I. Bar-Joseph, N. Sauer and T. Y. Chang, Appl. Phys. Lett **54,** 1203 (1989).
54. C. P. Yakymyshyn, J. F. Pinto and C. R. Pollock, Opt. Lett. **14,** 621 (1989).
55. A. Sennarogly and C. R. Pollock, J. Luminesc. **47,** 217 (1991).
56. E. Georgiou, J. F. Pinto and C. R. Pollock, Phys. Rev. B **35,** 7636 (1987).
57. D. Wandt, W. Gellermann, F. Luty and H. Welling, J. Appl. Phys. **61,** 864 (1987)
58. K. R. German, and C. R. Pollock, Opt. Lett. **12,** 474 (1985).
59. T. J. Carrig and C. R. Pollock, J. Appl. Phys. **69,** 3796 (1991).
60. G. Liftin and R. Beigang, J. Phys. E, Scient. Intrum. **11,** 984 (1978).
61. D. G. Parker, P. G. Say, A. M. Hansom and W. Sibbett, Electron. Lett. **23,** 527 (1987).
62. Tektronix Model No CSA 803, Tektronix Product Catalogue 1993 p 250.
63. E. K. Zavoiskii and S. D. Franchenko, Sov. Phys. Doklady **1,** 285 (1956).
64. D. J. Bradley, B. Liddy and W. E. Sleat, Opt. Commun. **26,** 273 (1978).

65. J. A. Armstrong, Appl. Phys. Lett. **10,** 16 (1967).

66. H. P. Weber, J. Appl. Phys. **38,** 2231 (1967).

67. M. Maier, W. Kaiser and J. A. Giordmaine, Phys. Rev. Lett. **17,** 1275 (1966).

68. J. L. A. Chilla and O. E. Martinez, Opt. Lett. **16,** 39 (1991).

69. K. Naganuma, K. Mogi and H. Yamada, Appl. Phys. Lett. **54,** 1201 (1989).

70. K. L. Sala, G. A. Kenney-Wallace and G. E. Hall, IEEE J. Quantum Electron. **QE-16,** 990 (1980)

71. R. S. Grant, Ph.D. Thesis, University of St. Andrews 1991.

72. F. Schimazu, Phys. Rev. Lett. **19,** 1097 (1967).

73. W. Koechner in *Solid-State Laser Engineering* (Springer-Verlag, New York, 1973), Chapter 12.

74. G. P. Agrawal, Nonlinear Fibre Optics (Academic Press, Boston, 1989)

75. D. Grischkowsky and A. C. Balant, Appl. Phys. Lett. **41,** 1 (1982).

76. A. Hasegawa and F. Tappert, Appl. Phys. Lett **23,** 142 (1973).

Chapter 2

The Actively Mode-Locked NaCl:OH^- Laser

2.1 Introduction

Active mode locking of the NaCl:OH^- colour-centre laser was first reported by Pinto[1] *et al.* and German and Pollock[2]. They used the technique of synchronous mode locking, using an actively mode-locked Nd:YAG pump laser, to obtain pulse durations of 5 ps duration. More detailed studies, including the effects of cavity length detuning, were later reported by Kurobori and co-workers[3] and Grant[4]. The shorter pulses available from the actively mode-locked Nd:YLF pump laser resulted in the generation of 2.7 ps duration pulses from the synchronously mode-locked NaCl:OH^- laser[3].

In this chapter a detailed study of the actively mode-locked NaCl:OH^- colour-centre laser is described. The laser resonator design is briefly outlined followed by the laser characteristics when mode locked via synchronous pumping and acousto-optic loss modulation. The passive mode-locking techniques described in Chapters 3 and 4 of this thesis require an initial intense pulse to start the mode-locking process and are based upon the mode-locked lasers described here.

Solitonic pulse compression in an anomalously dispersive, monomode optical fibre was subsequently investigated and results shall be presented for a novel pulse compressor constructed from a nonlinear optical-fibre loop mirror.

2.2 The laser resonator

A three-mirror resonator[5], illustrated in Figure 2.1, was used for the colour-centre laser. This resonator configuration was originally developed for continuous-wave dye lasers. It consists of a focusing section comprising a -10 cm radius of curvature (RoC) mirror and a -5 cm RoC mirror between which the colour-centre crystal is located and a long arm terminated by a plane output coupler. This resonator design allows small spot sizes, of the order of several tens of microns, to be achieved within the colour-centre crystal whilst maintaining a relatively low sensitivity to misalignment. The long arm of the cavity can be extended to lengths greater than 1 m

to accommodate tuning elements and to enable active mode locking. A simple Gaussian beam program was used to analyse the laser resonator.

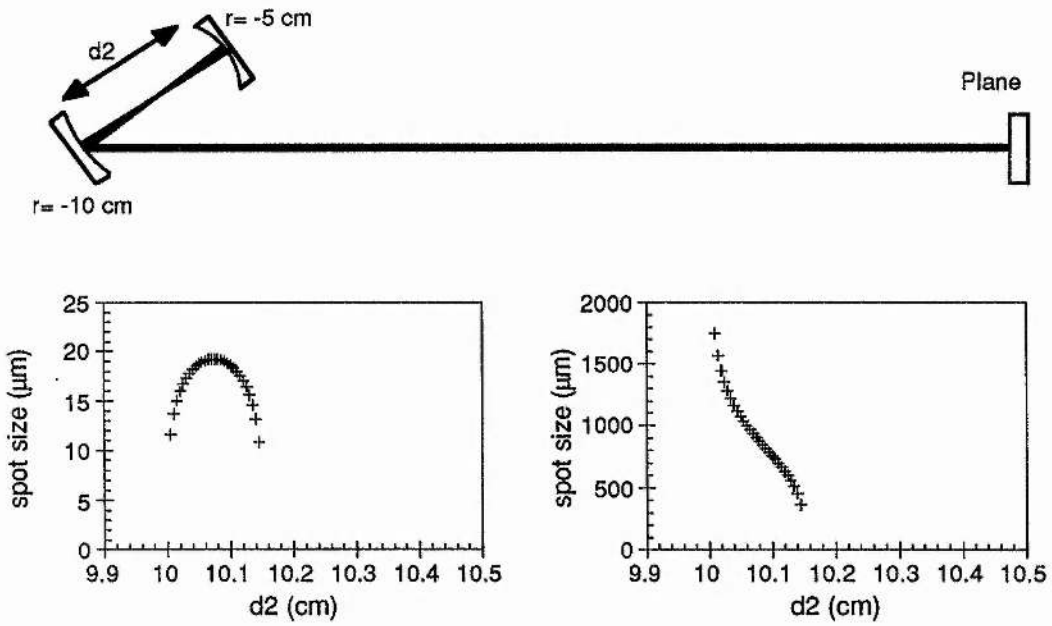

Figure 2.1. The three-mirror resonator and associated stability diagrams. The radius of the beam waist between the curved mirrors (left) and the radius on the plane output coupler are plotted as a function of the curved mirror separation.

Figure 2.1 shows the calculated beam waist sizes on the plane output coupler and between the focusing mirrors for a 183 cm long resonator. This resonator length corresponds to a round-trip frequency of 82 MHz and is compatible with active mode locking. When the mirrors are precisely 10 cm apart the beam in the long arm of the resonator is perfectly collimated and the radius of the beam waist between the focusing mirrors is zero. This represents one limit of the stability region. As the curved mirror separation is increased, the spot size increases to approximately 20 μm and then falls to zero at the other extreme of the stability region. At this point the size of the beam waist on the output coupler also tends to zero. In this arrangement the resonator is stable for approximately 1.5 mm adjustment of the separation of the focusing section. The extent of the stability range can be increased by reducing the length of the long resonator arm and harmonically mode locking the laser (a reduction in length from 172 cm to 81 cm doubles the stability region). However, this is undesirable because it leads to a reduction of the pulse energy. An alternative approach is to include a -1 m RoC mirror in the long arm approximately 50 - 60 cm from the output coupler as shown in Figure 2.2. This increases the range over which the separation of the focusing mirrors can be adjusted to roughly 4 mm. Graphs of the spot sizes on the output coupler and between the focusing mirrors are presented in

Figure 2.2. It can be seen that the inclusion of the -1 m RoC mirror also increases the radius of the beam waist in the focusing section from 20 μm to 30 μm. This allows better mode matching of the pump and laser beams in the colour-centre crystal.

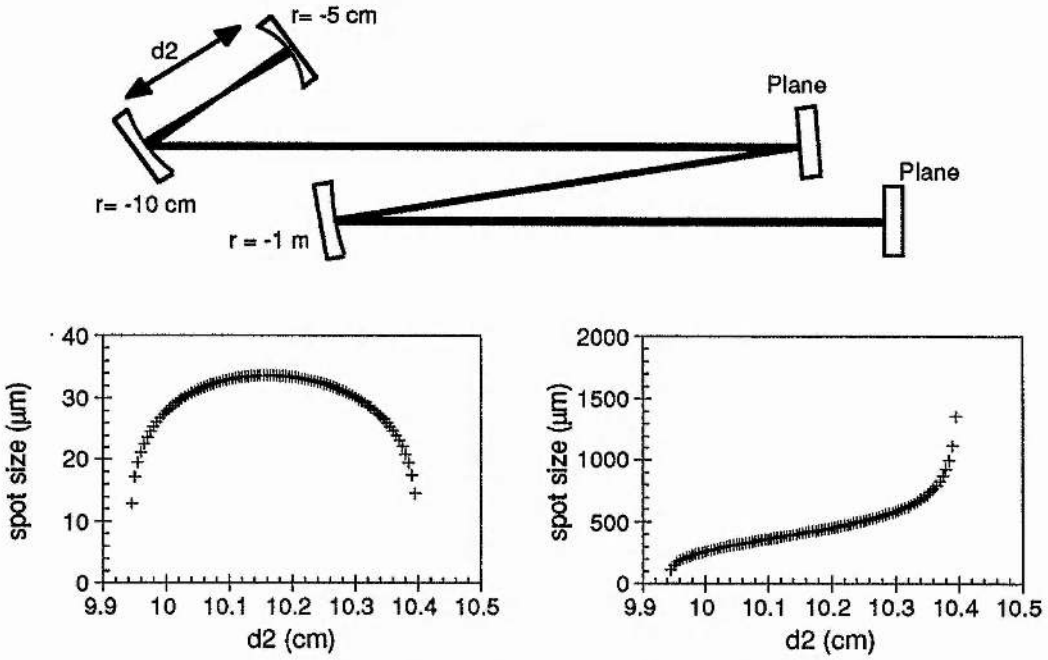

Figure 2.2. The extended three-mirror resonator. The radius of the beam waist in the focusing section (left) and on the plane output coupler are calculated as a function of the separation of the focusing mirrors.

Since the cryostat windows and the colour-centre crystal are positioned at Brewster's angle they will introduce considerable astigmatism to the intracavity beam. It is possible to compensate for this astigmatism by selecting an appropriate angle of incidence on the off axis, 10 cm radius of curvature mirror. The angle is calculated by solving[5]

$$\frac{2t_c\left(n_c^2-1\right)\sqrt{n_c^2+1}}{n_c^4}+\frac{4t_w\left(n_w^2-1\right)\sqrt{n_w^2+1}}{n_w^4}=R\sin\theta\tan\theta \qquad (2.1)$$

where t_c, n_g and t_w and n_w are the thicknesses and refractive indices of the colour-centre crystal and Dewar windows,
R is the radius of curvature of the mirror
and θ is the angle of incidence on the curved mirror.

For 2 mm thick infrasil windows (n_w = 1.45), and a 2 mm NaCl crystal having a refractive index of n_c = 1.53, the angle of incidence is $\theta = 13^o$ which corresponds to a folding angle of 26^o.

2.3 Synchronous mode locking

A schematic of the synchronously mode locked NaCl:OH⁻ laser is shown in Figure 2.3. An acousto-optically mode-locked Spectra-Physics 3800 Nd:YAG laser operating at 1064 nm was used to pump the colour-centre crystal. The laser produced 10 - 14 W of vertically polarised light and the pulses were typically 70 - 100 ps duration at 82 MHz repetition frequency. It exhibited 10% peak-to-peak amplitude noise which was reduced to approximately 2% by replacing the 50 cm radius of curvature resonator mirrors with 60 cm radius of curvature mirrors used in the Spectra-Physics 3000 series Nd:YAG lasers[4]. This modification reduced the output power of the laser by 20 - 30%.

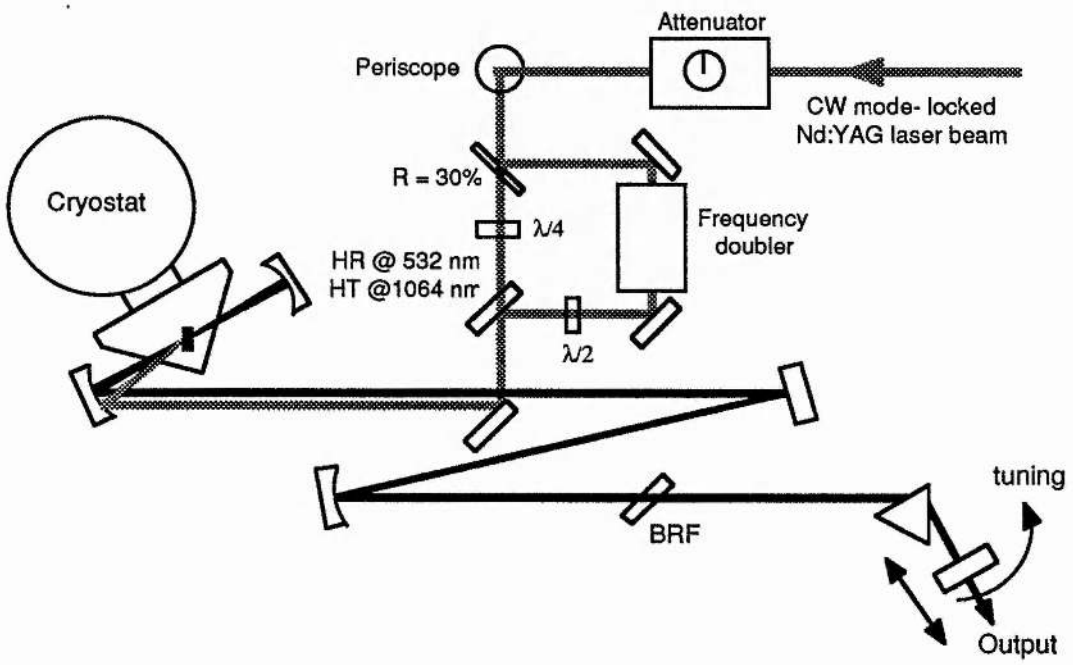

Figure 2.3. Schematic of the synchronously mode locked NaCl:OH⁻ laser.

The pump light was passed through a variable attenuator (Newport 935-3) and a periscope was used to adjust the height of the pump beam and to rotate its polarisation through 90 degrees. As mentioned in the previous chapter, the NaCl:OH⁻ crystal requires auxiliary illumination to reorient the active colour-centres. This was conveniently provided by diverting 30% of the pump beam to a Spectra-Physics model 3220-1 KTP frequency-doubling unit. The polarisation of the 1064 nm beam was set to be circular and the polarisation of the 532 nm light was rotated to horizontal using zero-order waveplates. The two beams were then combined using a harmonic beamsplitter. A high power aluminium mirror was placed at 45 degrees in the long arm of the resonator approximately 2 mm from the path of the intracavity beam. This was used to direct the pump beam parallel to the laser beam onto the

-10 cm radius of curvature cavity mirror which focused both the pump and colour-centre beams into the NaCl:OH⁻ crystal. This nearly collinear pumping configuration resulted in an incomplete overlap of the two beams within the colour-centre crystal but did not significantly impair the performance of the laser.

The laser resonator was extended to 183 cm using a -1 m radius of curvature mirror and the output coupler was mounted on a translation stage having 25 mm travel to allow fine adjustment of the cavity length. A Brewster-angled fused-silica prism and a 6.6 mm thick birefringent filter were incorporated in the long arm of the cavity resonator arm to facilitate tuning and to restrict the bandwidth of the mode-locked pulses. Output couplers having transmissions of 7%, 12% , 22% and 37% were used.

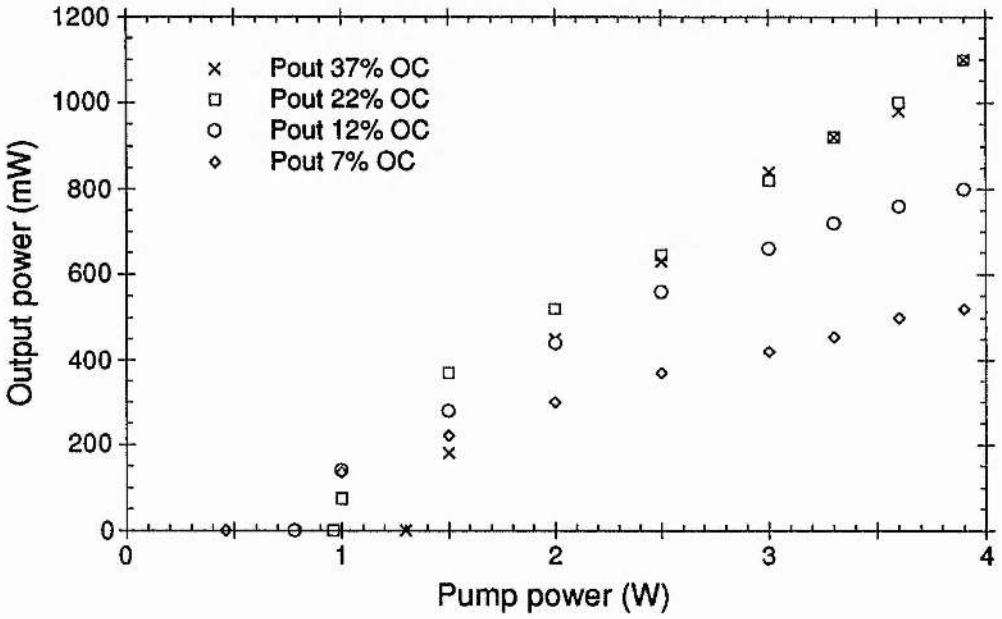

Figure 2.4. Power transfer characteristics for the synchronously mode locked laser for various output couplers.

A graph of the average output power of the synchronously mode locked colour-centre laser versus the input pump power for the various output couplers is presented as Figure 2.4. These measurements were taken at 1560 nm wavelength. A maximum output power of 1.1 W was obtained at a pump power of 3.9 W for both the 22% and the 37% output couplers, indicating an optimum output coupling at this wavelength of around 30%. Below 1.5 W of 1064 nm pump, the output power of the laser was affected by the power of the 532 nm centre-reorientation beam since the variable attenuator changed both the pump level and the power diverted to the frequency-doubling unit, rendering measurements of the true laser threshold impracticable. The output power of the laser was measured as a function of the power

of the 532 nm beam using a variable neutral density filter wheel placed at the output of the frequency doubler. Figure 2.5 shows the dependence of the laser output on the 532 nm power for a constant 1064 nm pump power of 3 W and an output coupling of 22%. As the 532 nm power is increased, the output power from the laser rapidly increases and saturates at 800 mW for approximately 5 mW of 532 nm average power.

When the laser length was detuned by several centimetres from the optimum mode locking position, the average output power decreased by approximately 30% This can be explained as follows: When the laser is synchronously mode locked the energetic laser pulses causes a rapid reduction in the upper-state population during pumping. This occurs on a time-scale much shorter than the lifetime of the upper laser level and so there is a minimal reduction in the upperstate population due to spontaneous emission. When the laser is detuned from mode locking, the stimulated emission rate during the pump pulse is reduced and so a greater fraction of the population inversion is lost to spontaneous emission. This results in a lower output power and an increase in the pump power required to reach threshold.

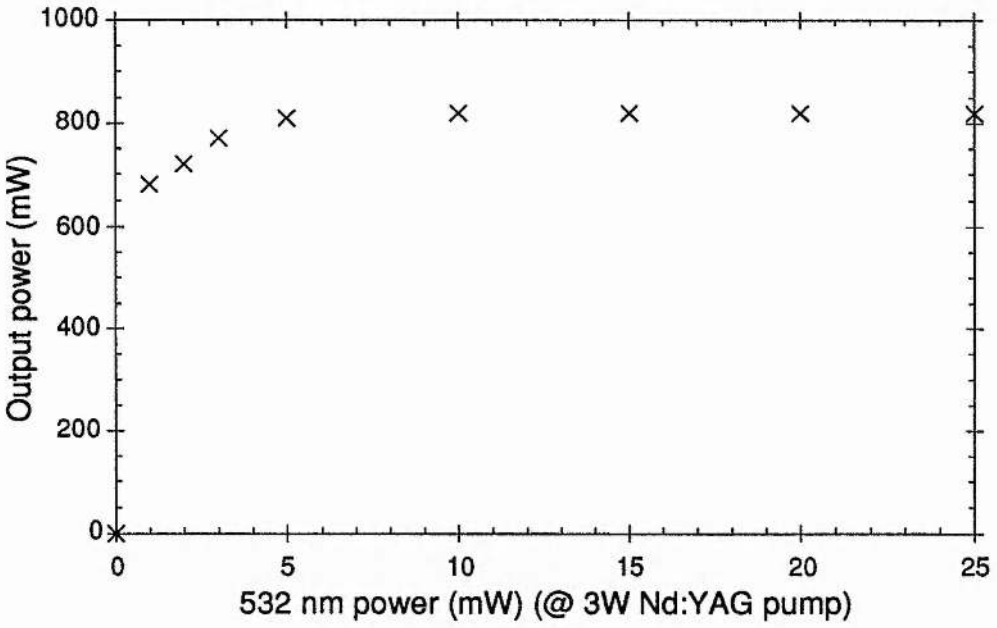

Figure 2.5. Output power as a function of 532 nm auxiliary illumination for a constant pump power of 3 W at 1064 nm.

The tuning characteristic of the laser was measured at a pump power of 3.5 W for each output coupler and are presented in Figure 2.6. The tuning ranges extended from 1440 nm to 1675 nm for the 7%, 12% and 22% output couplers with output powers in excess of 400 mW obtained from 1460 nm to 1660 nm. The tuning range for the 37% output coupler was 1470 - 1670 nm. The long wavelength tuning range

was limited by the dielectric coatings on the intracavity mirrors which extended from 1410 to 1680 nm. With suitable mirror coatings it should be possible to tune the laser wavelength to beyond 1.8 μm.

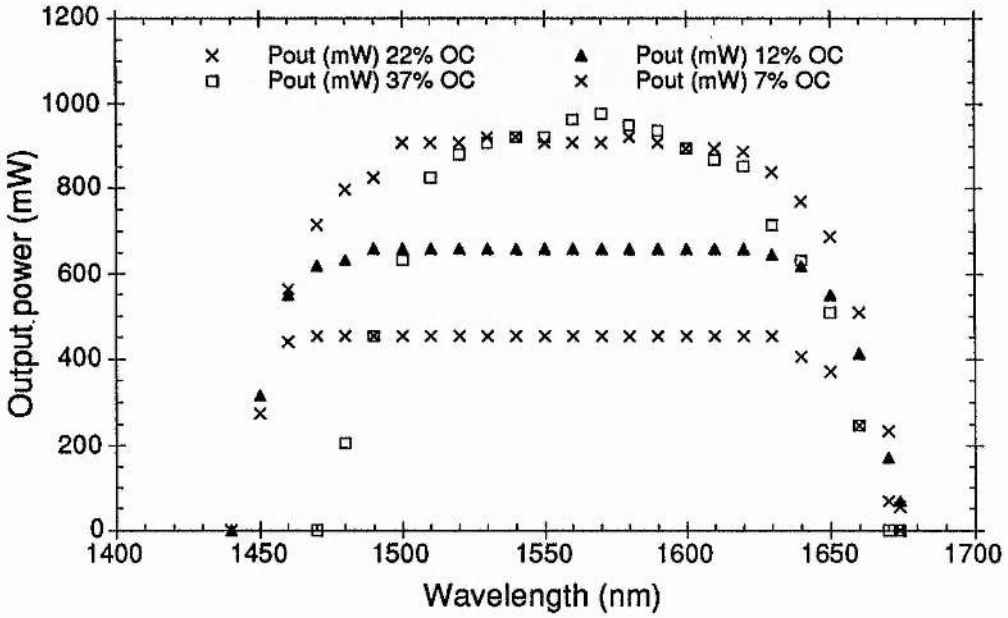

Figure 2.6. Tuning range of the synchronously mode locked laser. The dielectric mirror coatings prevented tuning above 1680 nm.

Figure 2.7 shows an autocorrelation and a spectrum of the optimum pulses obtained from the synchronously mode locked NaCl:OH⁻ laser. The pulse duration was 7.9 ps (Gaussian pulseshape assumed) and the bandwidth of the laser pulses was 0.19 nm which results in a duration-bandwidth product of 0.19. This value is much lower than the transform-limited, duration-bandwidth product of 0.44 for a Gaussian pulse and indicates that the pulse profile may be strongly asymmetric. The optimum pulse duration was measured to be essentially constant for all the output couplers and did not vary significantly across the tuning range. This indicates that the pulse duration was limited by the bandwidth of the 6.6 mm birefringent plate.

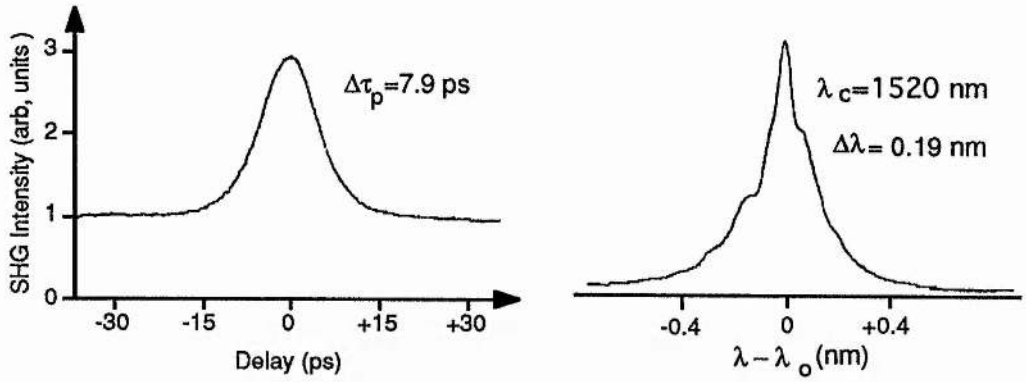

Figure 2.7. Autocorrelation and associated spectrum for the optimum pulses from the synchronously mode-locked laser.

The autocorrelations and spectra of the laser output were monitored as a function of cavity length detuning from the optimum cavity length for mode locking and are displayed as Figure 2.8. For negative detuning (*i.e.* a reduction in cavity length) the pulse duration decreased but satellite pulses were formed and a modulation appeared on the pulse spectrum. The separation between the pulses decreased with increasing cavity detuning. An autocorrelation and a spectrum of the laser output for a detuning of -60 μm are presented in Figure 2.8(a). The modulation on the spectrum arose from the double pulsing of the laser since the carrier frequency of the two pulses was the same. The period of the spectral modulation $\Delta\lambda$ is related to the temporal separation of the pulses $\Delta\tau$ by

$$\Delta\tau = \frac{\lambda^2}{c\Delta\lambda} \tag{2.2}$$

For the spectrum illustrated in Figure 2.8(a), the centre wavelength was 1520 nm and the period of the modulation was 0.236 nm which gives a temporal pulse separation of 33 ps. This is identical to the separation measured from the autocorrelation.

For positive detuning, Figure 2.8(b), the colour-centre produced noise bursts, indicated by the coherence spike on the autocorrelation. At a detuning of +60 μm, the duration of the noise burst was 15 ps and the coherence spike duration was 4.75 ps. The spectral bandwidth of the pulses increased to 1.1 nm to accommodate the coherence spike.

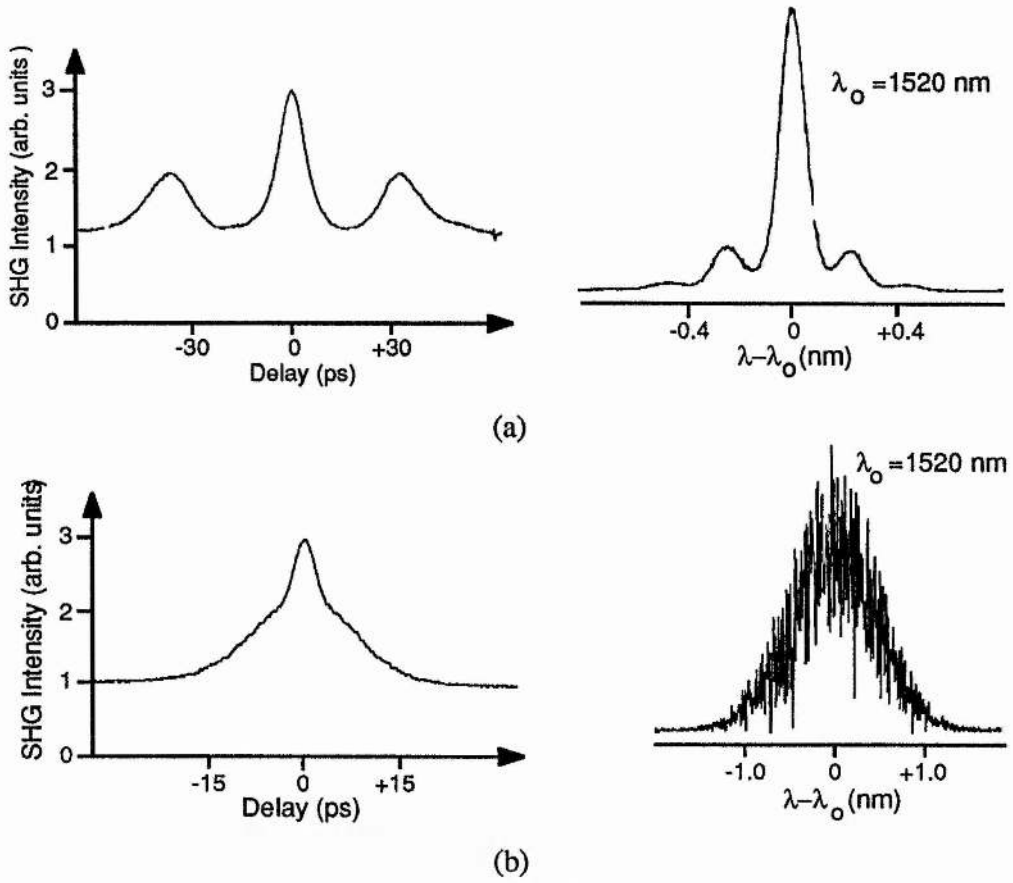

Figure 2.8. Detuning characteristics of the synchronously-pumped laser for: (a) a detuning of -60μm and (b) a detuning of +60 μm.

These detuning characteristics together with the large increase in output power when the correct cavity length for mode locking is achieved are very similar to the operating characteristics of synchronously mode-locked dye lasers[6]. The laser output may be qualitatively explained by considering the evolution of the gain in the vicinity of the pump laser pulse as shown in Figure 2.9.

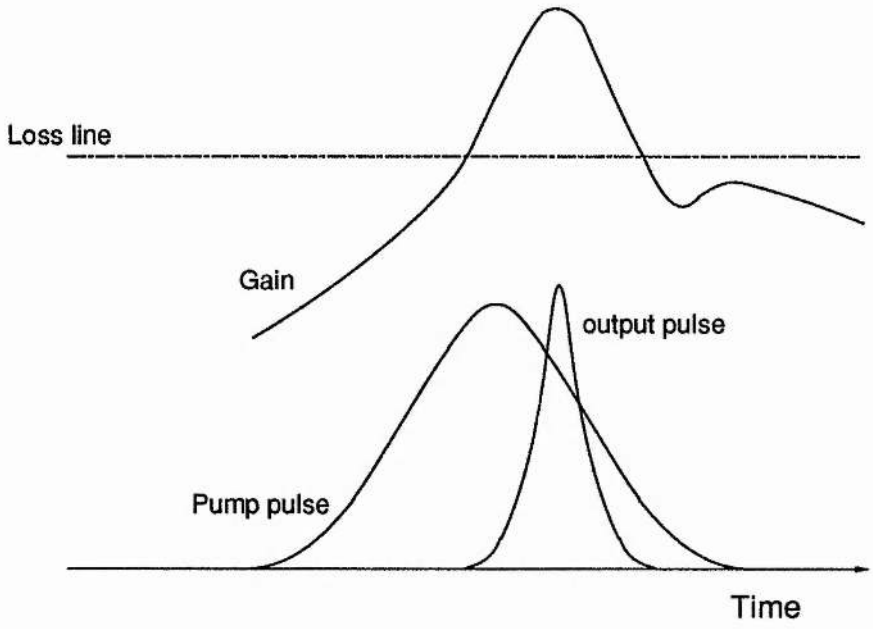

Figure 2.9. Schematic showing the evolution of the laser gain in the vicinity of the pump pulse.

The horizontal line in the figure represents the loss line of the laser cavity. Above this line there is net round-trip gain and laser oscillation can occur. During the pump pulse the gain rises and crosses the loss line. In the absence of the colour-centre laser pulse, the gain would continue to rise until the end of the pump pulse and would then slowly decrease due to spontaneous emission. However, in the presence of the mode-locked colour-centre laser pulses, the gain crosses the loss line and is then reduced due to stimulated emission. The energy of the colour-centre laser pulse saturates the gain, causing it to drop below the loss line and terminates the pulse. If the pump pulse is still present, the gain will begin to rise again. Thus, there are two pulse shortening mechanisms involved in the generation of the mode-locked pulses; the rising edge of the gain shapes the leading edge of the pulse, whereas gain saturation shapes its trailing edge.

In the steady state, the pulse repetition frequency of the mode-locked colour-centre laser must be the same as that of the pump laser. Cavity length detuning therefore changes the timing of the colour-centre laser pulse with respect to the pump pulse. If the cavity is negatively detuned, the synchronously mode-locked pulse is advanced towards the point where the gain crosses threshold. This shortens the leading edge of the pulse but reduces the overall gain seen by the pulse, resulting in a decrease in the output power. If a significant portion of the pump pulse remains after the transit of the colour-centre laser pulse, the gain will rise and cross the loss line, again resulting in the formation of satellite pulses. Positive cavity length detuning pushes the centre of the colour-centre pulse towards the trailing edge of the pump

pulse, preventing the formation of satellite pulses but increasing the pulse duration. Further lengthening of the cavity prevents complete mode locking causing the laser to produce noise bursts.

2.4 Acousto-optic mode locking

The NaCl:OH⁻ laser was acousto-optically mode locked by reconfiguring the Nd:YAG laser to cw operation and replacing the fused silica prism in the colour-centre laser with a Spectra-Physics Model 342 mode locker. The mode locker consists of a Brewster-angled prism onto which a radio-frequency (RF) transducer is bonded. This prism possessed ultrasonic resonances separated by 400 kHz and the transducer was designed to resonate at frequencies around 41 MHz, corresponding to a mode-locked pulse repetition frequency of 82 MHz and a cavity length of 1.83 m. The mode locker was driven by a Marconi model 2019 frequency synthesiser whose output was amplified to between 1 and 2 watts using a type CA 2832 broadband amplifier. A voltage standing-wave-ratio (SWR) meter was inserted between the mode locker and the amplifier so that the frequency of the RF drive signal could be matched to the mode-locker resonances. The lowest SWR value that could be achieved with this mode locker and synthesiser was 1.5. For acousto-optic mode lockers it is necessary to approach the mode-locker resonance from its low-frequency side. As the frequency of the RF signal is increased towards resonance, more power is coupled into the transducer. This heats the prism causing an increase in its resonant frequency which may be followed by increasing the drive frequency. If the drive frequency is increased above the resonant frequency of the mode locker , the power coupled into the device is reduced and the prism cools, decreasing its resonant frequency. This results in a further reduction of the power coupled into the mode locker causing more cooling and thermal runaway. The modulation depth of the mode locker was measured to be approximately 15% at a wavelength of 1550 nm for 2 W of incident RF power.

The optimum pulse duration and cavity length detuning were measured as a function of the laser output power for 22%, 12% and 7% output couplings and are displayed in Figure 2.10. Measurements of the pulse duration were obtained using an InGaAs PIN photodiode having a 3 dB bandwidth of 9.5 GHz and a Tektronix sampling oscilloscope. The resolution of the photodiode/sampler combination was approximately 50 ps. The cavity length detuning was measured with respect to the optimum cavity length for mode-locked operation at 30 mW output power.

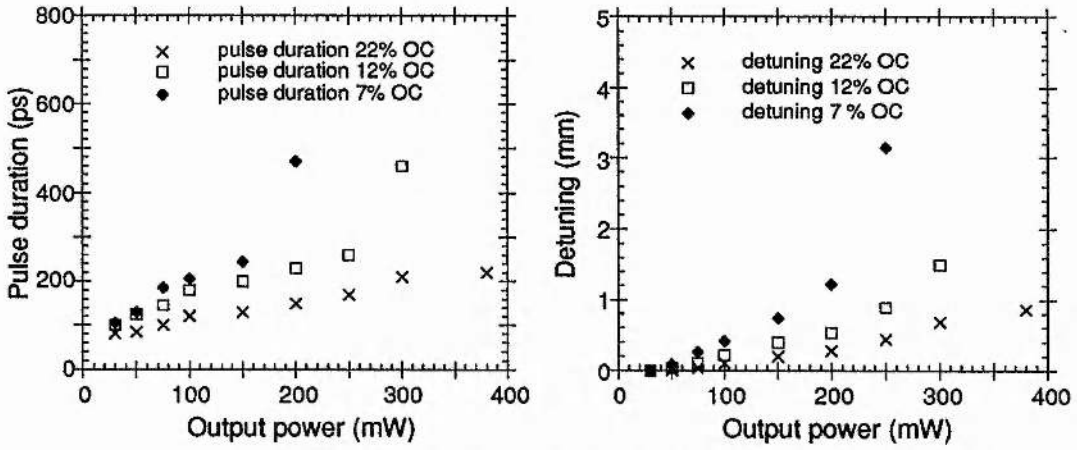

Figure 2.10. Variation of the minimum pulse duration (left) and optimum detuning (right) with output power for the acousto-optically mode locked laser.

From the data displayed in Figure 2.10, it can be seen that the pulse durations obtained from the acousto-optically mode-locked laser were significantly longer than those obtained by synchronous mode locking. This is a result of the large gain window and the relatively low modulation depth provided by the acousto-optic modulator. As the pump power was increased, it was necessary to lengthen the colour-centre laser cavity to avoid the formation of satellite pulses resulting from gain recovery. This retarded the colour-centre pulse with respect to the applied modulation, reducing the shaping on the leading edge of the pulse and increasing its duration.

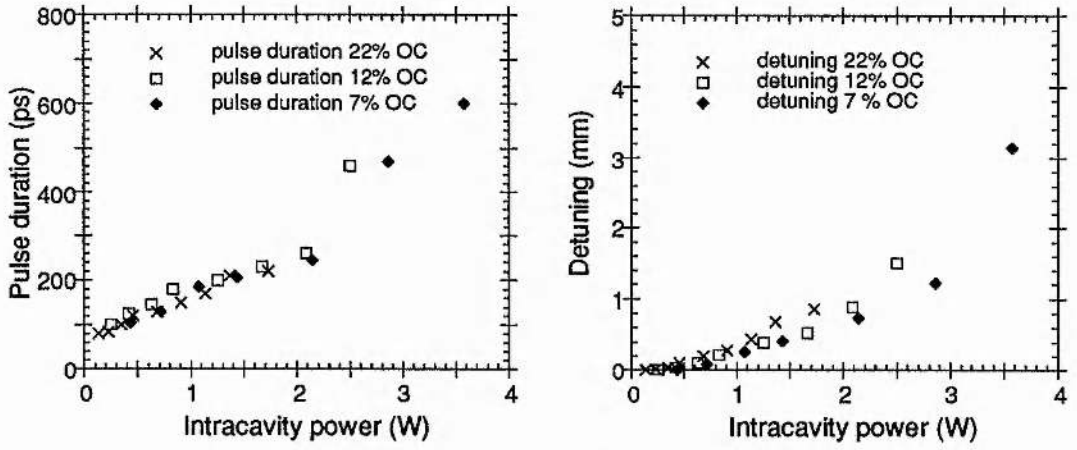

Figure 2.11. Variation of the minimum pulse duration (left) and optimum detuning (right) with intracavity power for the acousto-optically mode locked laser.

Figure 2.11 shows the data presented in Figure 2.10 replotted against the calculated intracavity power. It is obvious from these graphs that the mode-locked pulse duration and cavity length detuning varies with the intracavity pulse energy.

Therefore, to obtain the shortest pulses it is necessary to reduce the pulse energy by operating the laser close to its threshold. Also, to achieve a useful output power, a large output coupling should be used. This behaviour is again consistent with that of mode-locked dye lasers.

2.5 Solitonic pulse compression of the NaCl:OH⁻ laser pulses.

If pulses are propagated down a standard telecommunications optical fibre at wavelengths greater than 1.32 μm they will experience both a positive frequency chirp, due to self-phase modulation, and anomalous group-velocity dispersion. In this dispersion regime, the optical fibre will support bright solitons. For high input peak powers, the pulse will propagate as a higher-order soliton. These solitons are not spectrally and temporally invariant, but instead follow a periodic evolution as they propagate along the fibre. Figure 2.12 shows the calculated temporal evolution of an N = 4 soliton over 3 periods (after Ref 7). It is apparent that the pulse undergoes a narrowing at the beginning of each period. This is a general feature of all higher order solitons, the pulse shortening increasing for greater soliton numbers. By selecting an optical fibre so that its length corresponds to maximum pulse narrowing, for the given input pulse parameters, a simple pulse compressor can be constructed. This was first demonstrated by Mollenauer *et al.*[8] who compressed pulses of 7 ps duration from a synchronously mode-locked colour-centre laser to 260 fs. Subsequently compression factors of 110 have been demonstrated[9].

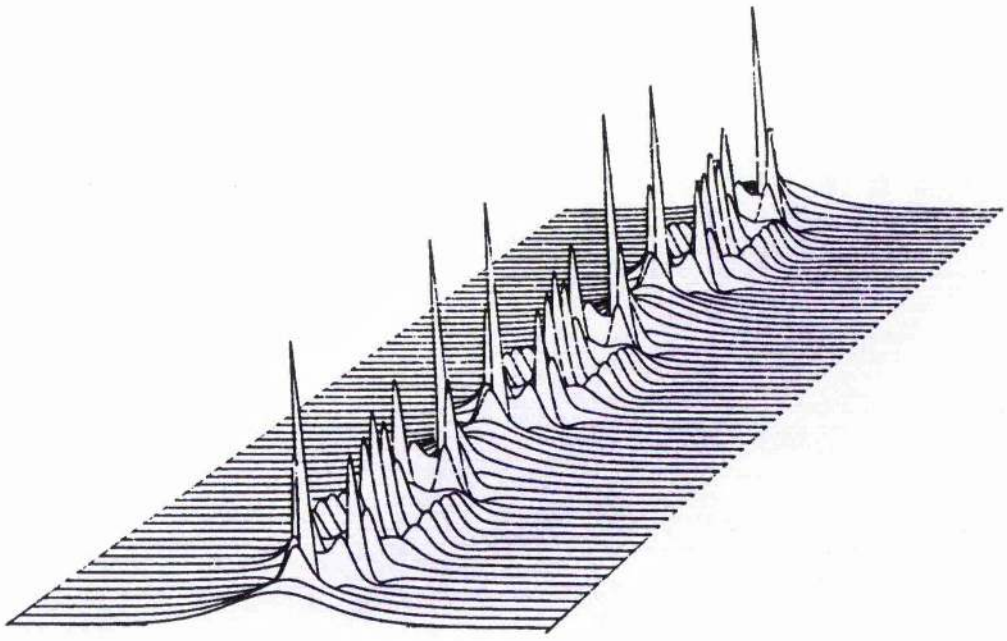

Figure 2.12. Temporal evolution of a N = 4 soliton over three soliton periods (adapted from Reference 7.).

To predict the output pulse duration and the required fibre length for a solitonic pulse compressor, it is necessary to solve the nonlinear Schroedinger equation. However, Dianov *et al.*[10] have shown that, for 10th order solitons and greater, the compression factor, F_c, and optimum fibre length, z_{opt} can be predicted by

$$F_c = 4.1N \tag{2.3}$$

$$z_{opt} = \left(\frac{0.32}{N} + \frac{1.1}{N^2}\right) z_o \tag{2.4}$$

where N is the soliton number and z_o is the soliton period. Although solitons only exist for integer values of N, the equation is valid for noninteger N.

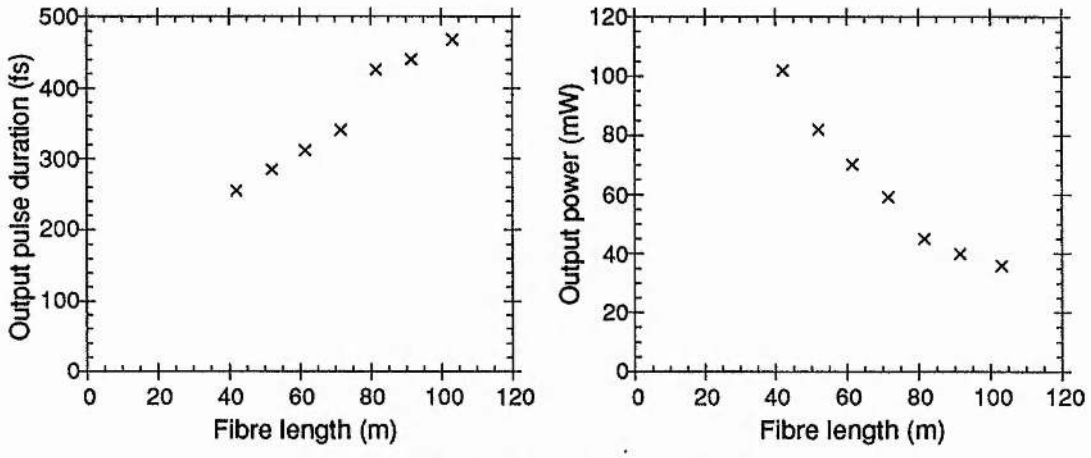

Figure 2.13. Variation of output pulse duration and power with fibre length for a soliton pulse compressor.

Pulses of 7.8 ps duration from the synchronously mode-locked NaCl:OH^- laser were coupled into various lengths of standard telecommunications optical fibre. The fibre nonlinearity was assumed to be $\gamma = 2\ W^{-1}km^{-1}$ and its group-velocity dispersion was estimated to be $\beta_2 = 20\ ps^2km^{-1}$. For the input pulse duration of 7.8 ps the soliton period was calculated to be 1540 m. The autocorrelations and spectra of the compressed pulses from the fibre were monitored and the input power was adjusted, using a neutral density attenuator wheel, to achieve maximum compression for each fibre length. Graphs of the output pulse duration and average output power are presented as Figure 2.13 . From the measured output powers, the soliton number, N, was calculated for each fibre length and substituted into equations 2.3 and 2.4 to obtain theoretical compression factors and optimum fibre lengths. Figure 2.14 displays graphs of the soliton number versus the reciprocal compression factor and the optimum fibre length normalised to the soliton period. The crosses indicate

experimentally obtained data whereas the solid lines show the values obtained from theory. The predicted compression factors are consistently a factor of 2.5 greater than the experimentally observed values and the optimum fibre length was calculated to be significantly less than those used in the experiment.

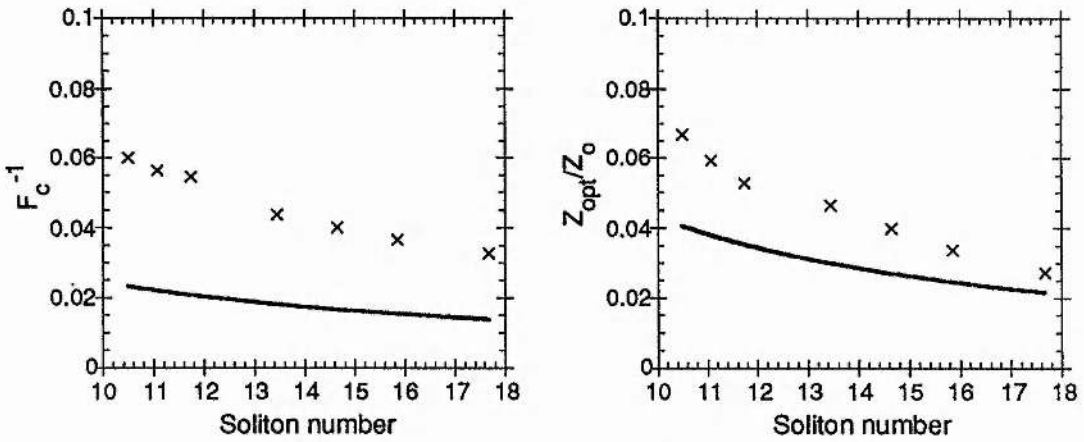

Figure 2.14. Dependence of the pulse compression factor and ratio of the fibre length to the soliton period as a function of the soliton number. Crosses represent experimental data and solid lines theory.

A typical autocorrelation and spectrum of the output from the soliton effect compressor is shown in Figure 2.15. In this case the pulses were compressed from 7.8 ps to 400 fs in an 85 m length of fibre. It is evident from the autocorrelation that only a portion of the input pulse is compressed. A significant fraction of the pulse remains uncompressed and appears as a broad background pedestal. This is an inherent feature of soliton effect compressors; the fraction of the input pulse which is compressed decreases monotonically with soliton number and hence compression factor. During the initial pulse narrowing phase of the soliton period, the evolution of the pulse is dominated by self-phase modulation. The self-phase modulation is linear only over the central region of the pulse and therefore it is only this region of the pulse that is compressed by the anomalous group-velocity dispersion. It is possible to partially suppress the pedestal by utilising the effect of nonlinear birefringence in a polarisation-maintaining fibre and polarising optics[8,11,12]. If both polarisation states of the optical fibre are excited unequally, the birefringence of the optical fibre becomes intensity dependent since each axis experiences a different refractive index change due to self-phase modulation. The output state of polarisation from the fibre compressor is therefore intensity dependent and the intense, compressed pulse can be separated from the low intensity pedestal using a polariser. In the remainder of this Chapter, a means of completely eliminating the pedestal using the nonlinear transmission properties of a fibre-loop mirror is described.

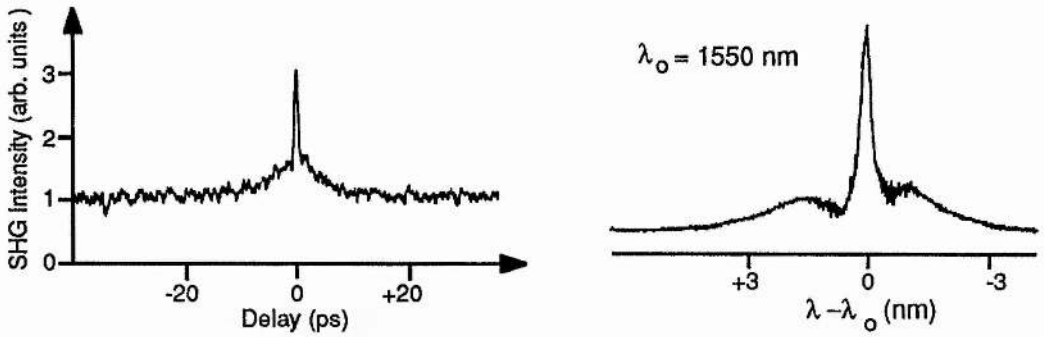

Figure 3.15. Typical output autocorrelation and spectrum from a soliton effect pulse compressor.

2.6 · Compression of the NaCl:OH⁻ laser pulses using a nonlinear loop-mirror

2.6.1 The optical fibre loop mirror.

A fibre-loop mirror[13] consists of a directional coupler with the output ports spliced together. A schematic of the device is shown in Figure 2.16. The device is a Sagnac interferometer: The light is input at port 1 and is split by the directional coupler. The cross-coupled light into port 3 experiences a $\pi/2$ radians phase lag with respect to the straight through light . The two waves traverse the loop and interfere at the directional coupler. In the absence of birefringence and external influences, such as magnetic fields or rotation, both propagating waves travel exactly the same optical path length and arrive at the coupler with a relative phase delay of $\pi/2$ radians. The output intensity from port 4 of the device is given by

$$I_{out} = I_{in}[1-4\alpha(1-\alpha)] \tag{2.5}$$

where α is the power splitting ratio of the coupler, and I_{in} and I_{out} are the input and output intensities respectively. The light which is not transmitted at the output port is reflected down the input fibre. By inspection of equation 2.5, it can be seen that for a coupling coefficient of 0.5, zero power is transmitted by the loop and the fibre loop acts as a 100% reflector. In practice, coupler loss and fibre loss may slightly affect the reflectivity of the loop mirror.

Birefringence may strongly affect the reflectivity of the device. For example, the inclusion of a half-wave plate in the loop can induce a further π radians phase shift between the counter propagating fields which will result in a reflection maximum where there was previously a minimum and vice versa. Thus a 100% reflecting mirror ($\alpha = 0.5$) would become fully transmitting.

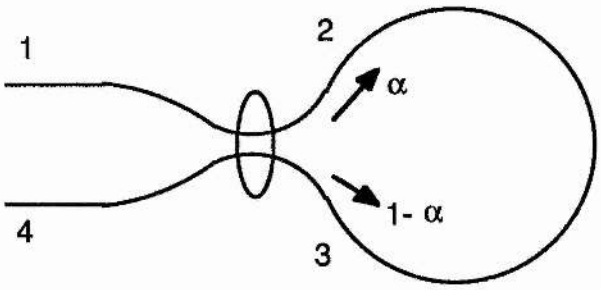

Figure 2.16. Schematic of a fibre loop mirror.

2.6.2 Nonlinear loop mirrors

At high input intensities, the light within the fibre loop will accumulate an additional phase shift due to the nonlinear effect of self-phase modulation. The additional phase difference between the counter-propagating fields is

$$\Delta\Phi = \frac{2\pi n_2 I_{in}}{\lambda} L(1-2\alpha) \tag{2.6}$$

Where λ is the wavelength, L is the fibre loop length and n_2 is the Kerr coefficient for the optical fibre. This phase shift will result in the loop mirror having an intensity-dependent transmission. The potential for the nonlinear loop mirror for pulse shaping and switching was first discussed theoretically by Doran and Wood[14] and subsequently, experiments were reported by Blow *et al.*[15] and Smith *et al.*[16]. The modified transmission of the device is given by[15]

$$\frac{I_{out}}{I_{in}} = 1-2\alpha(1-\alpha)[1+\cos(\Delta\Phi)] \tag{2.7}$$

From this equation it can be seen that when $\Delta\Phi$ is an odd multiple of π radians, 100% of the input field is transmited by the loop mirror. Also, for loop mirrors utilising 50/50 couplers ($\alpha = 0.5$) the SPM induced phase shift is identical for the two propagating fields and has therefore no effect on the transmission of the device. Therefore, to obtain a nonlinear response from the loop mirror it is necessary to break the symmetry of the device. This can be realised in two ways:

1. By using a coupler with $\alpha \neq 0.5$ the two propagating fields have different intensities and therefore accumulate different phase shifts. Figure 2.17 shows a graph of the transmission versus the product of the input power and loop length for coupling coefficients of α = 0.4, 0.3, and 0.2. The maximum transmission is unity for each coupling coefficient and the minimum transmission for the devices can be obtained

from equation 2.5. From this equation, it is apparent that the minimum transmission approaches zero as α approaches 0.5. Thus to construct a high contrast switch, it is necessary to use a coupler with α close to 0.5. However, high powers would be required to obtain the π radians phase difference between the two waves to obtain full switching.

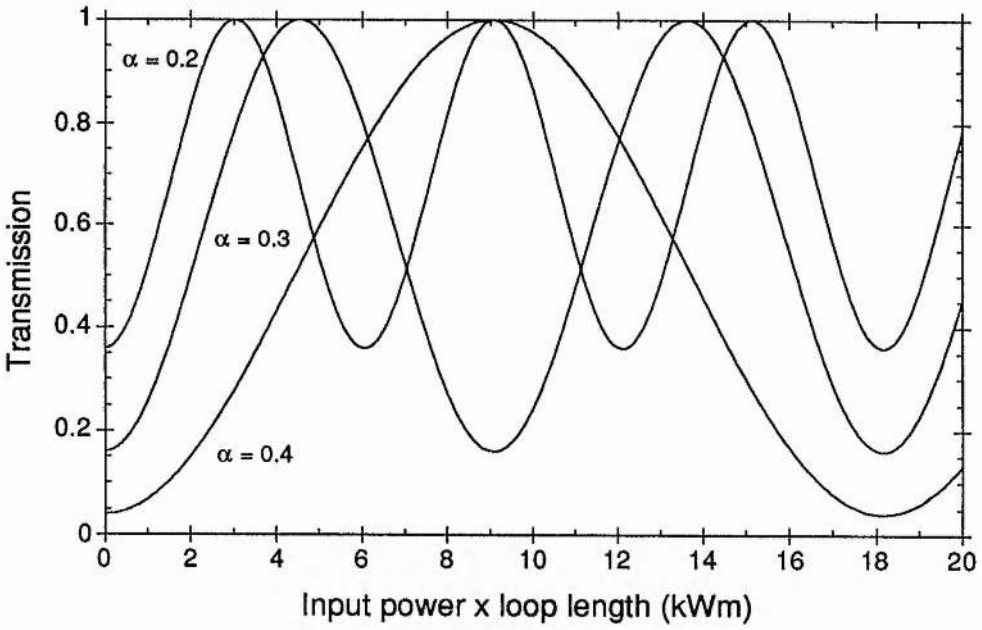

Figure 2.17. Transmission of a nonlinear loop mirror for various coupling coefficients.

2. By adding a discrete loss or gain asymmetrically within the loop. One example is the nonlinear-amplifying loop mirror,[17] where an amplifier of gain G is placed close to port 2 of the loop mirror shown in Figure 18. The clockwise propagating field is first amplified and then traverses the loop sustaining appreciable SPM, whereas the field propagating in the opposite direction traverses the majority of loop at low intensity, accumulating minimal self-phase modulation and is then amplified immediately before re-entering the directional coupler. For this device the SPM induced relative phase difference is

$$\Delta\Phi = \frac{2\pi n_2 I_{in}}{\lambda} L[\alpha(G+1)-1] \tag{2.8}$$

From this equation it can be seen that a non-zero relative phase difference can be achieved for $\alpha = 0.5$, and hence switching at full contrast can be realised.

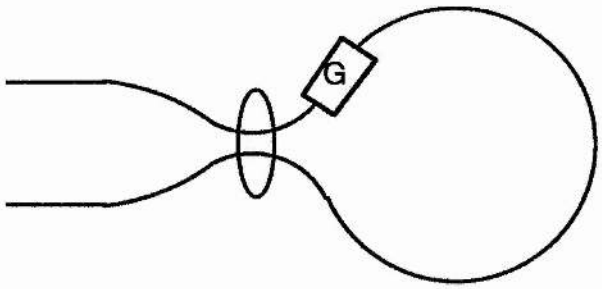

Figure 2.17. Schematic of a nonlinear amplifying loop mirror.

In the preceding analyses, the loop response for cw light was considered. For pulses, the transmission of the loop is more complicated since group-velocity dispersion will distort the pulse shape as it propagates round the loop. However if the dispersion length of the fibre is much less than its nonlinear length, dispersive effects may be ignored and the pulse transmission can be obtained by dividing the pulse into many cw segments and applying equation 2.7 to each one. A computer program was written to model the pulse shaping behaviour of the nonlinear loop mirror. Group-velocity dispersion was not included in the model.

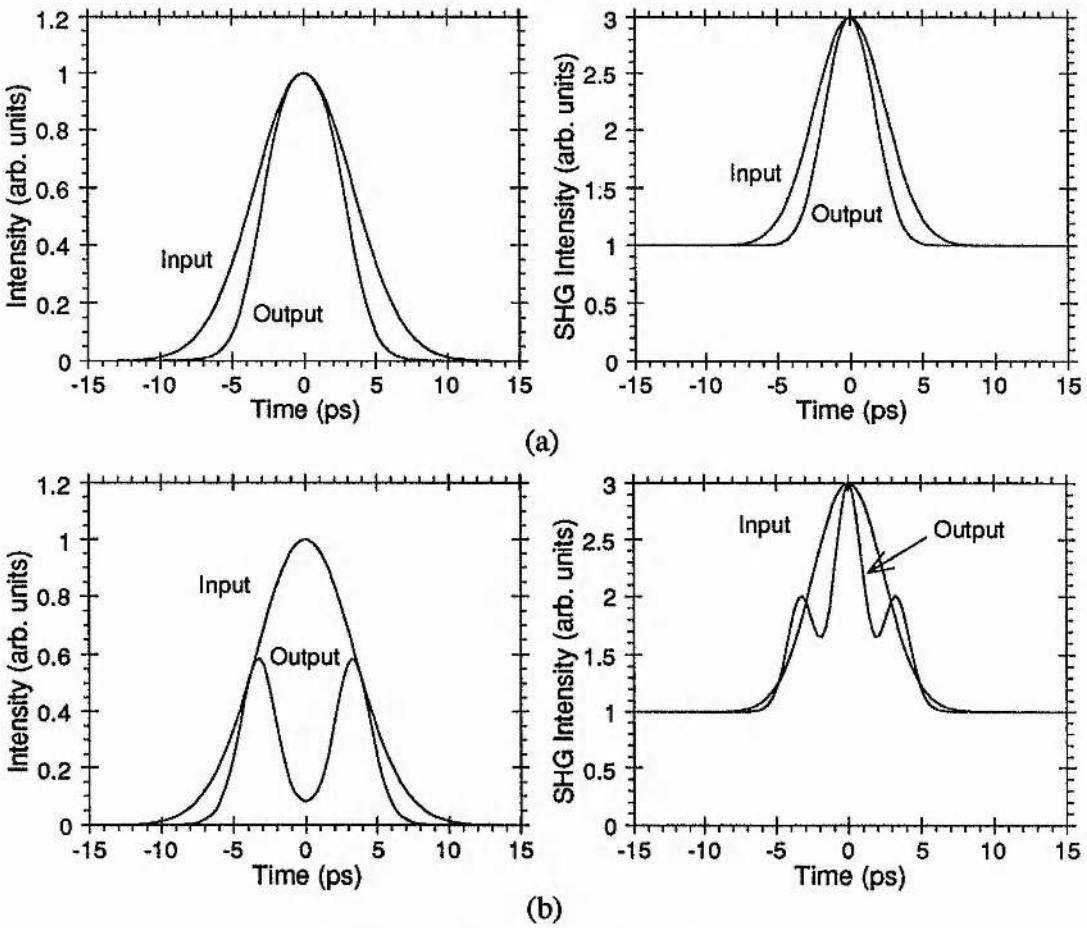

Figure 2.19. Calculated output pulse profiles (left) and autocorrelations(right) for 8 ps duration pulses having (a) 800 pJ and (b) 1500 pJ energies coupled into a nonlinear loop mirror.

Figure 2.19 shows the calculated intensity profiles (left) and autocorrelations (right) of 1.55 μm wavelength pulses coupled into a 100 m long loop mirror. The mode field area of the fibre was 75 μm^2 and the coupling coefficient was 0.4. Figure 2.19(a) shows the transmission of 8 ps duration pulses having an energy of 800 pJ. The intensity at the centre of the pulse corresponds to full transmission by the loop whereas the wings of the pulse, having a lower intensity, are only partially transmitted by the device. Increasing the peak intensity past the maximum transmission of the loop mirror results in pulse break-up. This is illustrated in Figure 2.19(b), where the input pulse energy is 1500 pJ. Clearly this device could be used to remove the pedestal component from the output of a soliton effect compressor. This is further illustrated in Figure 2.20, which shows the transmission of the same 800 pJ pulse as presented in Figure 2.19(a) but with a 5% peak-to-peak noise component included. This noise, which caused a clear increase in the background level of the autocorrelation, is almost completely removed by the nonlinear loop mirror.

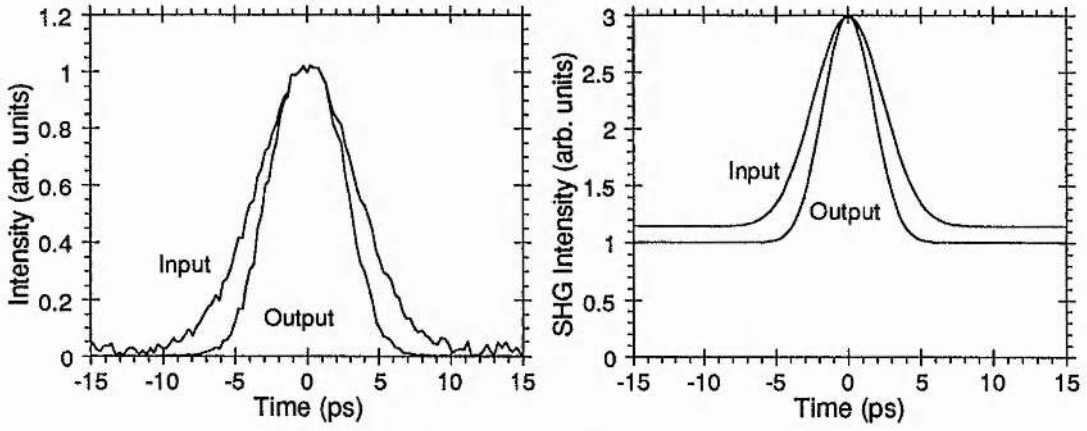

Figure 2.20. Calculated input and output pulse profiles and autocorrelations for an 8 ps duration, 800 pJ pulse having a 5% noise component after propagation through a nonlinear loop mirror.

An integrated pulse compressor with pedestal suppression was fabricated from a nonlinear fibre loop mirror. The device was fabricated from anomalously dispersive fibre so that the pulses were compressed by solitonic effects as they traversed the loop and the nonlinear transmission of the device was used to separate the pedestal from the compressed pulse.

2.6.3 Experiment

The experimental arrangement is illustrated in Figure 2.21. Synchronously mode-locked pulses from the NaCl:OH⁻ laser were coupled into a fibre loop mirror using a X 10 microscope objective. The loop mirror was constructed from standard optical fibre having zero group-velocity dispersion at 1.32 μm. The fused fibre

coupler had a splitting ratio of 0.61:0.31 and the loop was formed by joining the two output ports of the coupler using a temporary fibre splice. For this coupler, the calculated minimum device transmission was 4.8%. A 50/50 beamsplitter was placed before the input fibre to allow access to the light reflected by the loop mirror. The reflection from the front of the beamsplitter (shown by a dotted line) also enabled the input pulse train to be monitored. It was necessary to include an optical isolator (OFR 10-4-IR) between the colour-centre laser and the loop mirror to prevent the light reflected by the loop mirror from being fed back into the laser and interrupting the synchronous mode locking. The transmitted and reflected light was monitored using an autocorrelator and a scanning Fabry-Perot interferometer.

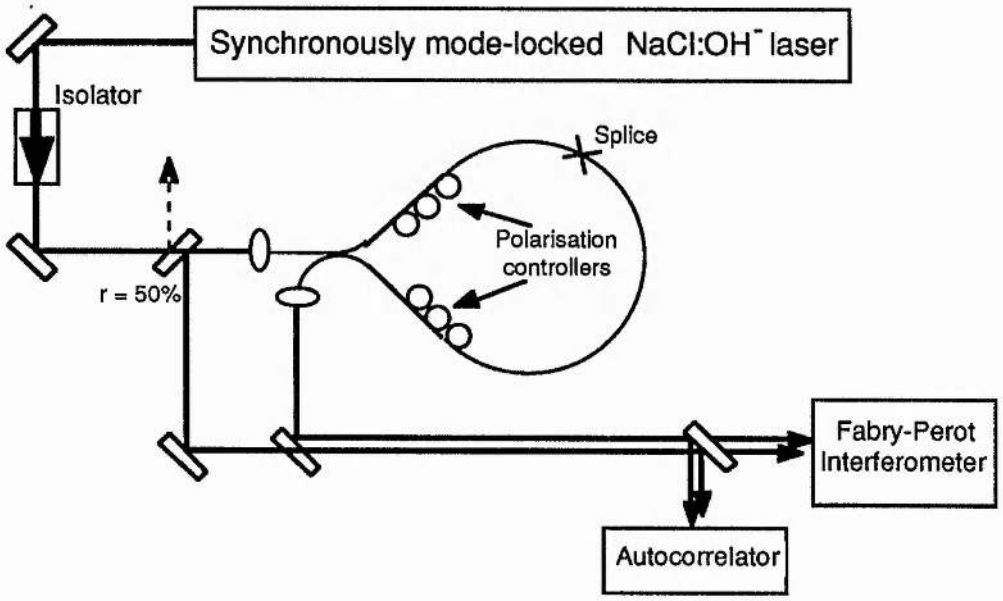

Figure 2.21. Schematic of the experimental arrangement used to observe pulse compression in a nonlinear loop mirror.

Pulses of 7.8ps duration at a centre wavelength of 1560 nm were coupled into the loop mirror and the autocorrelation of the compressed pulse transmitted by the loop was monitored. Polarisation controllers, located within the loop, were adjusted to obtain maximum transmission of the pedestal component whilst minimising the transmission of the uncompressed pulse. Measurements of the compressed pulse duration and average output power of the device were performed for various loop lengths and are presented in Figure 2.22.

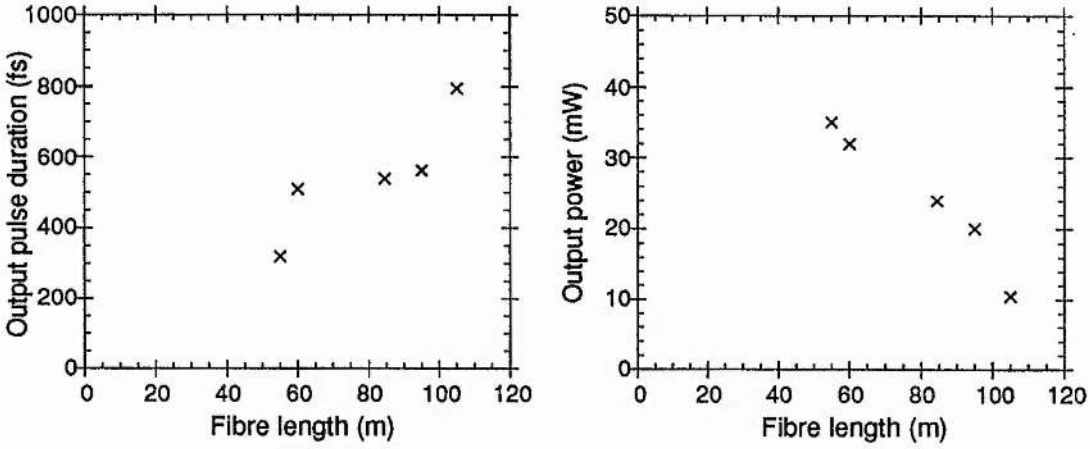

Figure 2.22. Output pulse duration and power as a function of loop length for the nonlinear loop mirror.

Figure 2.23 shows transmitted (top) and reflected (bottom) autocorrelations and spectra obtained using an 84 m long loop mirror. The intensity-dependent transmission of the device is clearly evident.

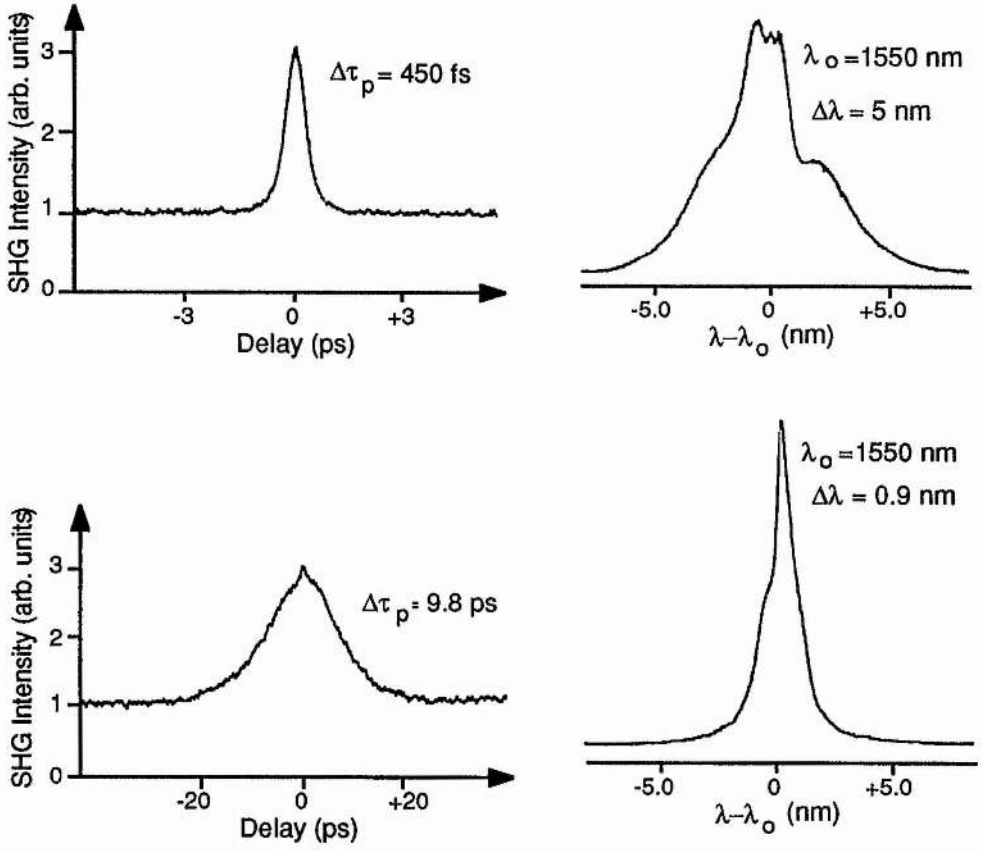

Figure 2.23. Transmitted (top) and reflected (bottom) autocorrelations and spectra for the nonlinear loop mirror pulse compressor.

The pulses had a duration of 450 fs and a bandwidth of 5 nm yielding a duration-bandwidth product of 0.28; whereas the reflected pulses were 9.8 ps in duration with a bandwidth of 0.9 nm giving a duration-bandwidth product of 1.1. For these results, the measured transmitted average power was 24 mW and the reflected power was 44 mW. By adjusting the polarisation controllers, the switching characteristic of the device could be reversed, that is, the compressed pulse was reflected and the pedestal was transmitted by the loop mirror.

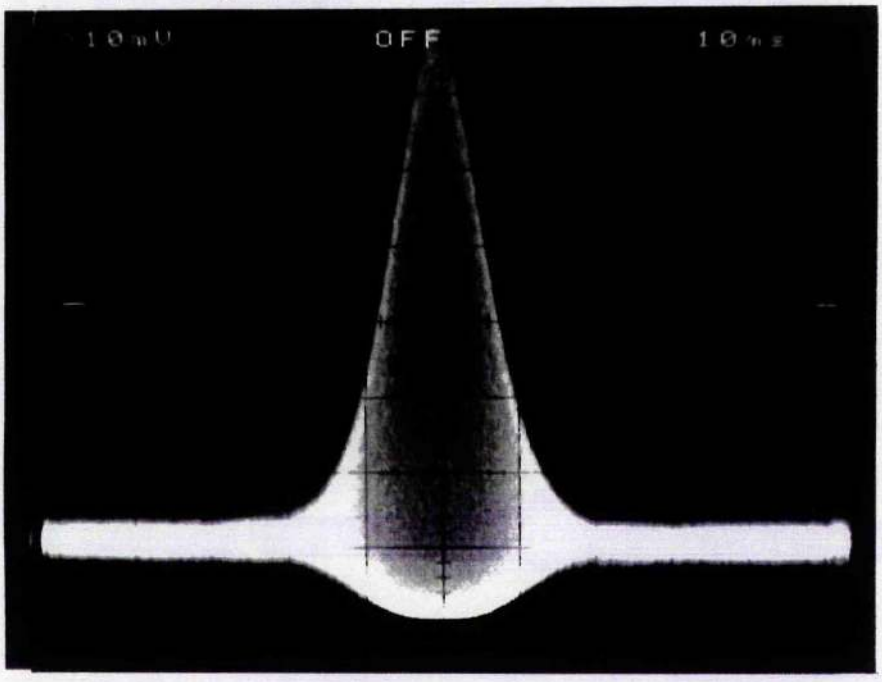

Figure 2.24. Interferometric autocorrelation of the output from the nonlinear fibre-loop mirror

Careful examination of the transmitted pulse showed no indication of any pedestal component. This was further verified by examination of the interferometric autocorrelation shown in Figure 2.24 which has an enhanced contrast ratio. A simple autocorrelation program was written to ascertain the minimum pedestal level detectable. Figure 2.25 shows both the computed intensity profiles (left) and background-free autocorrelations of 450 fs duration pulses superimposed upon broad 9.8 ps duration pedestals. The fraction of the total energy in the pedestals is 20%, 10% and 0%. Interestingly, the contrast between the short pulse and the pedestal is increased for the autocorrelation. This occurs because the short pulse performs a cross-correlation with the broad pulse. In the computed autocorrelation, the 10% pedestal is clearly distinguishable indicating that any pedestal component in the experimental results must contain less than 10% of the total pulse energy. Furthermore, any transmitted pedestal components could be further suppressed by using nonlinear birefringence in the output fibre.

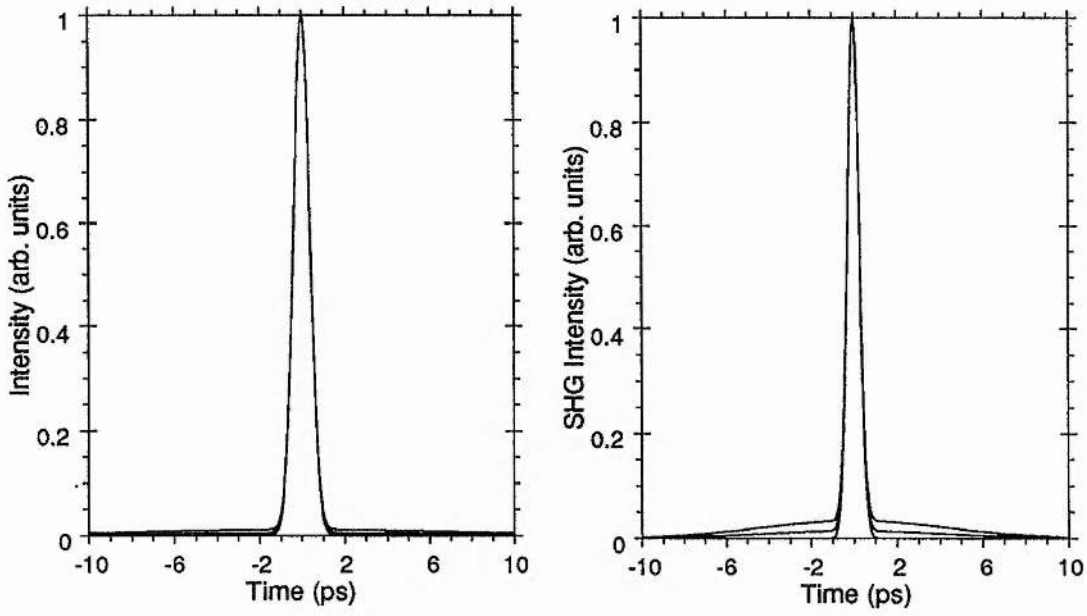

Figure 2.25. Calculated pulse profiles and their corresponding autocorrelations for 480 fs duration pulses superimposed on a 9.8 ps duration pulse possessing 10% and 20% of the total pulse energy. Note the increased visibility of the pedestal for the autocorrelations.

2.7 Summary

Synchronous mode locking of the NaCl:OH⁻ colour-centre laser has been investigated. This laser produced pulses of 8 ps duration at average output powers in excess of 1 W and was tunable from 1470 nm to 1660 nm. The cavity length detuning characteristics of the laser were studied and were found to be qualitatively similar to those observed for synchronously mode locked dye lasers. The laser was also mode locked using acousto-optic loss modulation and the performance of the laser was found to be inferior to the synchronously mode-locked laser. The shortest pulses obtained were 80 ps at an average output power of 30 mW, which rose to 210 ps for 300 mW of output power.

The pulses from the synchronously mode locked laser were compressed to less than 300 fs duration using a soliton-effect compressor. Using this scheme, only a small fraction of the mode-locked pulse (30%) was compressed, the remainder of the pulse featured as a broad background pedestal. A pulse compressor was formed from a nonlinear fibre-loop mirror. Solitonic compression occurred in the anomalously dispersive fibre loop while the nonlinear transmission of the loop mirror was used to separate the compressed pulse from the background pedestal. By comparing the output from the device to a computer model, the transmitted pedestal component was estimated to contain less than 5% of the total pulse energy.

References

1. J. F. Pinto, E. Georgiou and C. R. Pollock, Opt. Lett. **11,** 519 (1986).
2. K. R. German and C. R. Pollock, Opt. Lett. **12,** 474 (1986).
3. T. Kurobori, A. Nebel, R Beigang and H. Welling, Opt. Commun. **73,** 365 (1989).
4. R. S. Grant, PhD thesis, University of St. Andrews 1991.
5. H. W. Kogelnik, E. P. Ippen, A. Dienes and C. V. Shank, IEEE J. Quantum Electron. **QE-8,** 373 (1972).
6. C. P. Ausschnitt, R. K. Jain and J. P. Heritage, IEEE J. Quantum Electron. **QE-15,** 912 (1979).
7. K. J. Blow and N. J. Doran, IEE Proc. J, **134,** 138 (1987).
8. L. F. Mollenauer, R. H. Stolen, J. P. Gordon and W. J. Tomlinson, Opt. Lett. **8,** 289 (1983).
9. E. M. Dianov, A. Ya Karasik, P. V. Mamyshev, G. I. Onischukov, A. M. Prokhorov, M. F. Stel'makh and A. Fomichev, JETP Lett. **40,** 903 (1984).
10. E. M. Dianov, Z. S. Nikonova, A. M. Prokhorov and V. N. Serkin, Sov. Tech. Phys. Lett. **12,** 311 (1986).
11. R. H. Stolen, J. Botineau and A. Ashkin, Opt. Lett. **7,** 512 (1982).
12. B. Nikolaus, D. Grischowsky and A. Balant, Opt. Lett. **8,** 189 (1983).
13. D. B. Mortimore, J. Lightwave Tech. **6,** 1217 (1988).
14. N. J. Doran and D. Wood, Opt. Lett. **13,** 56 (1988).
15. K. J. Blow, N. J. Doran and B. K. Nayar, Opt. Lett. **14,** 754 (1989).
16. K. Smith, N. J. Doran and P. Wigley, Opt. Lett. **15,** 1294 (1990).
17. D. J. Richardson, R. I. Laming and D. N. Payne, Electron. Lett. **26,** 1779 (1990).

Chapter 3

The Coupled-Cavity Mode-Locked NaCl:OH^- Colour-Centre Laser

3.1 Introduction

In the previous chapter a method of producing sub-picosecond pulses from the synchronously mode-locked NaCl:OH^- laser using extracavity pulse compression was discussed. Although this proved to be a convenient means of generating ultrashort pulses, it is inefficient because only a fraction of each laser pulse is compressed. In this Chapter, results for a coupled-cavity mode-locked NaCl:OH^- laser are presented. This is a general passive mode-locking scheme. It is not wavelength specific and it is therefore particularly useful for lasers where saturable absorbers are either not convenient or available. Until the recent advent of self-mode locking, coupled-cavity techniques were widely used to generate ultrashort pulses from most near-infrared laser sources.

The chapter begins with a brief review of coupled cavity mode-locking. The construction of the laser is outlined and its performance when mode locked is described in detail. An amplitude modulation was observed on the output from the laser. A method of eliminating the modulation by adopting an alternative cavity geometry and frequency-referencing the coupled-cavity laser to the mode-locked Nd:YAG pump laser is presented. Finally, the phase noise performance of the frequency-referenced laser was measured. A reduction of two orders of magnitude in the timing jitter of the pump and colour-centre lasers could be obtained by replacing the frequency synthesiser in the Nd:YAG mode locker electronics by a crystal oscillator.

3.2 Coupled-cavity mode locking

The first coupled-cavity mode-locked laser was reported by Mollenauer and Stolen[1] in 1984. The laser consisted of a synchronously mode-locked KCl:$Tl^0(1)$ colour-centre laser which was coupled to an external control cavity containing a anomalously dispersive optical fibre. When the length of the control cavity was adjusted to be an integral multiple of the main cavity length, pulses as short as 210 fs

were produced. These pulses were considerably shorter than the 8 ps duration pulses obtained by the synchronous mode locking alone. At that time, the enhanced mode locking was attributed to temporal compression of the synchronously mode locked pulses due to the combined effects of self-phase modulation and anomalous group-velocity dispersion in the optical fibre. When the compressed pulses were reinjected into the main laser cavity they caused the laser itself to produce shorter pulses. This pulse compression continued until a steady state was reached. Experimental observations indicated that this occurred when the pulse propagating in the optical fibre was a N = 2 soliton and hence the laser was called 'The Soliton Laser'. By using an optical fibre of low group-velocity dispersion, pulses of 60 fs duration were obtained from the same laser[2]. It was subsequently noted that the laser behaved as though it was passively mode locked; the synchronous pumping only provided an initial intense feature to start the solitonic pulse shortening process[3], and a cw-pumped acousto-optically mode-locked soliton laser was demonstrated[4].

Blow and Wood[5] numerically modelled the effects of nonlinearity in the control cavity in the form of saturable absorbers or amplifiers. For the case of saturable amplification, they predicted that enhanced mode locking would still occur even though the pulses returning from the control cavity would be temporally broadened, indicating that solitonic effects were not necessary for short pulse generation. This was experimentally confirmed when Kean *et al.*[6,7] and Blow *et al.*[8,9] reported coupled-cavity mode locking when normally dispersive (and therefore non-soliton-supporting) optical fibres were used in the control cavity.

Mark *et al.*[10] and Ouellette and Piche[11] published theories suggesting that pulse compression resulted from the interference between the pulse travelling in the main laser cavity and the self-phase modulated pulse in the control cavity at the common mirror. The theory presented by Mark *et al.* is illustrated below with reference to Figure 3.1. The main laser cavity consists of the gain medium and mirrors M1 and M2, and the control cavity formed by M2,M3 contains a nonlinear element. The incident and reflected wave amplitudes on the partially transmitting mirror M2 reflectivity, r are given by a1 and b1 in the main cavity and a2 and b2 in the control cavity.

Light travelling in the main laser cavity is split at the common mirror (M2). A portion of the beam traverses the control cavity and is attenuated by factor L (<<1), while the remainder circulates around the mail cavity. Since the two cavity lengths are approximately the same, the pulses are interferometrically recombined at the beamsplitter. In the absence of any nonlinearity or group-velocity dispersion, the pulses returning from the control cavity are spectrally and temporally identical to those in the main laser cavity and so interference occurs uniformly across the pulse. In effect, the coupled cavity changes the reflectivity of the end mirror (M2) of the main

laser cavity. This change in reflectivity depends on the static phase mismatch ϕ between the laser cavities.

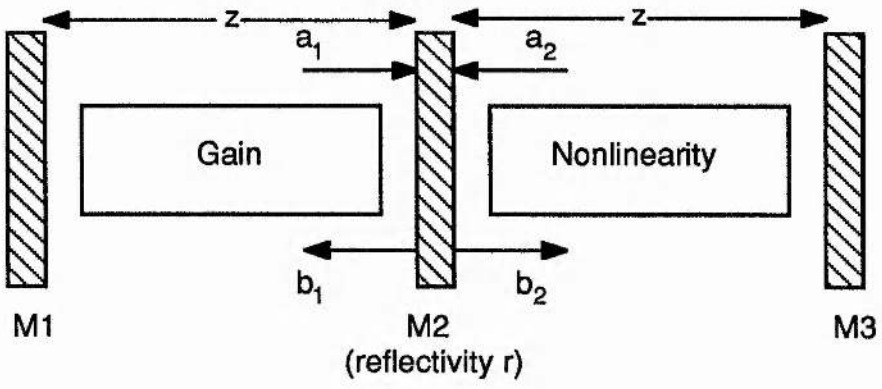

Figure 3.1. Simplified representation of a coupled-cavity mode-locked laser.

Now consider the effects of self-phase modulation (SPM) in the control cavity: The SPM causes a varying phase across the pulse in the control cavity, so when the pulses from the two cavities are interferometrically recombined the phase mismatch varies across the pulse, causes a temporally varying mirror reflectivity. If the static phase mismatch is chosen such that the reflectivity is increased at the pulse centre but decreased in its wings, a shorter pulse is returned to the main laser cavity. Mark *et al.* showed that the maximum change in reflectivity occurs for a static phase mismatch of $\phi = \pm \pi/2$. For $\phi = -\pi/2$ and a nonlinear phase shift of Φ (defined such that the phase shift is zero at the centre of the pulse, becoming negative in its wings) the amplitude reflectivity Γ = b1/a1 of mirror M2 as seen by the main laser cavity was given by

$$|\Gamma| \cong r + L(1-r^2)\Phi \tag{3.1}$$

From this equation it is clear that the mirror reflectivity is at a maximum for the centre of the pulse and decreases in the pulse wings. This is analogous to the effect of a fast saturable absorber in that the high intensity parts of the pulse experience less loss than lower intensity components.

Coupled-cavity mode-locking was subsequently observed for NaCl:OH^-[12], Ti:Al_2O_3[13,14], Nd:YAG[15], Nd:YLF[16], Nd:Glass[17] and Cr:forsterite[18] lasers. For these lasers, it was found that active mode locking was not required to initiate the coupled-cavity mode locking because the longitudinal mode beating in the laser cavity provided features of sufficient intensity to start the mode-locking process.

3.2.1 The laser configuration

A schematic of the coupled-cavity mode-locked NaCl:OH⁻ laser is shown in Figure 3.2. The NaCl:OH⁻ crystal pumping arrangement is described in Chapter 2. A nonlinear Fabry-Perot arrangement, based upon an extended three-mirror resonator was employed. The main cavity was formed by mirrors M1 through M5 and the output coupling provided by mirror M5 was 22 %. Birefringent filters (BRF) varying in thickness from 0.5 mm to 1 mm were incorporated in the cavity to tune the laser and to restrict the oscillating bandwidth. The length of the main cavity was 182 cm so that the laser could be synchronously pumped by the mode-locked Nd:YAG laser thus providing an intense noise burst for initiation of the enhanced mode-locking process. The control cavity, formed by mirrors M5 through M8 contained a 60 cm length of Corning dispersion-shifted single-mode optical fibre having zero group-velocity dispersion at approximately 1550 nm wavelength. This fibre is believed to be similar in construction to the fibre described in Ref. **19**, with a mode field diameter of 9.8 μm at 1550 nm wavelength, resulting in a fibre nonlinearity γ of approximately 2 $W^{1}km^{1}$.

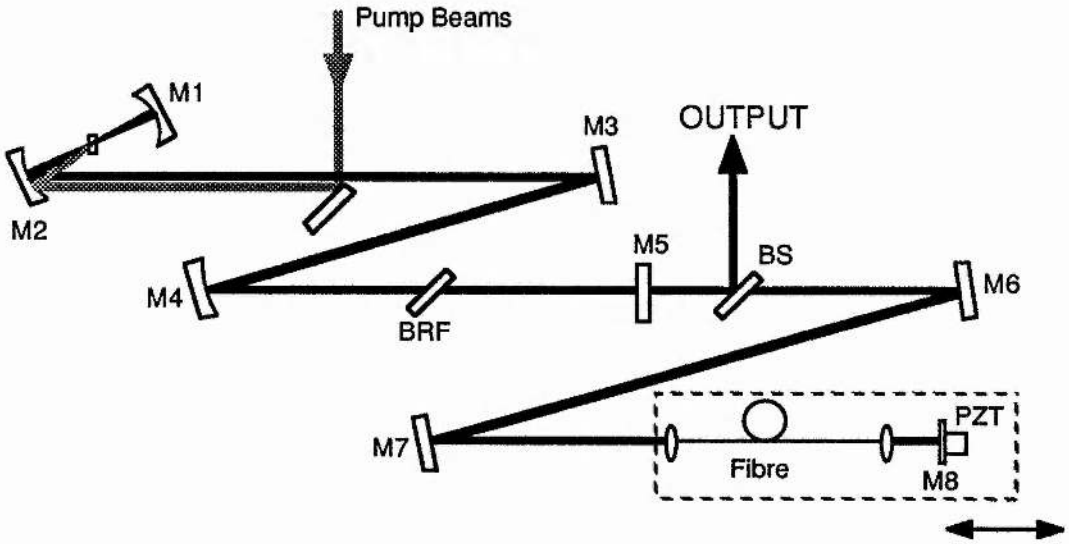

Figure 3.2. Schematic of the coupled-cavity mode-locked laser in a nonlinear Fabry-Perot configuration.

Light was coupled into and out from the optical fibre using Melles Griot 006 GLC 002 diode collimating lenses. All the lens surfaces were antireflection coated for 1550 nm operation with the exception of the surfaces closest to the optical fibre, which were uncoated. To minimise reflection from the fibre ends, the space between the lenses and the fibre ends was filled with a refractive index matching oil (Halocarbon 700 series) having an index of refraction of n = 1.42. The fluid was contained in perspex cylinders which were secured using O rings around the coupling

lenses. Motion of the lenses relative to the chucks holding the fibre ends was enabled by using a bellows arrangement (see Figure 3.3) to connect the perspex cylinders and fibre chucks (Newport model FPH - S). The lenses were mounted on Photon Control Microblock 3-axis positioners. The output from the fibre was focused onto mirror M8 and retroflected as this achieved greatest coupling efficiency in the backwards direction. The entire fibre coupling and end mirror assembly was mounted on a breadboard attached to Micro-Controle 50 mm translation stages so that adjustments to the length of the control cavity could be made with minimum change to the fibre coupling.

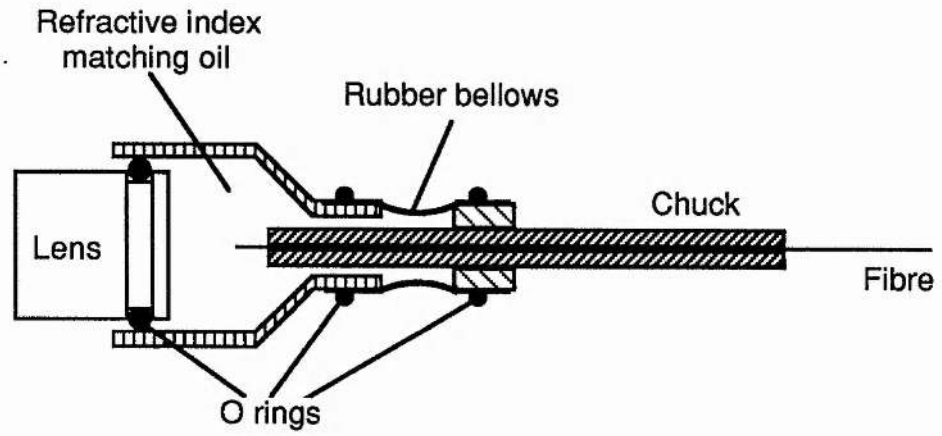

Figure 3.3. Schematic of the fibre coupling lens mount.

3.2.2 Electronic stabilisation scheme

Because the coupled-cavity mode-locking process relies on interference between the pulses from the main and control cavities at the common mirror M5, it is necessary to match the lengths of the two cavities to less than one optical cycle for stable continuous operation. It was therefore necessary to employ an active stabilisation scheme using an electronic feedback loop and a piezo-electric transducer attached to mirror M8.

The stabilisation scheme was based on the circuitry described by Mitschke and Mollenauer[3]. The system makes use of the modulation of the average output power that occurs as the length of one cavity is varied with respect to the other. This is clearly evidenced in Figure 3.4 which shows the variation of the average output power (top trace), and the SHG power generated from this light (lower trace), as the length of the control cavity is adjusted. The sharp increases of SHG power indicates that the onset of mode locking occurs at specific cavity lengths. This indicates that mode locking only occurs for a particular phase difference between the two interfering pulses. Since this phase difference can be associated with a specific

average power level, it is possible to maintain the length of the control cavity, and hence mode-locked operation, by adjusting its length to maintain an empirically preset average output power.

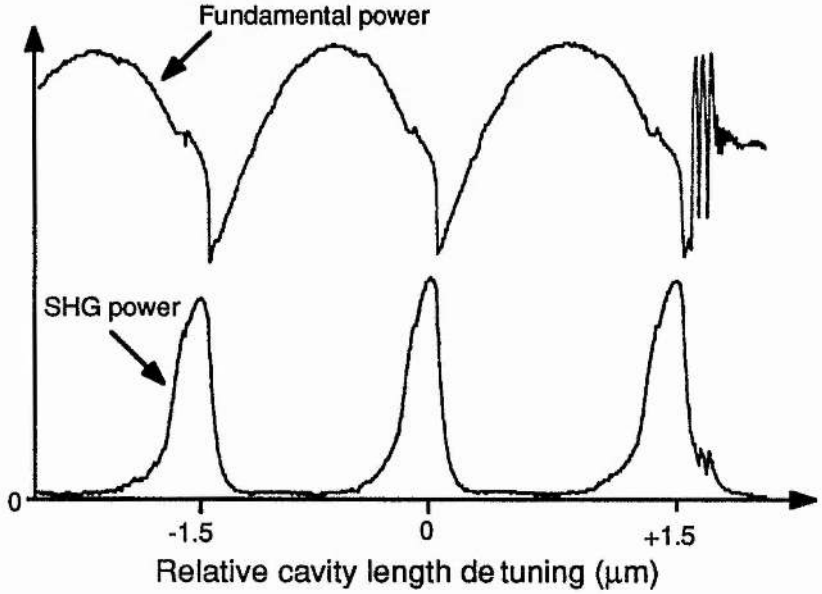

Figure 3.4. Variation of the fundamental and the second harmonic power from the laser as the length of the control cavity is scanned.

The basic circuitry is outlined in Figure 3.5. A portion of the laser output was directed onto a large-area germanium photodiode (Germanium Power Devices, GM 8). The photodiode signal was amplified using a low-noise (OP-07) operational amplifier. This signal was compared with an empirically preset reference voltage using a differential amplifier constructed from a low-noise, high-speed AD711 op-amp in order to obtain an error signal. Since each power level can correspond to two different phase differences the polarity of the feedback signal could be selected using a DPDT switch at the input to the comparator. The output from the comparator was then integrated and amplified to provide a 0 - 140 V, 50 mA maximum current signal to drive the 15 μm travel piezoelectric transducer (Photon control MGS 7.5) onto which a small dielectric mirror (M8) was mounted. The frequency of the feedback loop could be adjusted by selecting capacitors at the integrator. A reset circuit (not shown) was incorporated to set the piezoelectric transducer to a central position whenever it reached the end of its travel.

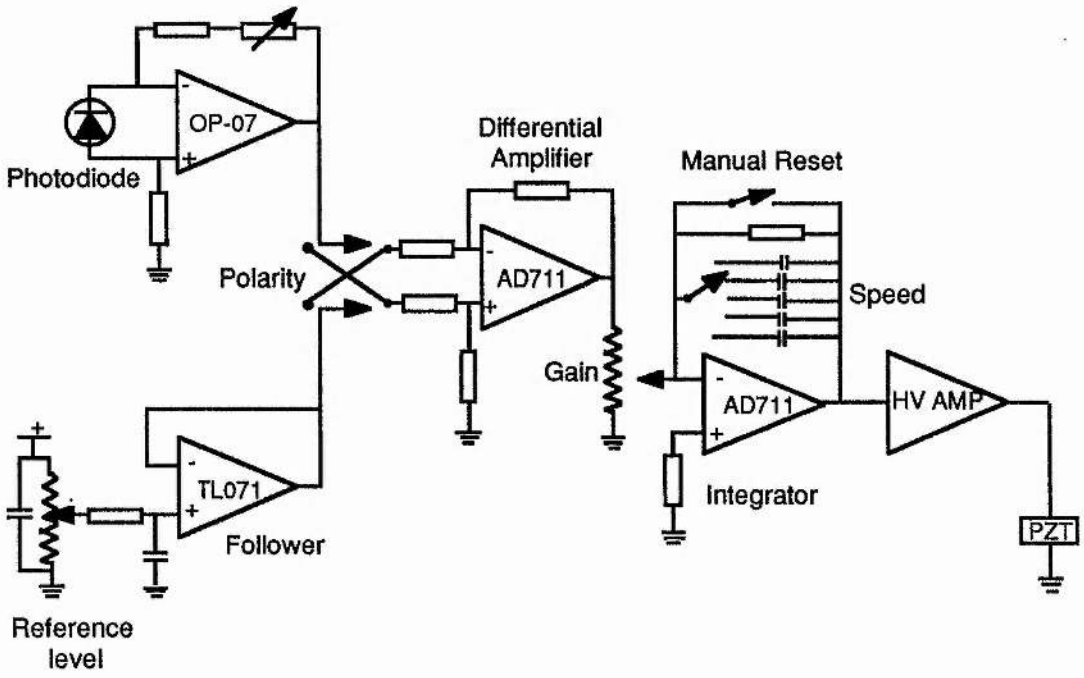

Figure 3.5. Circuit diagram of the stabilisation loop to maintain interferometric matching of the coupled-cavity lengths.

3.2.3 Results

To achieve coupled-cavity mode locking, the control cavity was blocked and the length of the main laser cavity was adjusted for optimum synchronous pumping. The control cavity was then unblocked and the coupling into the fibre, in both directions, was maximised. If the two cavity lengths were not matched, the synchronous mode locking was strongly inhibited by the asynchronous feedback from the control cavity. The approximate length of the control cavity was set by carefully measuring the length of the main laser cavity to within the travel of the fibre / end-mirror assembly. The entire assembly was then translated whilst monitoring the output from the autocorrelator. When mode locking occurred, signified by a large increase in the autocorrelation signal, the stabilisation circuitry was turned on and the reference level and feedback polarity were adjusted to achieve stable mode locking.

However, when the feedback loop was closed, a periodic modulation was observed on the output pulse train of the mode-locked laser. An example of this modulation is illustrated in Figure 3.6, which shows the autocorrelation of the laser pulses (left) and an oscillogram (right) of the pulse train measured using a germanium photodiode having a 700 ps rise time (Germanium Power Devices GM 4). By adjusting the relative lengths of the main and control cavities with respect to one another, the frequency of the amplitude modulation could be varied. It was concluded

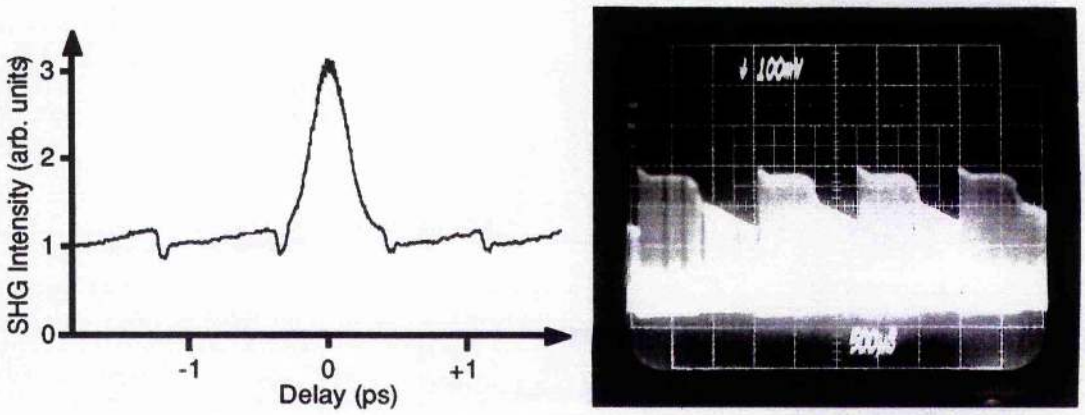

Figure 3.6. Autocorrelation and pulse train from the coupled-cavity mode-locked laser showing amplitude modulation resulting from mismatch of the pump and NaCl:OH⁻ laser cavity lengths.

that the modulation arose from the beating of the colour-centre laser pulse train with the gain modulation induced by the Nd:YAG laser pump pulses. This is a result of the passively mode locked nature of the coupled-cavity mode-locked laser[3]: the synchronous pumping only serves to initiate the mode-locking process, after which it performs no useful role. The pulse repetition rate of the colour-centre laser is determined by the optical path length of the resonator. Because the 150 ns upper-state lifetime of the active centres is relatively short (*c.f.* 1600 ns for KCl:$Tl^0(1)$[20]) the synchronous pumping imposes a significant modulation on the gain. For a pump pulse repetition frequency of 82 MHz, there is an 8% modulation of the small-signal gain over the 12.5 ns pulse period. This gain modulation manifests itself as a regular ramping of the output power as the pulse train of the colour-centre laser walks through the pump laser pulse train.

Typically, the modulation of the output power of the laser occurred at frequencies varying from several tens of hertz to a few kilohertz. These frequencies are within the bandwidth of the cavity matching stabilisation electronics. The stabilisation circuitry interpreted the amplitude modulation as a change in the relative cavity lengths and adjusted the length of the control cavity in an attempt to obtain a constant output power. It was therefore difficult to maintain the coupled-cavity mode locking.

It was found that coupled-cavity mode locking could be obtained when the main cavity length was negatively detuned by approximately 200 μm from the optimum length for synchronous mode locking. This cavity detuning corresponds to a frequency difference of approximately 18 kHz from the pump laser pulse repetition frequency. The bandwidth of the stabilisation feedback loop was only several kilohertz and therefore it did not respond to the amplitude modulation caused by the mismatch between the pump laser and colour-centre laser cavity lengths. It was subsequently possible to obtain stable mode locking for extended periods of time.

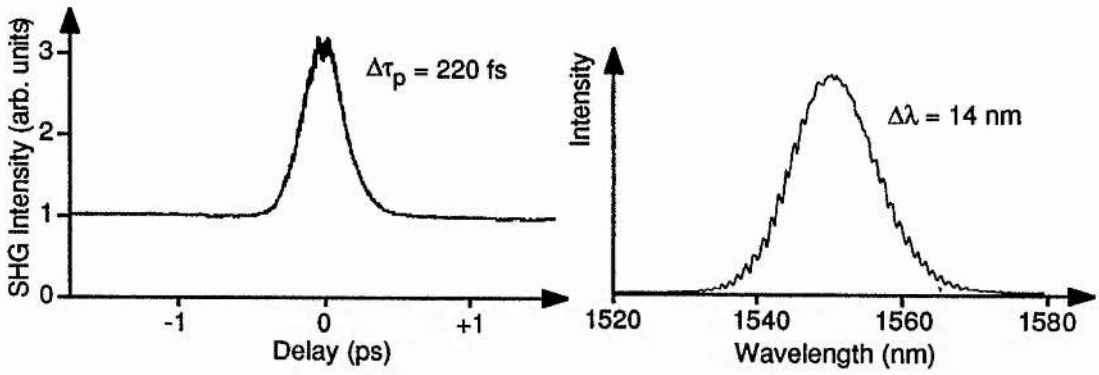

Figure 3.7. Autocorrelation and spectrum of the coupled-cavity mode-locked laser. A 0.8 mm thick birefringent filter was used to restrict the oscillating bandwidth.

Figure 3.7 shows an intensity autocorrelation (left) and a spectrum (right) of the coupled-cavity mode-locked laser pulses, taken at 90 mW output power. The pulse duration was 220 fs and the spectral bandwidth was 14 nm yielding a duration-bandwidth product of 0.38. The slight modulation on the spectrum of the laser pulses was ascribed to etalon effects within the laser cavity. The reflectivity of the main-cavity end mirror was 78% and the coupling efficiency into the optical fibre was measured to be greater than 80% in both directions. A 0.8 mm thick birefringent filter was included in the main laser cavity to restrict the bandwidth of the mode-locked pulses. The threshold for coupled-cavity mode locking was measured to occur at 70 mW output power and the mode locking became unstable at output powers in excess of 110 mW.

In order to obtain the maximum useful output power from the laser, the error signal for the interferometric stabilisation circuitry was derived from the light that was reflected out from the laser cavity after propagating through the optical fibre. From this beam it was also possible to measure the spectral and temporal profiles of the mode-locked pulses returning to the main laser cavity. Intensity and interferometric autocorrelations and a spectrum of the returning pulses are shown as Figure 3.8 (also taken at 90 mW output power). After propagation through the fibre, the pulses increased in duration to 265 fs and their spectrum was strongly broadened to 38 nm. This is consistent with the actions of self-phase modulation and small normal group-velocity dispersion. The strong frequency chirp on the returning pulses is clearly evident on the interferometric autocorrelation where the fringe visibility is largely reduced.

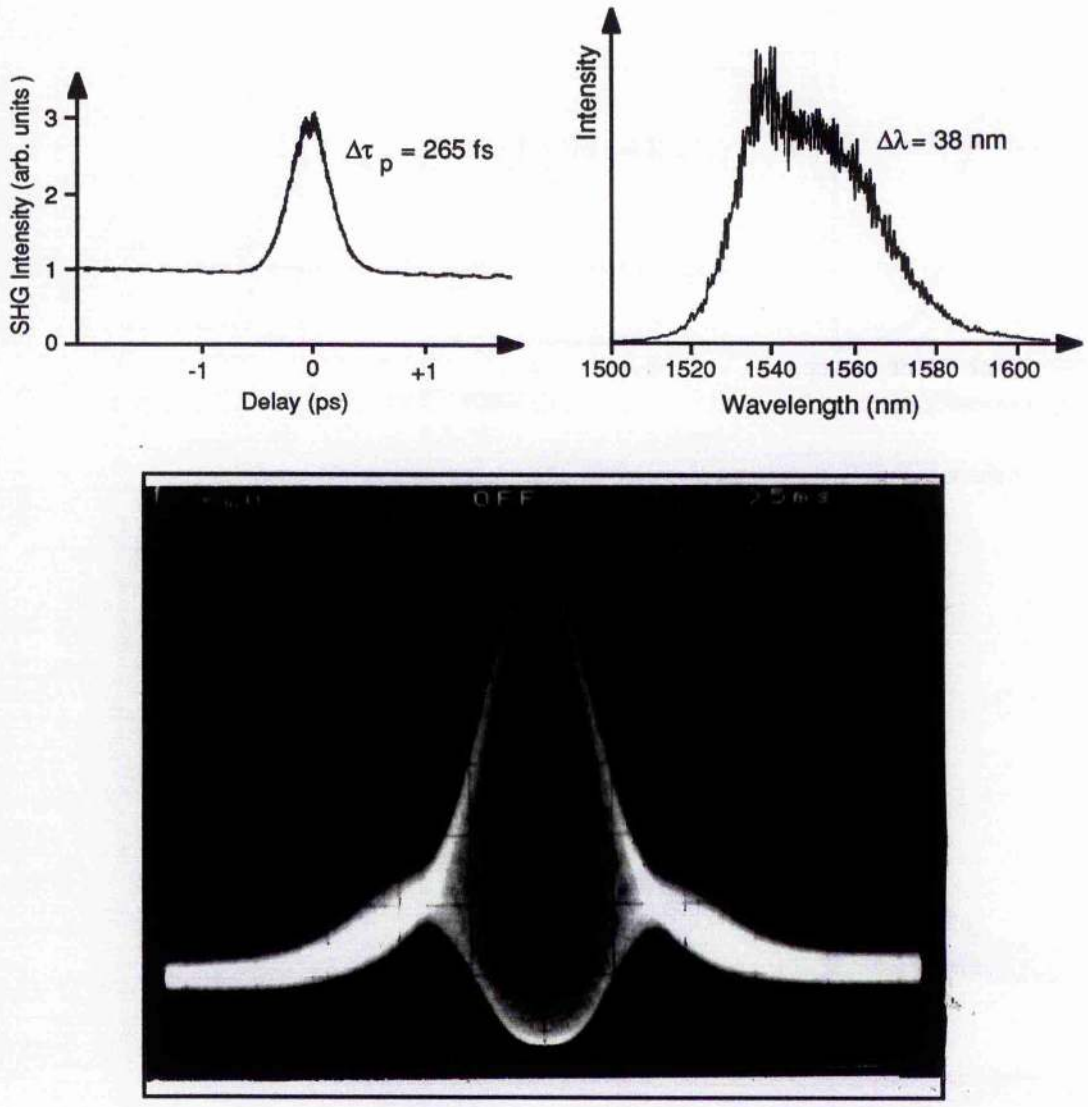

Figure 3.8. Autocorrelations and spectra of the pulses returning from the fibre.

Figure 3.9 shows the progression of the spectra for the laser pulses returning to the main cavity as the pump power to the NaCl:OH⁻ crystal was increased from threshold for mode locking to the maximum stable operating power. The spectra are annotated with the average power coupled into the optical fibre. For all of these results the measured output pulse duration was constant at 220 fs. This indicates that the birefringent filter located in the main laser cavity was the dominant pulse duration limiting element. As the power coupled into the fibre was increased the spectral bandwidth of the pulses in the control cavity increased through the intensity dependent effect of self-phase modulation. At 83 mW coupled power, the spectrum from the optical fibre possessed two peaks indicating a peak phase shift in excess of $3\pi/2$ radians. Above 2π radians peak phase shift mode locked operation became

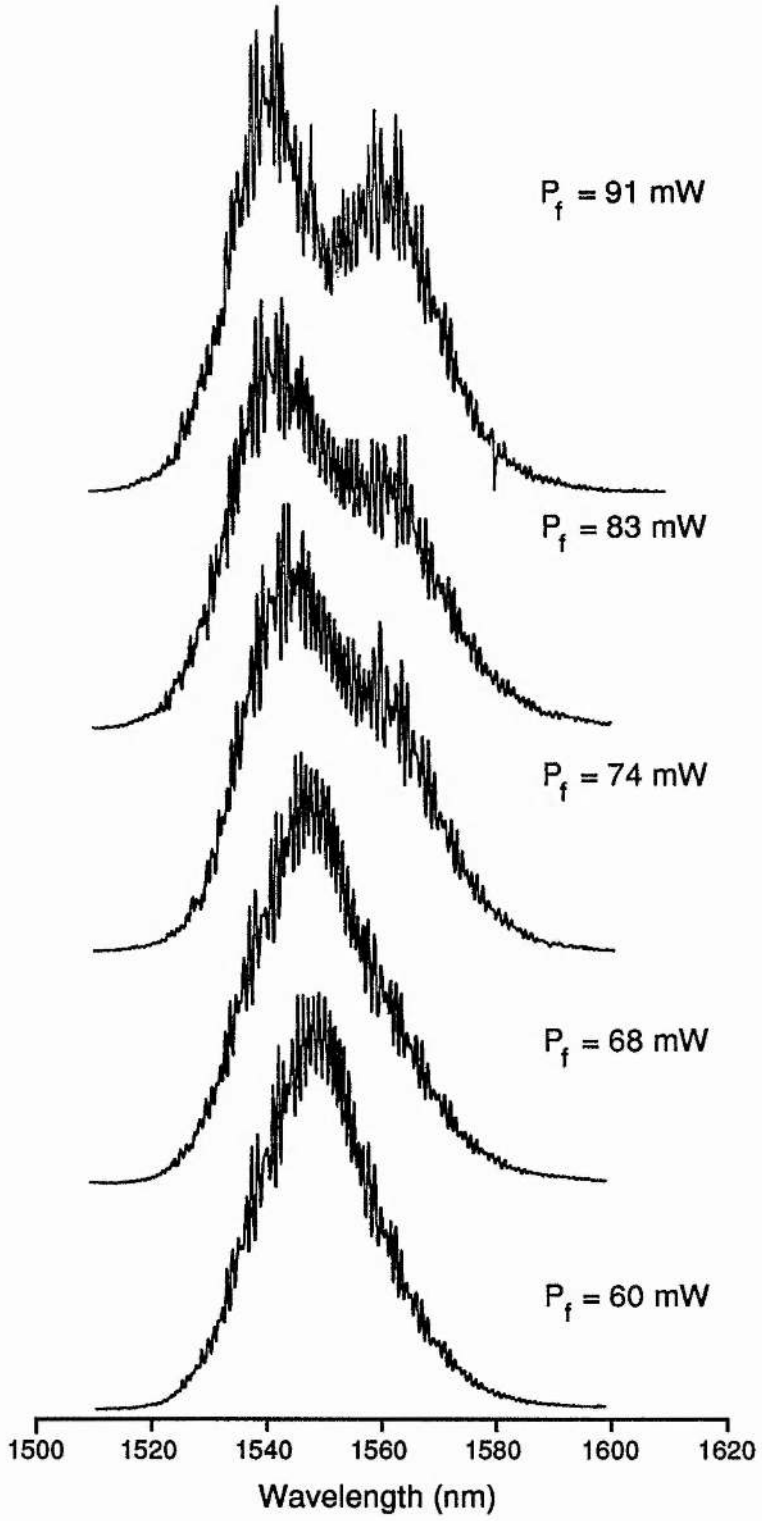

Figure 3.9. Progression of the spectrum returning from the fibre as the laser pump power is increased.

unstable since the interfering pulses experienced oscillating regions of constructive and destructive interference across the pulse.

By reducing the thickness of the birefringent filter from 0.8 mm to 0.5 mm, shorter duration pulses were obtained. An autocorrelation and a spectrum of the output pulses, together with an autocorrelation and a spectrum of the pulses returning from the control cavity are displayed in Figure 3.10. The output pulse duration was 140 fs and the bandwidth of the laser pulses was 21 nm, resulting in a duration

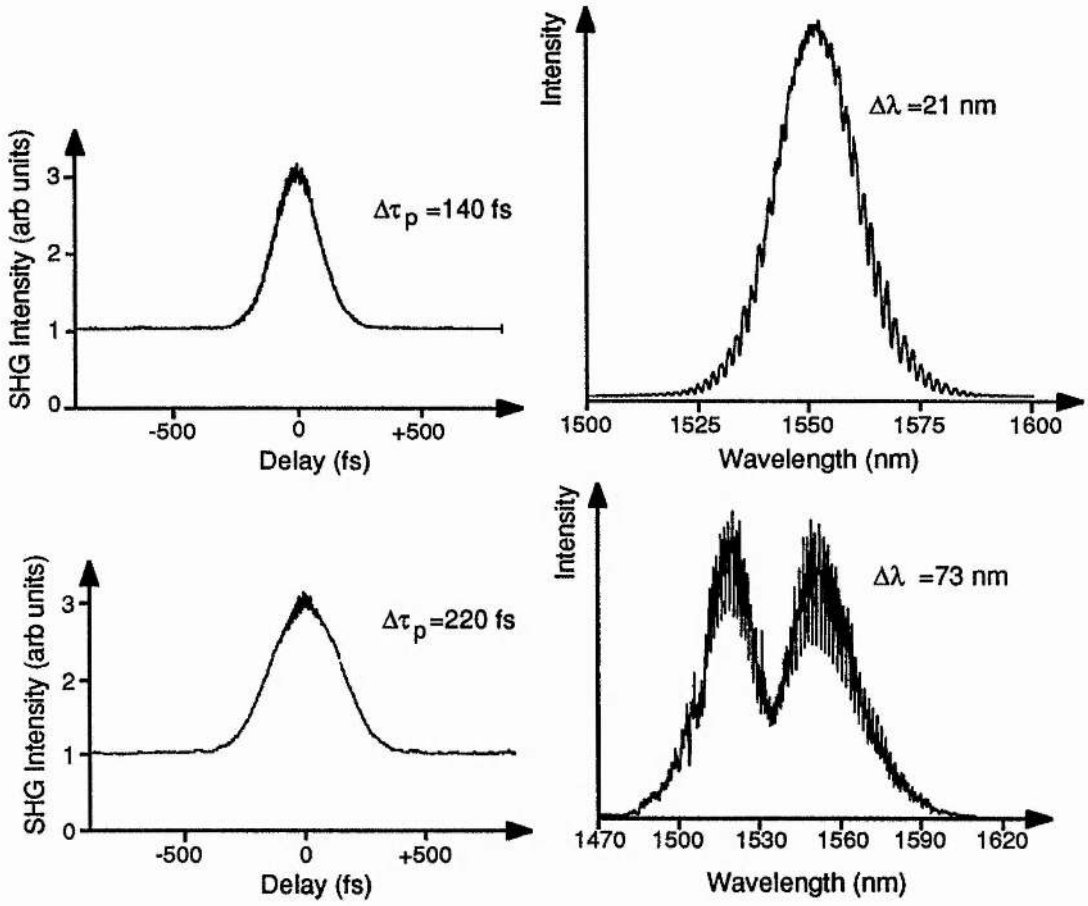

Figure 3.10. Autocorrelations and spectra of the output (top) and the pulses returning to the main cavity (bottom) for the coupled-cavity mode-locked NaCl:OH⁻laser. A 0.5 mm thick BRF was used to restrict the oscillating bandwidth.

bandwidth product of 0.36. The laser could be operated at output powers up to 95 mW, above which excessive phase shifts in the optical fibre resulted in multiple pulsing and unstable behaviour. It should be noted from Figure 3.10, that in addition to strong spectral broadening, the duration of the laser pulses was significantly increased to 220 fs after propagating through the optical fibre. For this pulse duration, it was believed that the group-velocity dispersion also played a role in limiting the output pulse duration, in addition to the birefringent filter. This hypothesis was

reinforced by the generally more stable performance of the laser when it was operated with the 0.5 mm thick BRF compared to the 0.8mm thick filter.

3.3 Amplitude stabilisation of the coupled-cavity mode-locked laser

For the results reported so far in this chapter, the output pulse train of the laser exhibited a sawtooth modulation arising from the beating of the pump and colour-centre laser pulse trains, although in most cases the modulation frequency was increased to beyond the response of the detectors used in the pulse diagnostics. It is obviously desirable to eliminate this modulation.

One method to overcome this amplitude modulation, which has been reported by Sucha[21], is to pump the colour-centre crystal using cw radiation and operate the laser in the self-starting regime. However, this approach is undesirable for several reasons. The powers required in the optical fibre in order to reach threshold are much higher for self-starting operation. For the generation of sub-100 fs duration pulses at high average powers, operation may be unreliable since the high powers necessary within the optical fibre may result in phase shifts in excess of 2π radians at threshold. The mismatch in length between the main and control cavities over which mode locking can be maintained is much less for the self-starting laser, increasing the requirements on the stabilisation electronics. Also, for many NaCl:OH⁻ laser systems, the green light required to reorient the active colour centres is generated by frequency-doubling a portion of the pump laser beam. By using a cw pump source, the efficiency of the frequency doubling stage is dramatically reduced and it may not be possible to generate sufficient second harmonic power, thus necessitating a (costly) auxiliary green source such as an air-cooled argon-ion laser. In this section, a different means of eliminating the amplitude modulation is described whilst retaining the benefits of low threshold power and relaxed cavity-matching tolerance obtained by using synchronous pumping for initiation. The approach used was to synchronise the pulse trains from the colour-centre laser and Nd:YAG pump laser by active control of the NaCl:OH⁻ laser cavity length to ensure coincidence between the Nd:YAG pulses and the circulating pulses in the colour-centre laser at the NaCl:OH⁻ crystal.

In the nonlinear Fabry-Perot arrangement, it was not possible to alter the repetition rate of the laser by translating one mirror since interferometric matching of the two laser cavities must be maintained. Translation of any one of the mirrors in this configuration leads to amplitude fluctuations and eventually, loss of coupled-cavity mode-locking if the mirror displacement is greater than $\lambda/10$. It was therefore necessary to reconfigure the laser into a nonlinear Michelson arrangement[22] as shown schematically in Figure 3.11. A beamsplitter having a reflectivity of 78% was included in the synchronously mode-locked laser cavity (M1 - M6) to form a Michelson interferometer with a linear branch BS,M4,M5,M6 and a nonlinear branch

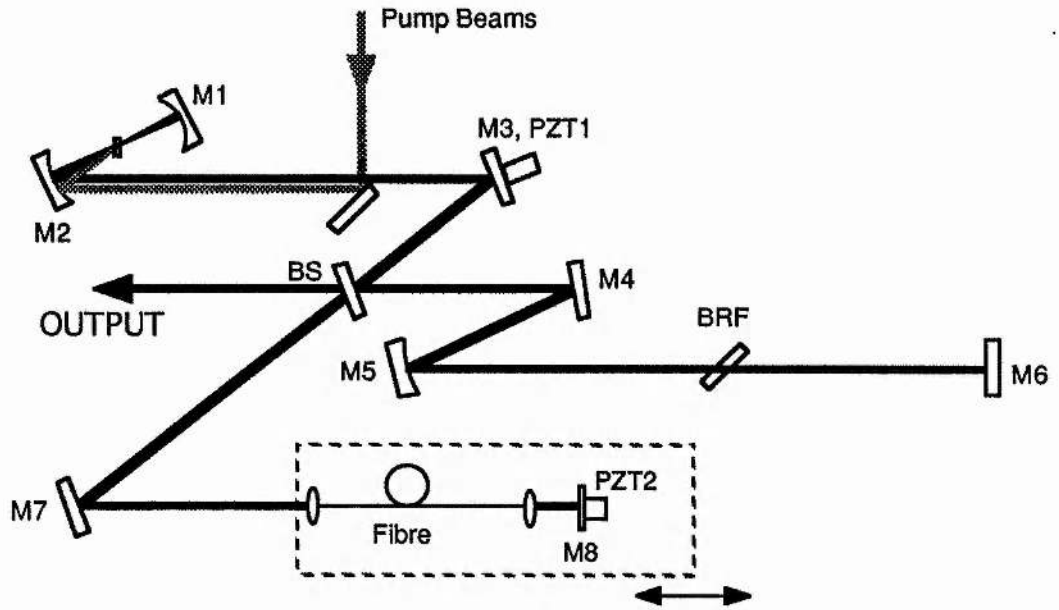

Figure 3.11. Schematic of the coupled-cavity mode-locked laser in the Michelson cavity arrangement. This configuration permits the length of the cavity to be adjusted, using PZT 1, so that it may be frequency referenced to the pump laser.

BS,M7,M8 containing the optical fibre. In this arrangement, it was possible to simultaneously adjust the lengths of the two coupled cavities by adjusting the position of a single mirror mounted on a piezoelectric transducer (PZT1, M3). This allowed the pulse repetition frequency of the laser to be adjusted with respect to that of the Nd:YAG pump laser, whilst maintaining the interferometric match of the nonlinear and linear branches.

The frequency-referencing circuitry is shown in Figure 3.12. The pulses from the pump and colour-centre lasers were detected using photodiodes (bandwidth > 500 MHz). The signals were amplified and the second harmonic of the pulse repetition frequencies were selected using bandpass filters (~5 MHz passband, ~2 dB insertion loss). The signal from the Nd:YAG laser was delayed with respect to that from the colour-centre laser using a variable delay line to take account of the different optical path lengths to the detectors and the different cable lengths. These two signals were mixed by a double-balanced mixer (DBM) (Mini-Circuits model SRA-1) to provide an error signal. This mixer was operated at elevated powers (3-5 dBm in excess of the manufacturer's recommended input powers) to reduce amplitude-to-phase noise conversion[23]. The error signal from the mixer was then integrated, amplified and compared to a reference voltage to produce a correction signal which was applied to the piezoelectric transducer on which mirror M3 had been mounted.

The bandwidth of the stabilisation scheme was limited to 2 kHz by the resonant frequency of the piezoelectric transducer.

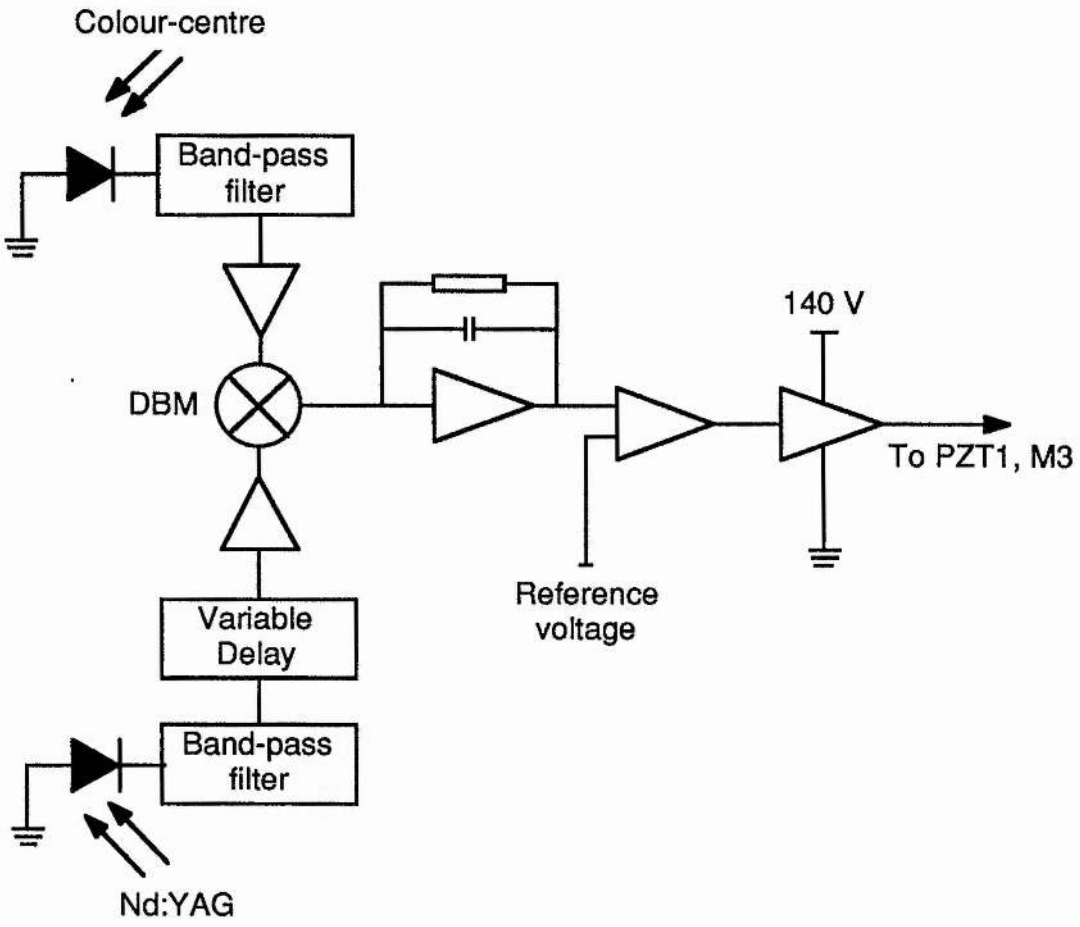

Figure 3.12. The frequency referencing circuit.

When coupled-cavity mode locking was achieved and the servo loop to maintain interferometric matching of the two branches of the laser was closed, the output from the double-balanced mixer, which corresponds to the frequency difference between the colour-centre and pump laser pulse trains, was monitored. The location of mirror M3 was adjusted to bring the pulse repetition frequency of the colour-centre laser to within 250 Hz of that of the pump laser (*i.e.* to within the 6 μm travel of the PZT). The feedback loop which provided the correction signal to PZT 1 was then closed, thus matching the period of the pulses from the two lasers and eliminating the sawtooth modulation. A typical pulse train from the frequency-referenced NaCl:OH⁻ colour-centre laser is reproduced as Figure 3.13. A further indication of the effectiveness of this stabilisation method is shown in the RF spectra of the laser output. Figure 3.14 shows the spectrum of the 2nd harmonic of the laser output before the stabilisation circuitry was turned on. Multiple sidebands arising

from the strong amplitude modulation extending to beyond 1 Mz from the carrier frequency are clearly evident. Whereas, with the feedback loop closed (Figure 3.14 right), it is clearly demonstrated that the modulation has been completely eliminated.

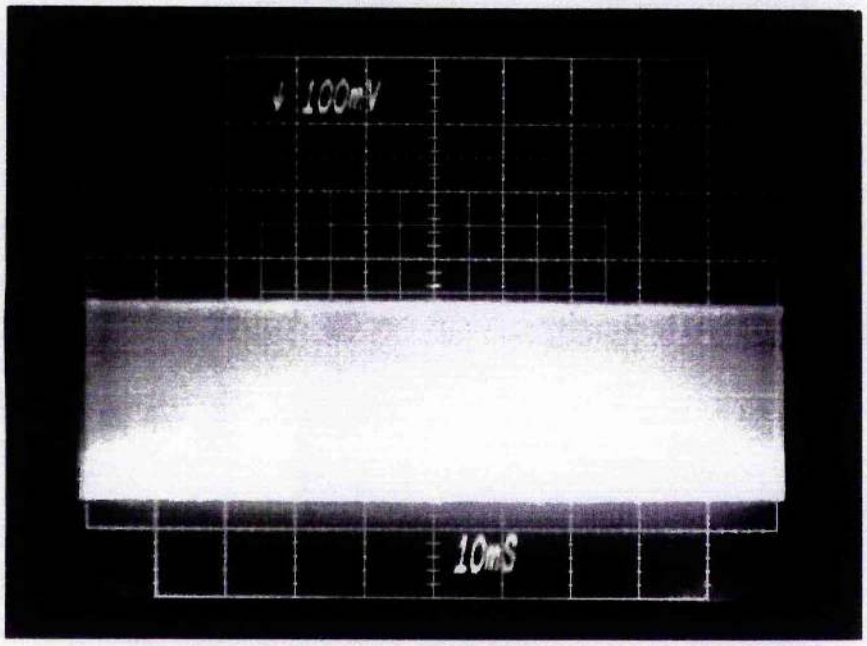

Figure 3.13. Pulse train from the frequency-referenced coupled-cavity mode-locked laser.

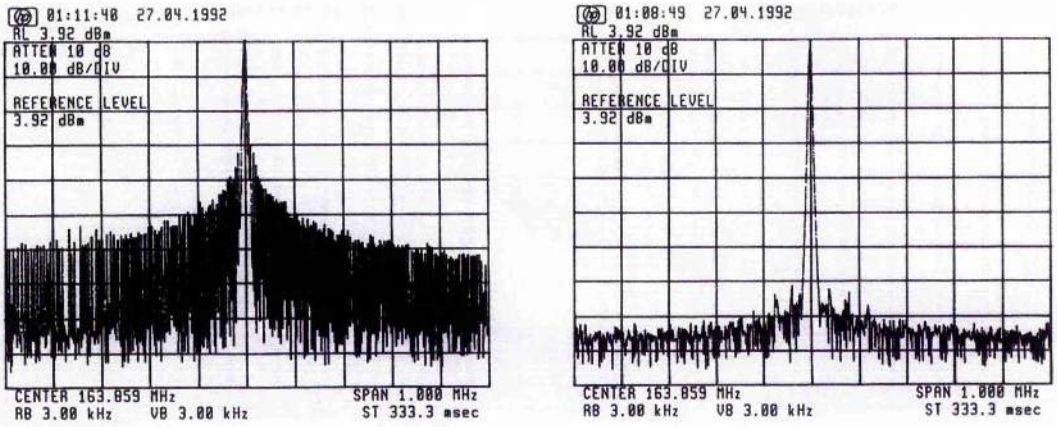

Figure 3.14. RF spectra of the unreferenced (left) and frequency referenced (right) coupled-cavity mode-locked laser.

When frequency referenced to the Nd:YAG pump laser the coupled-cavity mode-locked colour-centre laser produced pulses with durations of 110 fs with bandwidths of 24 nm, giving duration-bandwidth products of 0.33. A typical autocorrelation and spectrum of these pulses are presented in Figure 3.15 . The power

coupled into the optical fibre was ~ 32 mW. For these results the average output power from the laser was 50 mW. Unstable operation occurred at higher powers due to excessive phase shifts in the fibre within the nonlinear cavity branch. In practice greater output powers can be achieved by using shorter fibre lengths in preference to reducing the power coupled into the fibre. This is because the latter may compromise the performance of the laser by reducing the coupling between the two cavity branches.

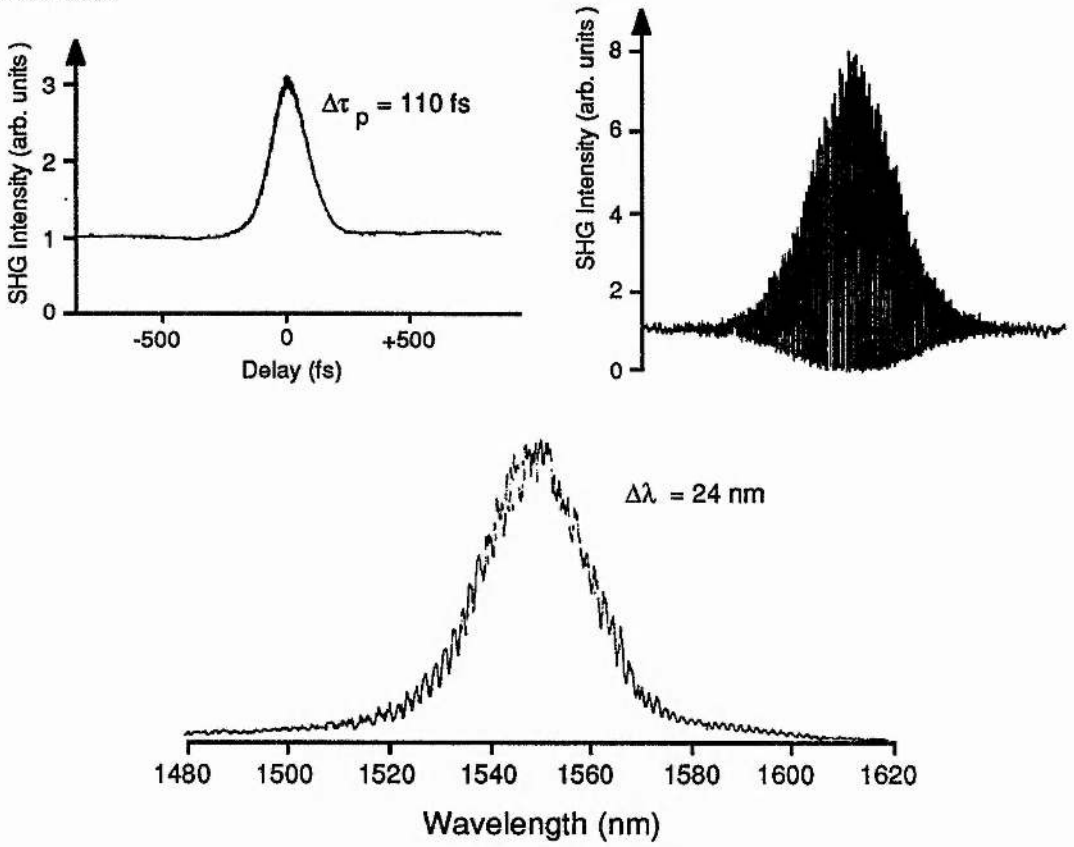

Figure 3.13. Autocorrelations and spectra of the frequency-referenced coupled-cavity mode-locked NaCl:OH⁻ laser.

3.4 Phase noise measurements of the coupled-cavity mode-locked laser.

In mode-locked laser systems, phase noise manifests itself as a variation in the temporal separation of the mode-locked pulses, that is a pulse-to-pulse timing jitter. Although the variation in the temporal separation of two successive pulses may be small, it can accumulate over thousands of round trips. Since frequency is the first derivative of phase with respect to time, frequency noise and phase noise are aspects of the same phenomenon. For pump-probe experiments using two laser sources, electro-optic sampling experiments and pulse duration measurements using synchroscan streak cameras, the phase noise of the laser systems may limit the

temporal resolution of the measurements. It is therefore important to be able to characterise the noise performance of mode-locked laser systems to assess the suitability of these systems for such experiments and also, to identify sources of and means of reducing the phase noise of mode-locked lasers.

In actively mode-locked lasers the pulse repetition frequency is determined by the applied modulation signal, and as such the phase noise of these lasers tends to follow that of the modulator. For example, the phase noise of the synchronously mode-locked dye laser was found to replicate that of the mode-locked argon-ion laser used to pump it[24]. In acousto-optically mode-locked lasers and semiconductor lasers mode locked by current modulation, the phase noise of the electronic drive circuitry will transferred directly onto the pulse train. It is therefore necessary to use low phase noise electronics to obtain low noise performance from these lasers.

In passively mode-locked lasers, however, the pulse repetition frequency is determined primarily by the optical path length of the laser cavity. The phase noise of these systems mainly arises from cavity length fluctuations caused by thermal, mechanical and acoustic noise in the laboratory environment. Some phase noise may arise from amplitude-to-phase noise conversion through the refractive index changes that accompany gain saturation and self-phase modulation, although they are usually small. Hence, to obtain low phase noise performance from a passively mode-locked laser, both passive and active cavity stabilisation together with a low noise pump are required.

In 1986, Von der Linde[24] described a powerful technique to characterise the phase noise of mode-locked lasers based on an analysis of the power spectrum of the mode-locked pulse train. The salient features of the theory behind the technique are outlined below. For a more detailed description the reader should consult Reference **24**.

The intensity of a noisy pulse train may be written as

$$F(t) = F_o(t) + F_o(t)A(t) + F_o(t)TJ(t) \tag{3.2}$$

where $F_o(t)$ represents the perfectly mode-locked, noise-free pulse train,
$A(t)$ is a function describing random amplitude fluctuations
and $TJ(t)$ represents the temporal jitter of the pulses with average period T.

The power spectrum of the pulse train is given by the Fourier transform of the intensity autocorrelation function. This is

$$P_f(\omega)=\left(\frac{2\pi}{T}\right)^2\left|\tilde{f}(\omega)\right|^2\sum_{n=-\infty}^{n=+\infty}\left[\delta(\omega_n)+P_A(\omega_n)+(2\pi)^2n^2P_J(\omega_n)\right] \qquad (3.3)$$

The three terms in the summation are a series of delta functions, $\delta(\omega)$, separated harmonically by the pulse repetition frequency representing a noise-free pulse train. The delta functions are accompanied by amplitude noise and phase noise sidebands of spectral densities $P_A(\omega)$ and $P_J(\omega)$, respectively.

By inspection of equation 3.3, it can be seen that the amplitude noise remains constant with harmonic number n whereas the phase noise increases with the square of the harmonic number. This is represented graphically in Figure 3.16.

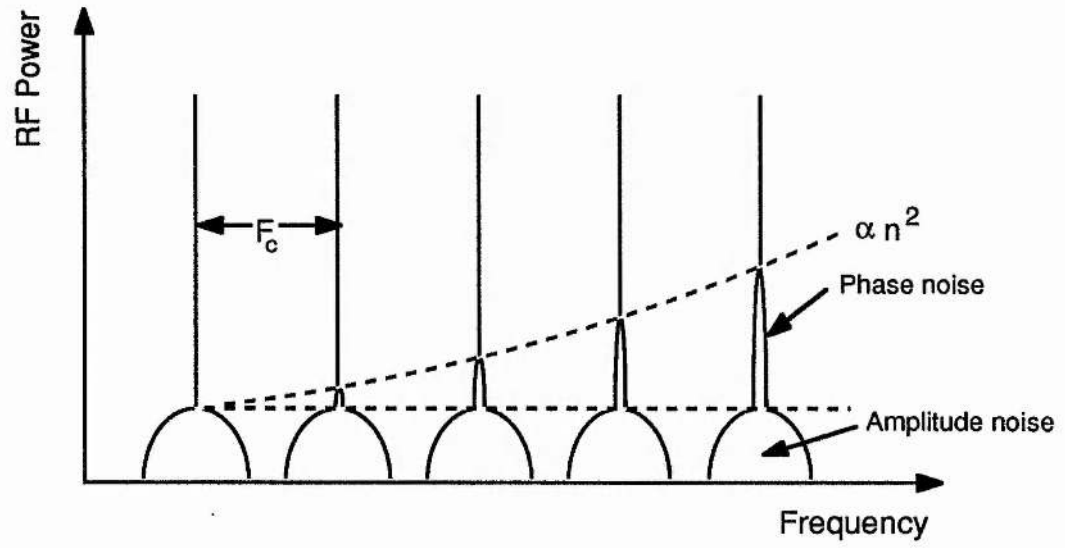

Figure 3.16 Representation of the RF power spectrum of a mode-locked laser showing the dependence of the phase noise on the square of the harmonic number.

By measuring the power spectrum using a broad-bandwidth photodetector and spectrum analyser combination, the noise properties of the laser can be accurately determined: amplitude noise can be determined by examining the sidebands around the fundamental harmonic, where only the amplitude noise is present, and the phase noise can be extracted from the noise side-bands attending higher harmonics of the pulse repetition frequency.

In practice, the phase noise of a mode-locked laser is evaluated as follows:

1. The power spectra of the laser pulse train is measured at the fundamental pulse repetition frequency and at a higher harmonic (n) using a

photodiode and a spectrum analyser. The measurement is performed for various resolution bandwidths of the analyser.

2. The phase noise and amplitude noise components are separated using the n^2 dependence of the phase noise and the single-sideband phase noise power spectrum $L_f(f)$ is plotted. This is a log-log graph of the ratio of the power in the noise sideband in a 1Hz bandwidth to the power in the carrier (units: $dBcHz^{-1}$).

3. The rms timing jitter σ_J in any frequency interval $[f_l, f_h]$ can then be readily obtained by linearising the single sideband noise spectrum and integrating it over the interval then applying the relation

$$\sigma_J[f_l, f_h] = \frac{1}{2\pi f_o}\sqrt{2\int_{f_l}^{f_h} 10^{L_f(f)/10} df} \qquad (3.4)$$

(The rms phase noise is simply $\phi_{rms} = 2\pi f_o \sigma_J$)

Using the above algorithm, the phase noise of the coupled-cavity mode-locked NaCl:OH⁻ laser was measured using a 9.5 GHz bandwidth InGaAs PIN photodiode and an HP 70000 series spectrum analyser. The data from the analyser was collected and processed using a portable computer and an in-house-developed software package. Measurements of the phase noise of the Nd:YAG pump laser and the synchronously mode-locked colour laser were also performed and their relevance to the noise of the coupled cavity mode-locked laser noise performance shall be discussed.

The phase-noise characteristics of coupled-cavity mode-locked laser are slightly different from those of other passively mode-locked lasers. Strong amplitude-to-phase noise conversion occurs since the interferometric matching of the two cavities is obtained through adjusting the control cavity length to maintain a constant output power: any amplitude noise on the pulse train will be interpreted as cavity length drift and will result in unnecessary changes to the length of the control cavity, thus introducing phase noise.

It was not possible to measure the phase noise of the free-running coupled-cavity mode-locked laser as it did not fall within (or indeed anywhere near) the small-signal criterion[25]. This could be seen from the RF spectrum of the free-running laser (Fig. 3.14) where multiple sidebands arising from the amplitude modulation are clearly evident. However, once the amplitude modulation was eliminated using the active feedback circuitry, it was possible to measure the phase noise of the laser. Figure 3.17 shows the single-sideband phase noise spectrum, calculated from the 1st and 10th harmonics of the pulse train. The dotted line indicates the limit for the small-signal deviation criterion. The rms timing jitter was measured to be 590 ps in the 50 -

500 Hz frequency range and 7.8 ps for the 500 Hz - 5 kHz frequency band. The value obtained for the 50 - 500 Hz interval represents an upper bound to the phase noise since it violates the small signal criterion.

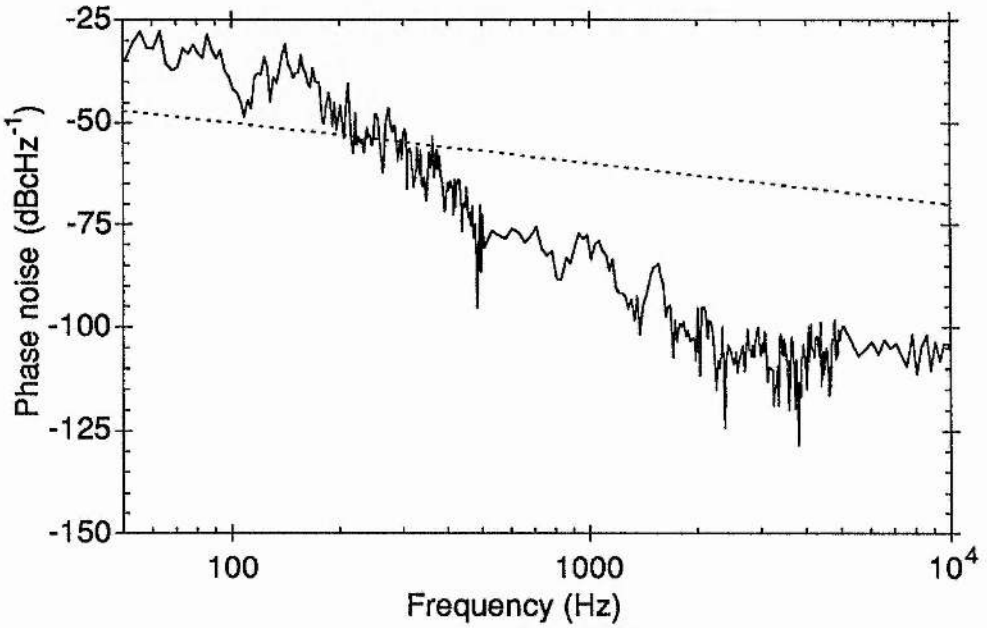

Figure 3.17. Single-sideband phase noise of the frequency-referenced coupled-cavity mode-locked NaCl:OH⁻ colour-centre laser.

In the amplitude stabilised format, the phase noise of the coupled-cavity mode-locked laser was expected to follow that of the Nd:YAG pump laser since it was directly frequency-referenced to the pump laser pulse train. To verify this, the phase noise of the Nd:YAG laser was measured using a silicon photodiode having a 2 GHz bandwidth. The single-sideband phase noise spectrum (again calculated from the 1st and 10th harmonics) is reproduced as Figure 3.18. The two phase noise spectra are very similar in shape, although the timing jitter of the Nd:YAG laser was slightly less than the colour-centre laser at 125 ps from 50 - 500 Hz, and 10 ps from 500 Hz to 5 kHz. The increase in the noise on the colour-centre pulse train was believed to originate from amplitude-to-phase noise conversion arising from amplitude noise on the pump laser output. A phase noise spectrum of the synchronously mode-locked laser (i.e. with the coupled cavity blocked) is reproduced as Figure 3.19. As was expected, for an actively mode-locked laser, its rms timing jitter of 170 ps [50 Hz, 500 Hz] and 12 ps [500 Hz, 5 kHz] closely follows that of the pump laser.

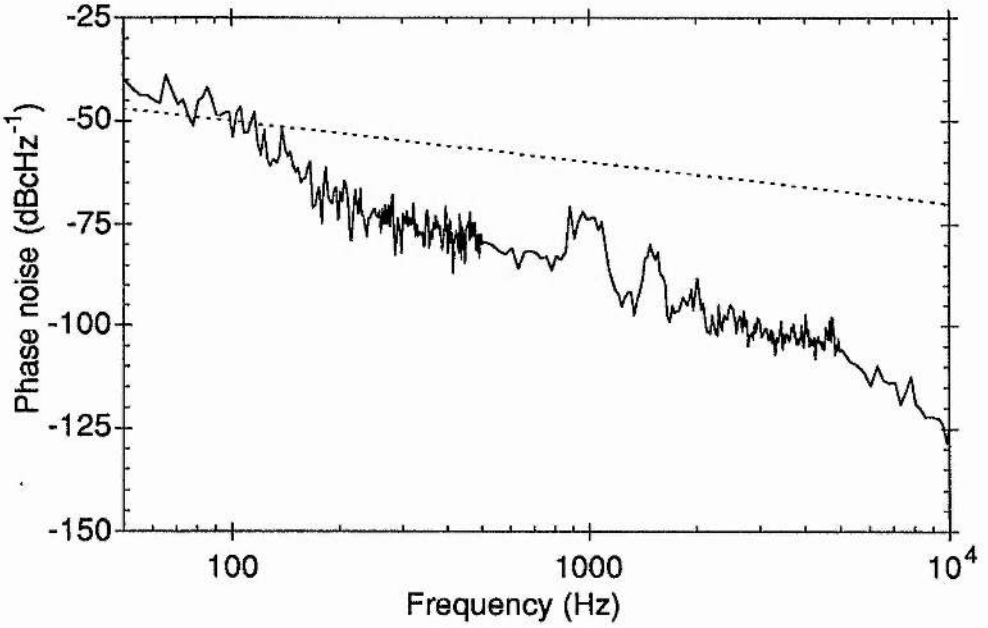

Figure 3.18. Single-sideband phase noise spectrum of the Nd:YAG pump laser.

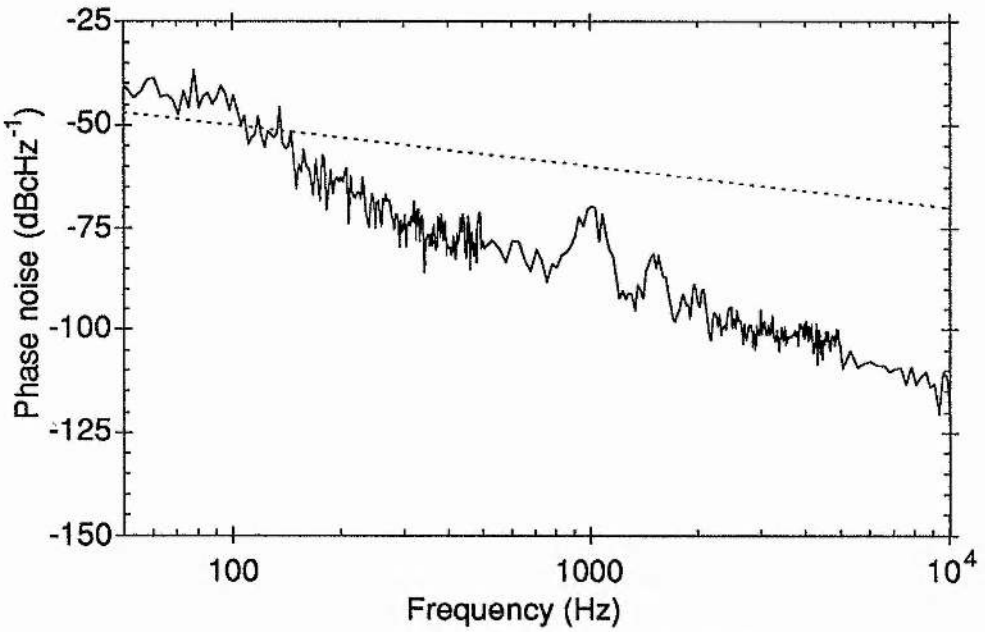

Figure 3.19. Single-sideband phase noise of the synchronously mode-locked NaCl:OH⁻ laser.

Since the phase noise of actively mode-locked lasers predominantly arises from the applied modulation, the source of the large timing jitter present in the Nd:YAG pump laser pulse train was deduced to be the acousto-optic modulator drive electronics. The RF spectrum from the Spectra-Physics Model 452 mode locker driver was measured using the spectrum analyser and this spectrum was compared to the RF spectra obtained from the mode-locked Nd:YAG laser. Figure 3.20 shows, from

bottom up, the signal from the mode locker drive circuitry and the 1st and 10th harmonics of the Nd:YAG pulse train. The close correlation between the shapes of the spectra, together with the 20 dB rise in the sideband power relative to the carrier for the 10th harmonic indicate that the dominant source of timing jitter in the Nd:YAG laser pulse train was, indeed, the mode locker driver unit.

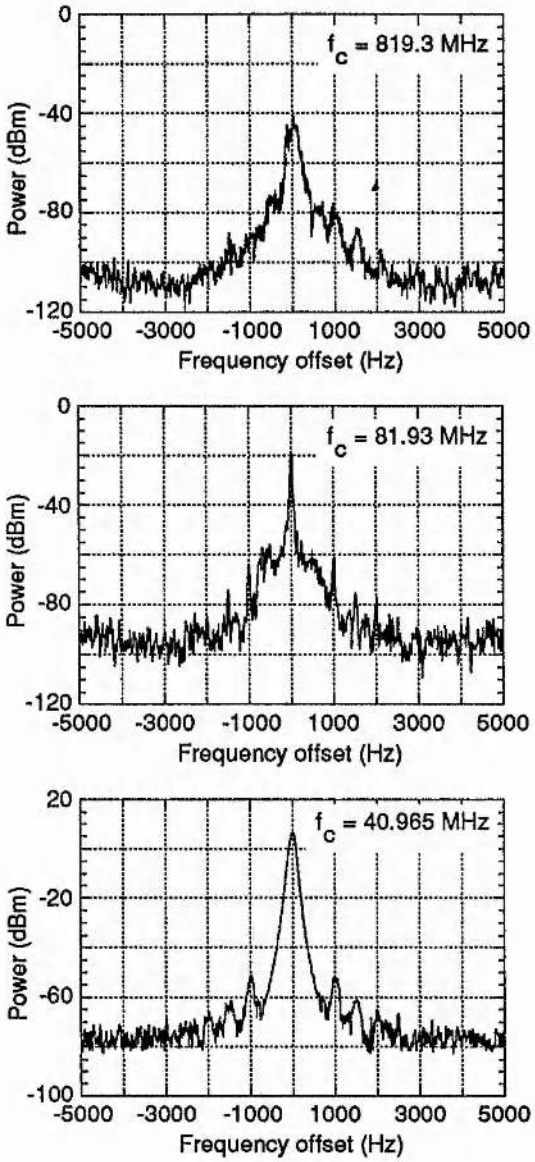

Figure 3.20 RF spectra of the Srectra-Physics frequency synthesiser and the fundamental and 10th harmonics of the coupled-cavity mode-locked laser (from bottom up).

To reduce the phase noise of the Nd:YAG laser, and hence the phase noise of the frequency-referenced mode-locked NaCl:OH⁻ laser, the frequency synthesiser in the Spectra-Physics mode-locker system was replaced by a home-built crystal

oscillator. RF spectra of the oscillator are shown in Figure 3.21, together with the corresponding spectra of the Spectra-Physics synthesiser for comparison.

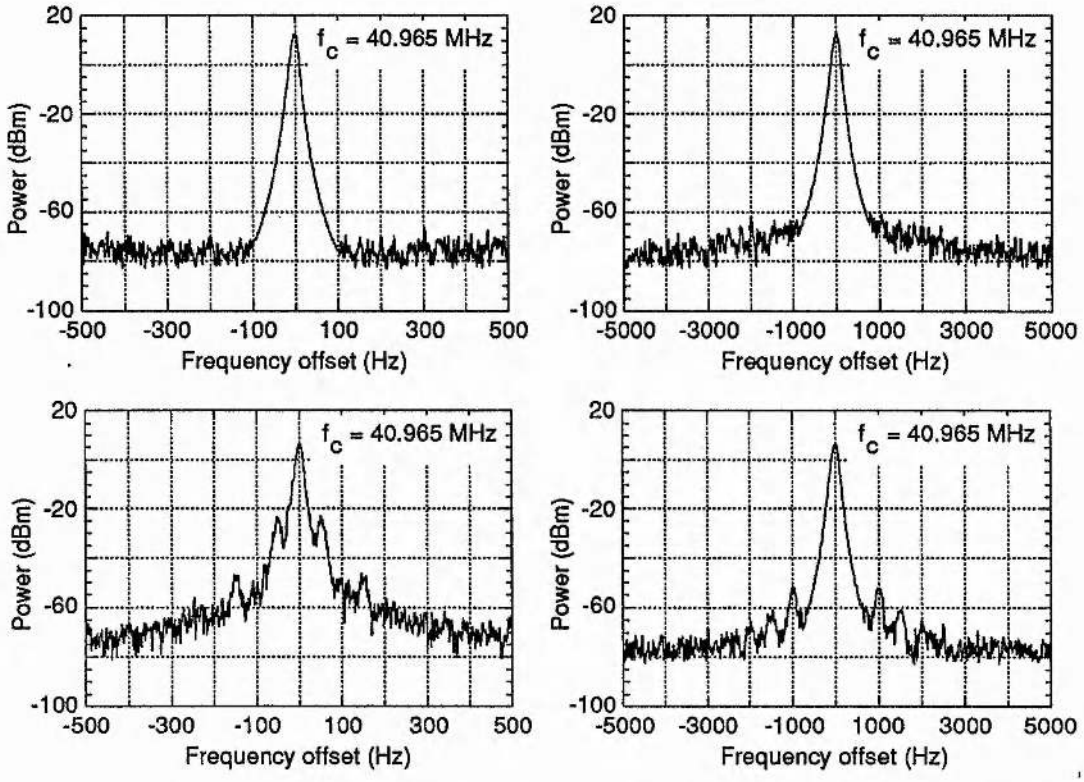

Figure 3.21. RF spectra of the crystal oscillator (top) and the Spectra-Physics frequency synthesiser (bottom).

The single-sideband phase noise of the Nd:YAG laser when mode locked using the low noise crystal oscillator is reproduced as Figure 3.22. The rms timing jitter was 1.7 ps [50 Hz, 500 Hz] and 630 fs [500 Hz, 5 kHz], which represents a phase noise reduction of almost two orders of magnitude. The noise of the coupled-cavity mode-locked laser was subsequently measured and a similar reduction of the phase noise was observed. The single-side band phase noise spectrum for this laser is presented as Figure 3.23 and the rms timing jitter was 1.4 ps [50 Hz, 500 Hz] and 300 fs [500 Hz, 5 kHz]. For these results, the power in the noise sidebands was at least 20 dB less than the limit set by the small signal criterion. The power spectra of the fundamental, 10^{th} and 30^{th} harmonics of the laser output are given in Figure 3.24 for frequency spans of 1 kHz and 10 kHz. The 20 dB and 30 dB rises in the sideband power relative to the carrier observed for the 10th and 30th harmonics respectively, is consistent with the n^2 dependence of the phase noise power with harmonic number.

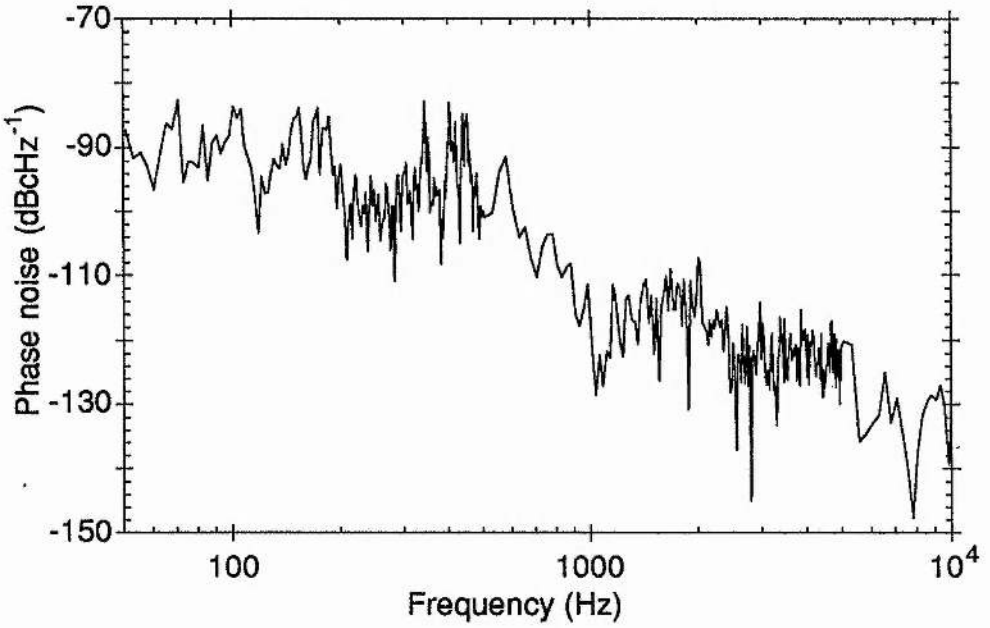

Figure 3.22. Phase noise spectrum of the Nd:YAG laser when its mode locker was driven by a crystal oscillator.

Measurements of the phase noise on the synchronously mode-locked colour-centre laser pulse train were also performed. As expected its phase noise mimicked that of the pump laser with rms timing jitter values of 1.5 ps and 700 fs in the 50 – 500 Hz and 500 Hz - 5 kHz frequency bands respectively.

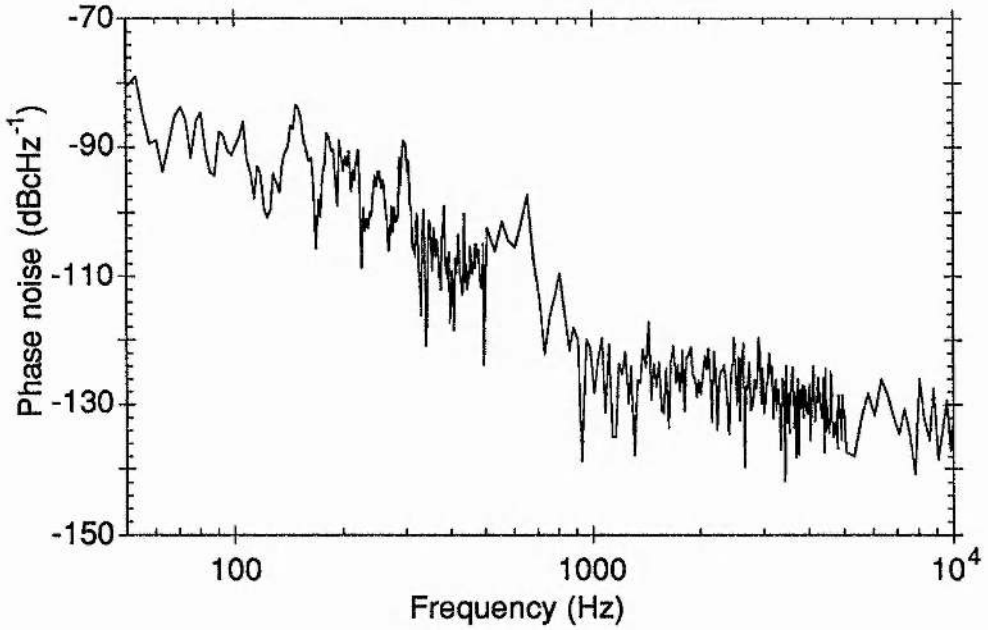

Figure 3.23. Phase noise spectrum of the coupled-cavity mode-locked colour-centre laser when the pump laser mode-locker signal was derived from a crystal oscillator.

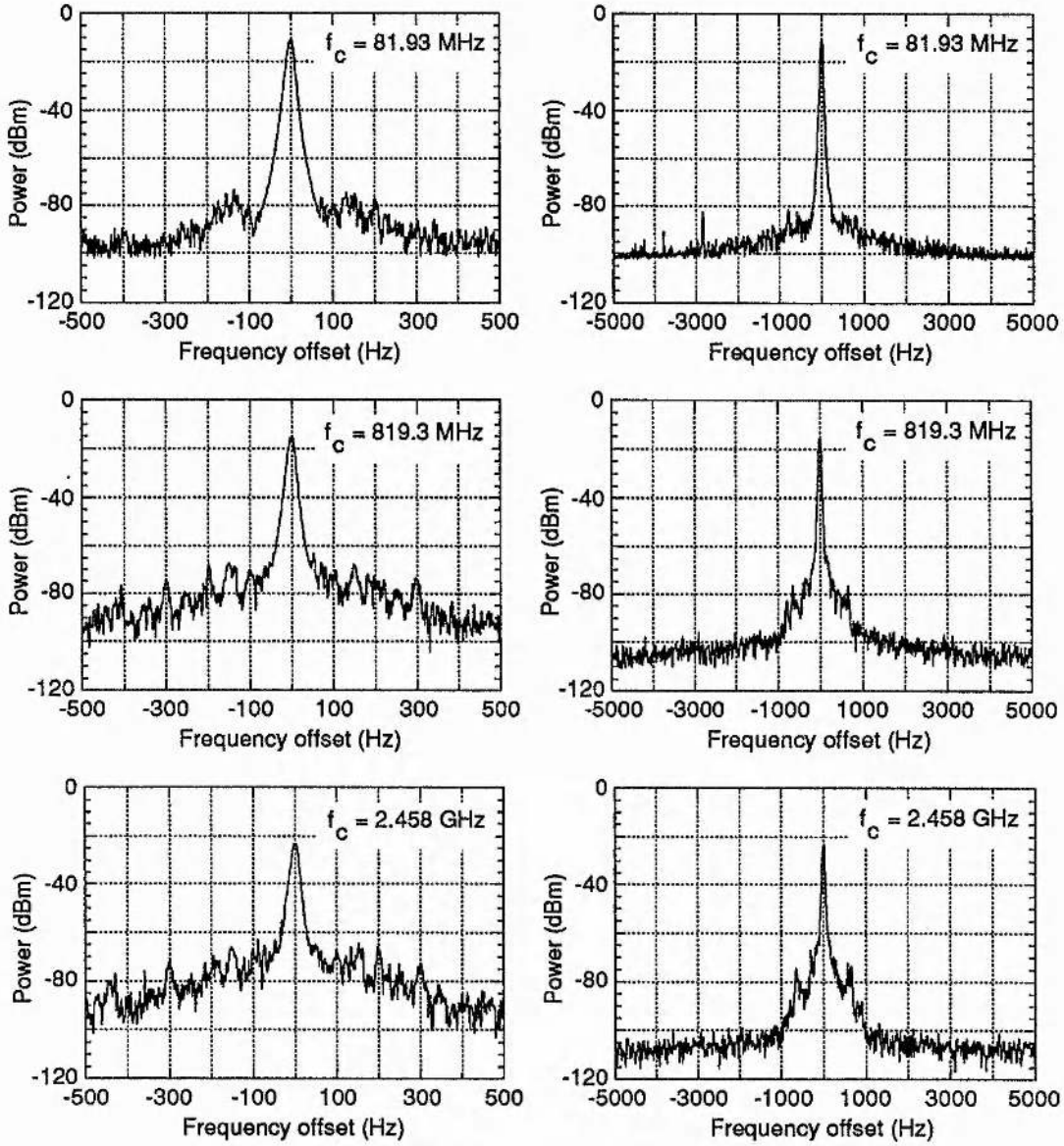

Figure 3.24. Rf power spectra of the fundamental, 10th and 30th harmonics of the mode-locked pulse train for 1 kHz (left) and 10 kHz (right) frequency spans.

This overall reduction of phase noise resulted in an improvement to the stability of the amplitude-stabilised NaCl:OH⁻ laser, since the frequency referencing circuitry did not have to work as hard to follow the frequency fluctuations of the Nd:YAG laser pulse train (since phase noise ≡ frequency noise). The phase noise performance of the lasers is sumarised in Table 3.1.

The timing jitter of this laser was considerably worse than the jitter figures of 170 fs [50 Hz, 500 Hz] and 100fs [500 Hz, 5 kHz] reported for the frequency referenced coupled-cavity mode-locked KCl:Tl^0(1) colour-centre laser by Walker

	Timing jitter (ps)	
	50 - 500 Hz	500Hz - 5 kHz
Nd:YAG (synthesiser)	125	10
(crystal oscillator)	1.7	0.63
Active ML NaClOH⁻ (synthesiser)	170	12
(crystal oscillator)	1.5	0.7
Coupled-cavity NaCl:OH⁻ (synthesiser)	590	10
(crystal oscillator)	1.4	0.3

Table 3.1. Summary of timing jitter values.

et al.[23]. The reasons for this are as follows: The long upper-state lifetime of 1600 ns for the active centres in KCl:Tl^0(1) means that the synchronous pumping causes minimal gain modulation (~0.2%) which does not affect the output of the coupled-cavity laser once mode locking has been established. The phase noise of the pump laser has therefore a greatly reduced influence on the phase noise of the colour centre laser. In their experiments, Walker and co-workers used an acousto-optic 'noise eater' on the output of the Nd:YAG pump laser to reduce its amplitude noise to below 1%. This reduced the phase noise arising from amplitude-to phase noise conversion. For the unreferenced KCl:Tl^0(1) laser this resulted in a phase noise reduction of greater than one order of magnitude. The NaCl:OH^- laser was frequency referenced to the pump laser pulse train, and therefore, its phase noise followed that of the pump laser. In Walker's experiments, the colour-centre laser was directly referenced to the low-noise crystal oscillator. So, to obtain lower phase noise, it would be necessary to further reduce the phase noise of the Nd:YAG laser. Sub-picosecond rms timing jitter values for an acousto-optically mode-locked Nd:YAG laser have been reported by Rodwell *et al.*[26] An electronic phase-locked loop incorporating a voltage-controlled phase-shifter to vary the phase of the RF signal to the mode locker was used to reduce the laser phase noise. This method was first used by Cotter[27] to reduce the phase noise of a mode-locked argon-ion laser.

3.5 Summary

Coupled-cavity mode locking was demonstrated using a nonlinear Fabry-Perot cavity configuration. In this arrangement, a sawtooth modulation was observed on the

output pulse train. The modulation was a result of beating between the colour-centre and Nd:YAG laser pulse trains in the NaCl:OH^- crystal. By frequency referencing the two lasers, the amplitude modulation could be avoided. In order to achieve this, the coupled-cavity laser had to be reconfigured into a nonlinear Michelson cavity arrangement so that its length could be adjusted to equal that of the pump laser whilst maintaining the interferometric matching of the two cavity branches.

The phase noise of the frequency-referenced colour-centre laser was also studied in detail. The phase noise was found to follow that of the mode-locked Nd:YAG pump laser. By replacing the frequency synthesiser in the Nd:YAG mode locker unit with a low noise crystal oscillator, the timing jitter on the Nd:YAG laser pulse train was substantially reduced from 125 ps to 1.7 ps in the 50 Hz to 500 Hz frequency interval. This resulted in a similar reduction to the timing jitter of the coupled-cavity mode-locked NaCl:OH^- laser to 1.4 ps from 50 - 500 Hz and 300 fs from 500 Hz to 5 kHz.

References

1. L. F. Mollenauer and R. H. Stolen, Opt. Lett. **9,** 13 (1984).
2. F. M. Mitschke and L. F. Mollenauer, Opt. Lett. **12,** 407 (1987).
3. F. M. Mitschke and L. F. Mollenauer, IEEE J. Quantum Electron. **QE-22,** 2242 (1986).
4. J. F. Pinto, C. P. Yakymyshyn and C. R. Pollock, Opt. Lett. **13,** 383 (1988).
5. K. J. Blow and D. Wood, J. Opt. Soc. Am. B **5,** 629 (1988).
6. P. N. Kean, R. S. Grant, D. W. Crust, X. Zhu, D. Burns and W. Sibbett, in *Technical Digest of Conference on Lasers and Electro-Optics* (Optical Society of America, Washington, D.C., 1988), paper PD7.
7. P. N. Kean, X. Zhu, D. W. Crust, R. S. Grant, N. Langford and W. Sibbett, Opt. Lett. **14,** 39 (1989).
8. K. J. Blow, D. S. Forrester and B. P. Nelson in Ultrafast Phenomena IV (Springer-Verlag, Berlin, 1988), pp 67-69.
9. K. J. Blow and B. P. Nelson, Opt. Lett. **13,** 1026 (1988).
10. J. Mark, L. Y. Liu, K. L. Hall, H. A. Haus and E. P. Ippen, Opt. Lett. **14,** 48 (1989).
11. F. Ouelette and M. Pichet, Opt. Commun., **60,** 99 (1986).
12. C. P. Yakymyshyn, J. F. Pinto and C. R. Pollock, Opt. Lett. **14,** 621 (1989).
13. P. M. W. French, J. A. R. Williams and J. R. Taylor, Opt. Lett. **14,** 686 (1989).
14. J. Goodberlet, J. Wang, J. G. Fujimoto and P. A. Schulz, Opt. Lett. **14,** 1125 (1989).
15. L. Y. Liu, J. M. Huxley, E. P. Ippen and H. A. Haus, Opt. Lett. **15,** 553 (1990).
16. C. Speilmann, F. Krausz, E. Wintner and A. J. Schmidt, in *Digest of the Topical Meeting on Ultrafast Phenomena* (Optical Society of America, Washington, D.C., 1990), paper PD10.
17. J. K. Chee, E. C. Cheung, M. N. Kong and J. M. Liu, in *Digest of the Topical Meeting on Ultrafast Phenomena* (Optical Society of America, Washington, D.C., 1990), paper MA2.
18. A. Sennaroglu, T. J. Carrig and C. R. Pollock, Opt. Lett. **17,** 553 (1992).
19. V. A. Bhagavatula, M. S. Spotz and W. F. Lowe, Opt. Lett. **9,** 186 (1984).
20. L. F. Mollenauer, N. D. Vieira, and L. Szeto, Phys. Rev. B **27,** 5332 (1983).
21. G. Sucha, Opt. Lett. **16,** 922 (1991).
22. R. S. Grant and W. Sibbett, Opt. Commun. **86,** 177 (1991).
23. D. R. Walker, D. W. Crust, W. E. Sleat and W. Sibbett, IEEE J. Quantum Electron. **28,** 289 (1992).
24. D. von der Linde, Appl. Phys. B **39,** 201 (1986).
25. Hewlett Packard Applination Note No 207.
26. M. J. W. Rodwell, D. M. Bloom and K. J. Weingarten, IEEE J. Quantum Electron. **25,** 817 (1989).
27. D. Cotter, in Ultrafast Phenomena IV, (D. A. Auston and K. B. Eisenthal, Eds. New York: Springer-Verlag, 1984), pp 78-80.

Chapter 4

The Self-Mode-locked NaCl:OH^- Laser

4.21 Introduction.

In Chapter 3, the performance of a coupled-cavity mode-locked NaCl:OH^- laser was described. This passive mode-locking technique converted spectral modulation arising from the optical Kerr effect in an optical fibre into amplitude modulation using interference obtained by constructing the laser as an interferometer. In this chapter, a further passive mode-locking technique which resulted in the sub-100 fs duration pulses from the NaCl:OH^-, laser is described. This technique, called self-mode locking, also utilises the optical Kerr effect, but does not rely upon interference, rendering coupled cavities (and the associated stabilisation electronics) unnecessary. Following a brief review of self-mode locking, a discussion of the physical mechanisms involved in the self-mode locking process is presented. The laser design, including intracavity group-velocity dispersion compensation, is discussed, and the overall performance of the mode-locked laser is described.

The first observations of self-mode locking were reported in 1990 by Spence and co-workers[1,2] They observed self-mode locking in a commercial Ti:Al_2O_3 laser[3] thats resonator had been extended to 2m long. Pulses of 2 ps duration were obtained from the laser with no active mode-locking elements within the cavity. These pulses were strongly frequency chirped (~ 10 times the transform-limited duration bandwidth product) as a result of the combined actions of self-phase modulation and normal group-velocity dispersion in the Ti:Al_2O_3 crystal. By employing intracavity group-velocity dispersion compensation using a prism pair made from SF14 glass, the mode-locked pulse duration was reduced to 60 fs. It was observed that the laser operated in two transverse modes and that a mechanical perturbation to the laser cavity was required to start the mode-locking process. Simultaneously, there were also reports of anomalously short pulse durations from actively and passively mode-locked Ti:Al_2O_3 lasers.[4-7]

At that time the mode-locking process was unclear. It was suggested that mode locking may be a result of interference between two transverse modes of the laser resonator[8,2] or two polarisations in a similar manner to coupled-cavity mode locking. For this case the two cavities were superimposed and therefore were always

the same length, removing the need for active cavity length control. The role of solitonic pulse shaping was also suggested[5].

The following year Negus[9], Salin[10] and Piche[11] published theories predicting that mode locking was a result of beam shaping in the laser cavity arising from self-focusing in the gain medium. Subsequently self-mode locking was reported for Nd:YLF[12], Nd:YAG[13], Cr:LiSAF[14,15], Cr:LiSCAF, Cr:LiCAF[16] and Cr:forsterite[17] laser systems. For some of these systems[12,18] , there was insufficient self-focusing in the gain medium to obtain self-mode locking and so an additional nonlinear element was included in the laser cavity.

By taking steps to minimise the third-order dispersion in the laser cavity by reducing the length of the gain medium and selecting suitable prism material pulse durations of 10.9 fs were obtained from a self-mode-locked Ti:Al_2O_3 laser[19]. This is the shortest pulse ever generated directly from a laser.

4.2 Mechanisms for mode locking.

Two pulse shortening mechanisms have been proposed for the generation of stable, self-mode-locked pulses. Both mechanisms can be attributed to the optical Kerr effect.

4.2.1 Self-focusing / defocusing of the intracavity beam.

The optical Kerr effect in the nonlinear element induces a varying refractive index across the laser beam. This manifests itself as an intensity-dependent lens: For a material with a positive Kerr coefficient ($n_2 > 0$) the lens is converging and the laser beam is said to be self-focused, and conversely for negative n_2 values, a diverging lens is created and the beam is self-defocused.

For a converging lens, the focal length of the nonlinear Kerr lens may be roughly approximated by assuming a self-induced quadratic index variation across the beam.[20]

The focal length is given by:-

$$f_{nl} = \frac{\pi a \omega_o^4}{8 n_2 n_o P_o z} \tag{4.1}$$

where: ω_0 is the 1/e amplitude beam radius,
P_o is the instantaneous peak power,
n_2 is the Kerr coefficient,
n_o is the background refractive index,
z is the interaction length

and a is a correction factor which accounts for the difference between the assumed quadratic index profile and a gaussian index profile ($3 < a < 7$).

Assuming the interaction length to be the confocal parameter of a Gaussian beam, waist ω_o *i.e.*

$$z = \frac{\pi n_o \omega_o^2}{\lambda} \tag{4.2}$$

the focal length of the lens may be expressed as

$$f_{nl} = \frac{\lambda a \omega_o^2 \tau_p P_{ave}}{8 n_2 n_o T_p} \tag{4.3}$$

where: τ_p is the pulse duration, P_{ave} is the average power and T is the period of the laser pulses. Assuming a beam waist of 20 μm, n_2 = 32 x 10-20 m^2W^{-1}, n_o = 1.9, P_{ave} = 1 W, T = 12.5 ns, and a=5. The focal length of the lens is 6.5 mm for a 150 fs pulse, 6.5 cm for a pulse of 1.5 ps duration and 4.3 m for a pulse duration of 100 ps.

The intensity-dependent lens causes a change in the resonator stability characteristics. If the change in the resonator stability is such that the output power from the laser is greater when self-focusing occurs then self mode locking may result.

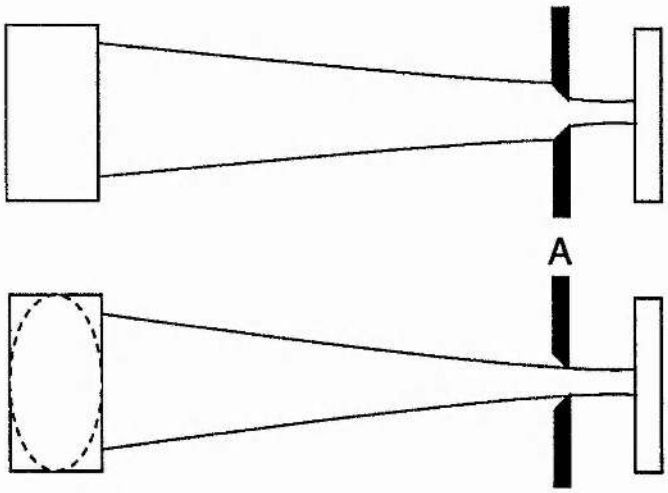

Figure 4.1. Schematic representation of the construction of a fast saturable absorber using the effect of self focusing and an aperture.

This geometrical effect is simply illustrated by considering the combined action of self-focusing in a nonlinear element and an intracavity aperture, shown in Figure 4.1.

CW laser operation is illustrated in top section of Figure 4.1: The peak intracavity intensity is low. The focal length of the Kerr lens is many times the length of the laser cavity and therefore has a negligible effect on the resonator stability. The insertion of an aperture at A constricts the transverse mode of the laser beam and reduces the output power of the laser. In effect, the insertion of the aperture can be regarded as the introduction of an intracavity loss.

If an intense pulse is excited in the laser, the focal length of the Kerr lens decreases. This causes a reduction in the spot size of the beam at A, thereby reducing the effect of the intracavity aperture and causing a reduction of the intracavity loss. Since the optical Kerr effect is essentially instantaneous, the reduction in the intracavity loss only occurs for the duration of the intense feature. This is entirely analogous to the action of a fast saturable absorber.

In practice, an intracavity aperture is not always required as the beam shaping introduced by the intensity-dependent lens may cause changes in the size and/or location of the beam waist in the gain medium.

4.2.2 Self-phase modulation and group velocity dispersion.

As a consequence of the high intensities that occur within self-mode-locked laser cavities, the circulating pulses will experience considerable self-phase modulation. This, together with the observation that stable femtosecond duration pulses can only obtained for cavities possessing overall anomalous group-velocity dispersion, has led to the suggestion that solitonic effects play an important role in the self-mode-locking process. These effects have been observed in passively mode-locked dye lasers[21,22]. However, although the combined actions of SPM and anomalous GVD can result in pulse shortening, they cannot be solely responsible for mode locking, since the processes do not discriminate against inter-pulse radiation. An additional amplitude modulation is required to ensure that there is a net loss before and after the mode-locked pulse. Furthermore, for the long pulse durations and low intracavity peak powers present during the initial stages of mode locking there would be negligible solitonic effects. Therefore, although the interplay between SPM and GVD determines the steady-state pulse duration it only becomes important once the mode-locked pulse sequence has been established.

4.3 Initiation of the self-mode-locking process.

In the previous section it was described how the action of self-focusing of the intracavity beam together with the appropriate cavity geometry leads to pulse shaping and mode-locking. To start the mode-locking process, however, an initial primitive pulse (or noise burst) of sufficient intensity to cause some self-focusing in the nonlinear element is required. Several methods to initiate self-mode-locking have

been reported. These are: (i) A mechanical perturbation to the laser, (ii) passive amplitude modulation and (iii) active amplitude modulation.

(i) For many self-mode-locked lasers, a mechanical perturbation to the laser cavity, such as tapping a cavity mirror mount, can generate a noise burst of sufficient intensity to start the mode-locking process. Although this is a simple and easy way to initiate mode locking, the laser will only remain mode locked for a short time until a further perturbation will cause the mode locking to cease.

(ii) The inclusion of a saturable absorber in the laser cavity can produce an intense, primitive pulse to start self-mode locking[5]. Mode locking has been reported for organic dye or semiconductor-doped glass[23] saturable absorbers. This method of initiation may compromise the tuning range of the laser since the absorption is wavelength dependent. However, the amplitude modulation required to obtain the primitive pulse is generally small. In this instance, weak absorber solutions or thin samples of doped glass may be used to initiate the mode locking. This has enabled absorber solutions containing several different organic dyes to be used to initiate mode-locking, reducing the wavelength tuning restrictions of the laser.[24]

(iii) Active amplitude modulation is commonly used to initiate self-mode locking. Two methods are generally used: Gain modulation by synchronous pumping[25], and loss modulation using an acousto-optic modulator[26]. One disadvantage of using active modulation to start self-mode locking arises from the passively mode-locked nature of self-mode-locked lasers. The pulse-repetition frequency of the laser is determined primarily by the optical path length of the laser cavity. This may be a slightly different frequency to the applied modulation, and a low-frequency modulation on the output of the laser will result.

Both synchronous pumping and acousto-optic loss modulation were used to initiate self-mode locking of the NaCl:OH^- colour-centre laser and will be described later.

4.4 Optical properties of Schott SF59 glass.

For the NaCl:OH^- colour-centre laser, the relatively low intracavity powers and short crystal length resulted in insufficient self-focusing to cause self-mode locking. It was therefore opted to include an additional nonlinear element within the laser cavity, similar to that used by Malcolm and co-workers, to facilitate self-mode locking in a Nd:YLF laser[12].

Schott Glass Works produce a range of lead-silicate optical glasses. These glasses have an enhanced nonlinear index of refraction compared to fused silica. The enhancement arises from the highly polarisable Pb^{2+} cations in the glass structure and increases with increasing lead content. Schott SF59 glass is one of this category glasses. It contains approximately 50 % mol PbO resulting in a density of 6.26 gcm^{-3}

(~ 2.5 times that of fused silica). The glass is transparent from 400 nm to beyond 2.5 μm. The linear refractive index is 1.90 at a wavelength of 1550 nm.

4.4.1 Kerr coefficient of SF59 glass.

The Kerr coefficient of SF59 glass has been measured by several groups[27-29]. It has been determined using the method of degenerate four-wave mixing [Ref. 28,29] and by a dual-wavelength pump-probe technique [ref. 27]. Reported values for n_2 are given in Table 4.1. All the measurements were performed at wavelengths considerably shorter than 1.55 μm.

Wavelength (nm)	n2 (x $10^{-20}m^2W^{-1}$)	Measurement method	Reference	n2 predicted by ref 30
650	32	Pump-probe	27	157
1064	70	DFWM	28	111
1064	54	DFWM	29	111

Table 4.1. Reported measurements of the Kerr coefficient of SF59 glass.

Recently Sheik-Bahae *et al.*[30] published a model which predicts the magnitude and dispersion of the Kerr coefficient for semiconductors and wide-bandgap solids. The dispersion of n_2 scales with the fourth power of the bandgap energy, as predicted by Wherrett[31]. The model takes account of contributions to n_2 arising from two-photon absorption, Raman transitions and the Stark effect. The scaled form of n_2 is given by[30]

$$n_2 = \frac{4\pi}{cn_o} K' \frac{\sqrt{E_p}}{n_o E_g^4} G_2\left(\frac{\hbar\omega}{E_g}\right) \tag{4.4}$$

where: c is the velocity of light (= 3 x 10^8 ms^{-1}),
K' is a material-independent constant = 0.86 x 10^{-8},
E_g is the band gap of the solid in eV,
$G_2\left(\frac{\hbar\omega}{E_g}\right)$ is the dispersion function for n_2 given in Appendix 2
and E_p is 21 eV for most materials.

Using equation 4.4, it was possible to calculate n_2 given the bandgap energy. From the transmission data for SF59[32], E_g was estimated to be 3.3 eV. The variation

of the Kerr coefficient with wavelength is shown in Figure 4.2. where the large enhancement of n_2 around 750 nm arises from the two-photon contribution to the Kerr coefficient.

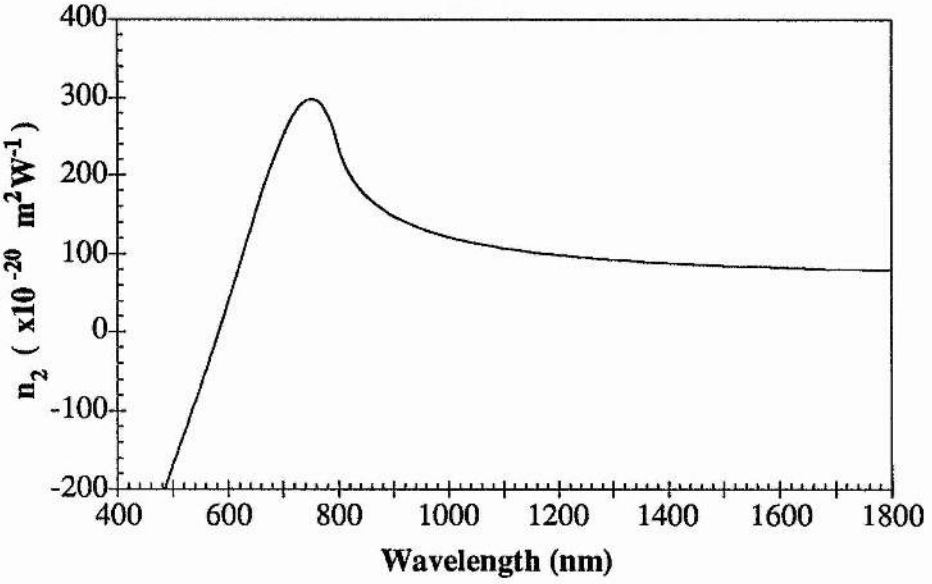

Figure 4.2. Dispersion of the Kerr coefficient of SF59 glass calculated from Reference 30

4.4.2 Experimental determination of the group-velocity dispersion of the SF59 glass

When the self-mode-locked laser was initially designed, only a Cauchy style expansion was available for the refractive index of the SF59 glass. This expansion is only accurate from 365 nm to 1014 nm and so it was necessary to determine the GVD of the SF59 glass experimentally.

In Chapter 1. it was stated that if a transform-limited, Gaussian pulse is propagated through a dispersive medium, it maintains its Gaussian profile but is temporally broadened by the factor:

$$\frac{T_{out}}{T_{in}} = \left[1 + \left(\frac{\beta_2 z}{T_{in}^2}\right)^2\right]^{\frac{1}{2}} \qquad 4.5$$

where T_{in} and T_{out} are the input and output pulse durations respectively (fs), z is the path length in the material (mm), and β_2 is the GVD of the material (fs^2mm^{-1}).

An attempt was made to measure the GVD of the SF59 glass by propagating pulses of 90 fs duration (FWHM) through the SF59 glass and measuring the ratio of

the dispersed pulse duration to the input pulse duration. The test pulses were obtained from a coupled-cavity mode-locked KCl:Tl^0(1) laser operating at a wavelength of 1516 nm. However, when these pulses were propagated through a fused silica rod, pulse narrowing was observed. This indicated that the pulses from the laser were not, in fact, transform limited but possessed an initial frequency chirp. It was therefore necessary to ascertain the magnitude to this chirp before the GVD of the SF59 glass could be evaluated.

A frequency-chirped, Gaussian, pulse may be represented by[33]

$$U(0,T) = \exp\left(-\frac{1+ic}{2}\frac{T^2}{T_0^2}\right) \tag{4.6}$$

where c is a chirp parameter; $c > 0$ representing upchirp, $c < 0$ downchirp and T_0 is the pulse duration, related to the fwhm pulse duration by $T_{fwhm} = 1.665T_0$. After propagation through a dispersive medium, the pulse still retains its Gaussian profile but is broadened by the factor

$$\frac{T_{out}}{T_{in}} = \left[\left(1+\frac{c\beta_2 z}{T_0^2}\right)^2 + \left(\frac{\beta_2 z}{T_0^2}\right)^2\right]^{\frac{1}{2}} \tag{4.7}$$

It can be seen from equation 4.7 that the pulse broadening as a function of z depends upon the signs of β_2 and c. If β_2 and c are of the same sign, the pulse always broadens with increasing z. However, if β_2 and c are of opposite signs the pulse initially narrows and then broadens as z increases. To determine c, the laser beam was propagated through two different lengths of fused silica rod of known GVD and $\frac{T_{out}}{T_{in}}$ was measured. Values for z, β_2 and $\frac{T_{out}}{T_{in}}$ are given in Table 4.2.

Material	Length (mm)	β_2 (fs^2mm^{-1}) (λ=1516 nm)	$\frac{T_{out}}{T_{in}}$
SiO_2	100	-24.03	0.87
SiO_2	200	-24.03	1.52
SF59	8.45	?	1.23

Table 4.2. Ratio of input and output pulse durations after propagating through various lengths of fused silica and the SF 59 glass.

Squaring equation 4.7, expanding and substituting values for z β_2 and $\frac{T_{out}}{T_{in}}$ gives for the 100 mm and 200 mm long fused silica rods

$$\left(100\frac{\beta_2}{T_0^2}c\right)^2 + 200\frac{\beta_2}{T_0^2}c + \left[1+\left(100\frac{\beta_2}{T_0^2}\right)^2 - 0.87^2\right] = 0 \qquad (4.8)$$

$$\left(200\frac{\beta_2}{T_0^2}c\right)^2 + 400\frac{\beta_2}{T_0^2}c + \left[1+\left(200\frac{\beta_2}{T_0^2}\right)^2 - 1.52^2\right] = 0 \qquad (4.9)$$

Multiplying 4.8 by -4 and adding to 4.9 gives $c = 0.746$

Substituting c into equation 4.7 along with z and $\frac{T_{out}}{T_{in}}$ yields a quadratic equation in β_2 which, when solved gives

$$\beta_2 = +99.7 \text{ or } -455.4 \text{ fs}^2 \text{ mm}^{-1} \qquad (4.10)$$

To determine which root of the equation corresponds to the correct value for β_2, the pulses from the laser were negatively chirped by passing them through the 200 mm long fused silica rod. The pulses were then propagated through the SF59 glass. It was noted that the broadening was reduced from a factor of 1.52 to 1.13, indicating that the Schott glass had a dispersion of opposite sign to fused silica; i.e. $\beta_2 = +99.7$ fs^{2}mm^{-1} at 1516 nm.

Subsequent to these measurements Schott Glass published a new catalogue which included Sellmeier expansions for all their glasses. Calculating β_2 from their expansion gave $\beta_2 = +101.1$, in close agreement with the experimentally obtained value.

4.5 Modelling of the laser cavity.

To obtain a qualitative understanding of how self-focusing in the nonlinear element affects the stability of the laser resonator, a simple gaussian-beam analysis of various cavity configurations was undertaken.

Initially the asymmetric four-mirror cavity illustrated in Figure 4.3 was analysed. The cavity consisted of two plane end mirrors (M1, M4) and a focusing section comprising two -10 cm radius of curvature (RoC) mirrors. In the analysis, the size of the beam waists at the end mirrors and the size and location of the waist in the focusing section were calculated as the separation of the focusing mirrors was varied.

The length of the longer cavity arm was 122 cm and the overall length of the resonator was maintained at 183 cm by adjusting the shorter arm of the cavity. This length was chosen so that the laser could be acousto-optically mode locked using standard modulators and electronics or synchronously pumped by a main-frame Nd:YAG laser. The results of this analysis are shown in Figure 4.4. It is apparent that there are two stability regions for this cavity: a region where the beam is focused onto mirror M4, and a region where the beam is collimated onto M4.

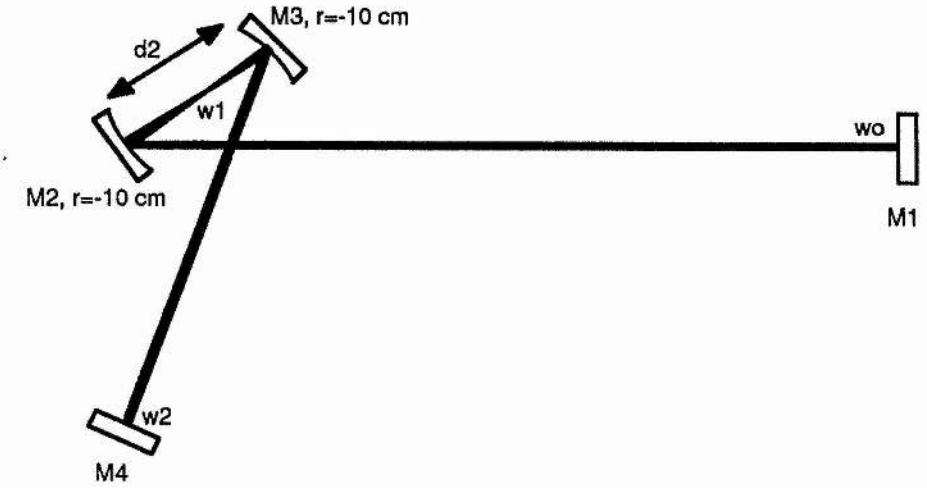

Figure 4.3. The four -mirror resonator.

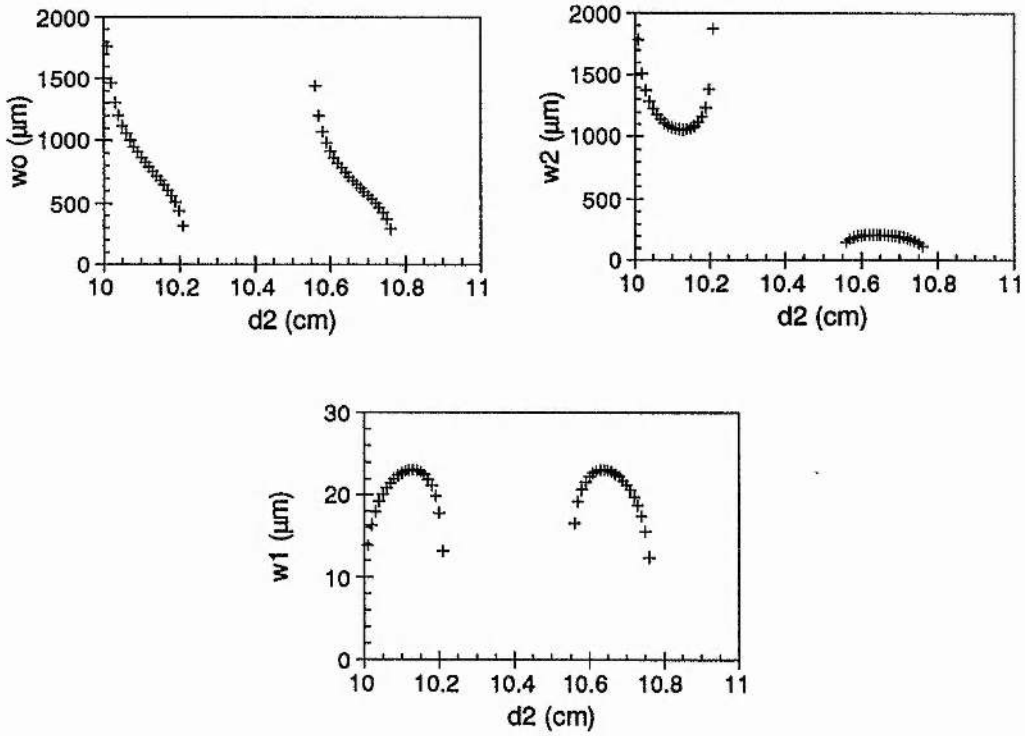

Figure 4.4. Beam waist sizes for the four-mirror cavity.

The six-mirror cavity illustrated in Figure 4.5 was then analysed. This cavity was constructed from two plane end mirrors (M1, M6), a focusing section around the gain medium consisting of two -10 cm RoC mirrors (M2, M3) and a tighter focusing section encompassing the nonlinear glass constructed from -5 cm RoC mirrors (M4, M5). In the model, the separation of the -10 cm RoC mirrors was kept constant at 10.13 cm. This corresponds to the centre of the stability range for the four-mirror cavity when the beam is collimated onto M4. Beam waists and locations were calculated as the separation of the -5 cm RoC mirrors was varied for several distances between the two focusing sections. Again the overall cavity length was maintained at 183 cm.

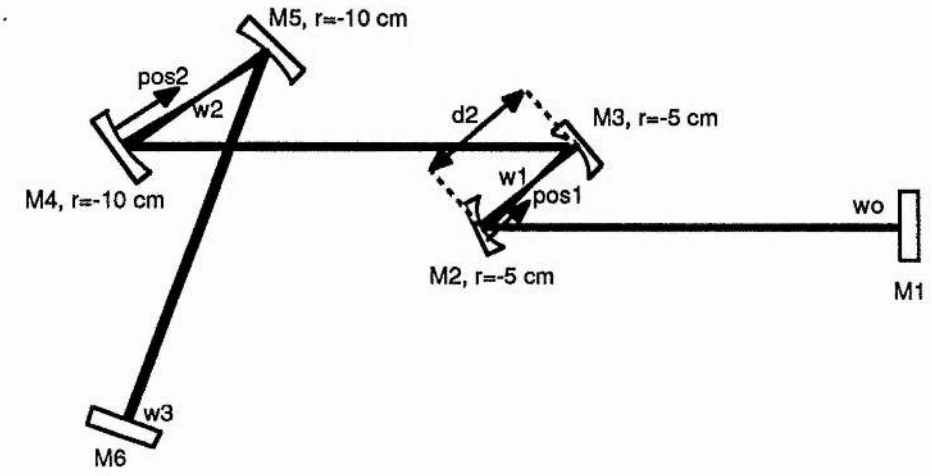

Figure 4.5. The six-mirror resonator.

It was noted that there were two stability regions for this laser resonator. The extent and separation of these regions varied with the separation of the two focusing sections. When these sections were approximately 55 cm apart, the stability regions merged. Also, the total stability range of the resonator was a maximum for this separation. For this configuration, Figure 4.6 shows graphs of beam waist sizes and locations as a function of the separation of the -5 cm RoC mirrors.

The effect of self-focusing within the laser resonator was subsequently modelled by including a converging lens with a 5 cm focal length between the -5 cm RoC mirrors. In the model, the separation of the -10 cm RoC mirrors was 10.13 cm and the distance between the focusing sections was 54.5 cm. The dimensions of the waists at the end mirrors and the sizes and locations of the beam waists between the focusing mirrors was calculated as the separation of the -5 cm RoC mirrors was varied. These calculations were performed for various locations of the converging lens within the tight-focusing section. The data for the waist sizes and positions was

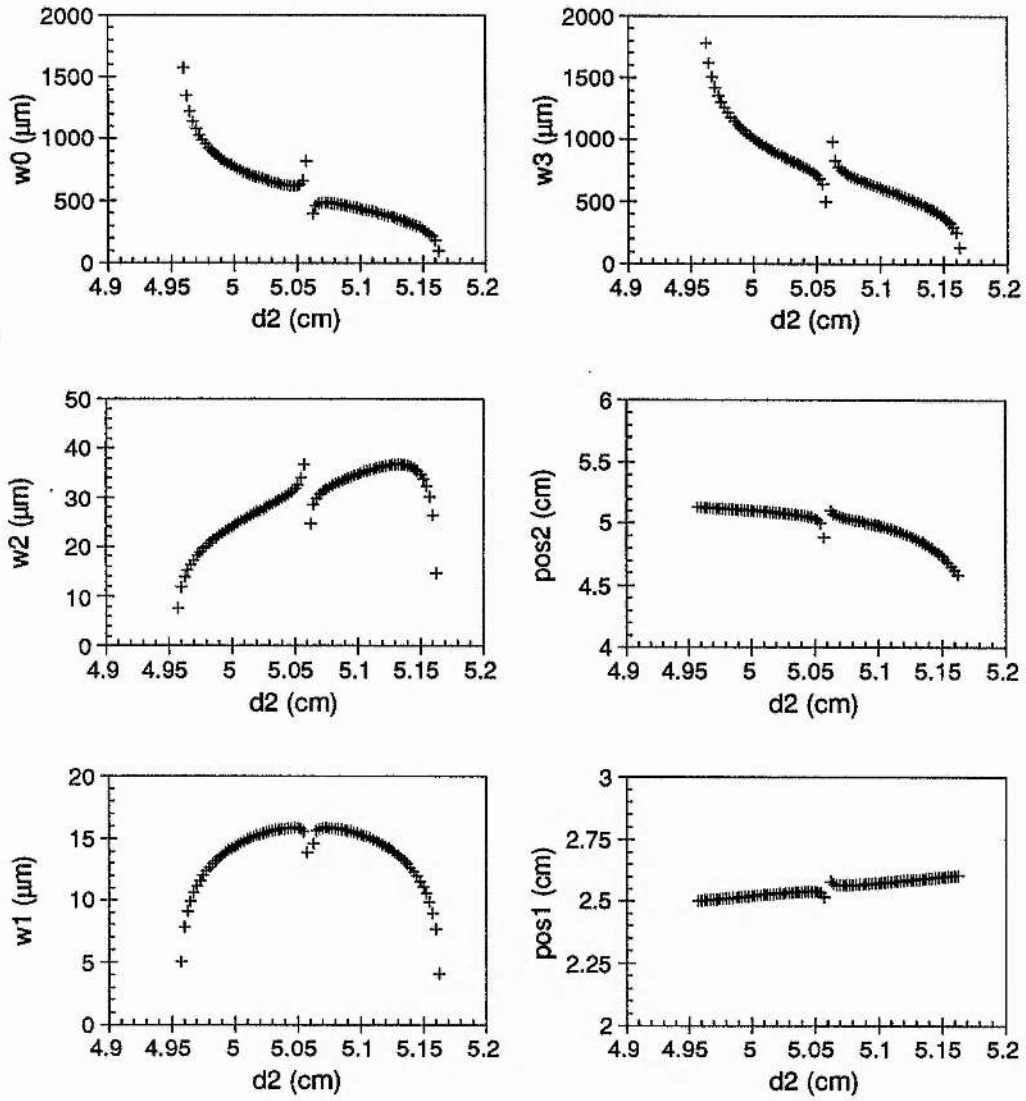

Figure 4.6. Beam waist sizes and locations for the six-mirror cavity. The distance between M1 and M2 is 55 cm.

divided by the corresponding data previously obtained for the six-mirror resonator in the absence of self-focusing (i.e. without the converging lens).

Results obtained for three different locations of the lens between the -5 cm RoC mirrors are shown in Figures 4.7, 4.8 and 4.9; Fig. 4.7 shows the fractional change in the beam waist sizes when the lens is placed 45 % of the distance between M2 and M3 (*i.e.* closer to M2); Fig. 4.8 shows data obtained when the lens is placed in the centre of M2 and M3; and Fig. 4.9 shows data for the lens placed 55 % of the distance between M2 and M3.

Large changes in waist sizes occur for both asymmetric lens locations (Figs 4.7 and 4.9). This indicates that the insertion of an aperture at one of the resonator end mirrors may cause mode locking. However, when the lens is placed in

the centre of the focusing section, the changes in the waist sizes are small as shown in Fig. 4.8 (note the change in scale).

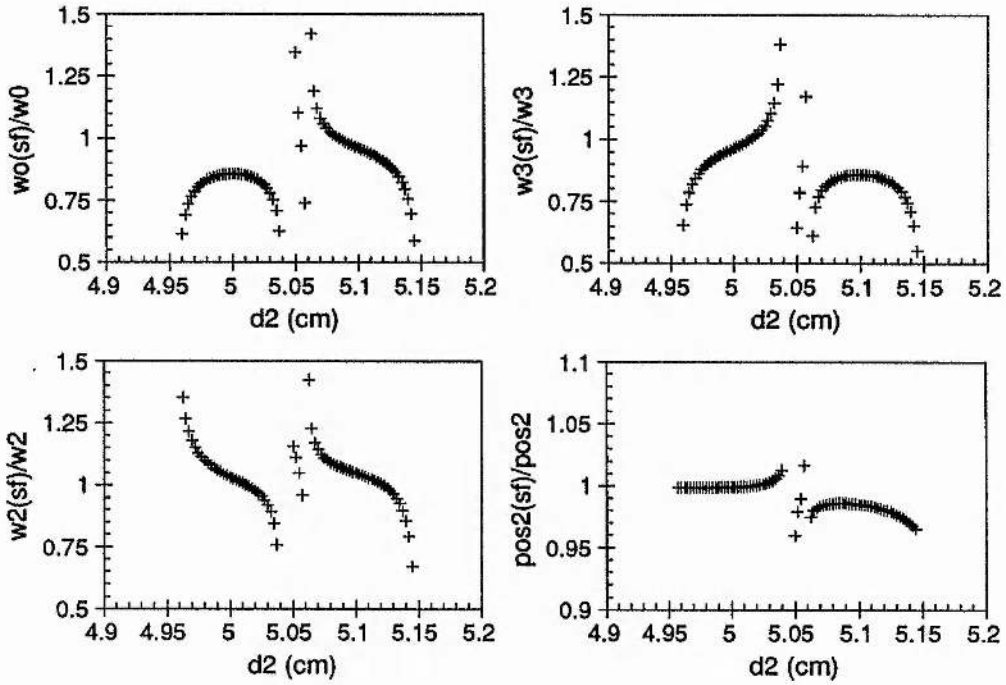

Figure 4.7. Beam waist sizes and locations when a 5 cm focal length lens in included asymmetrically in the tight focusing section. The lens is located towards mirror M2.

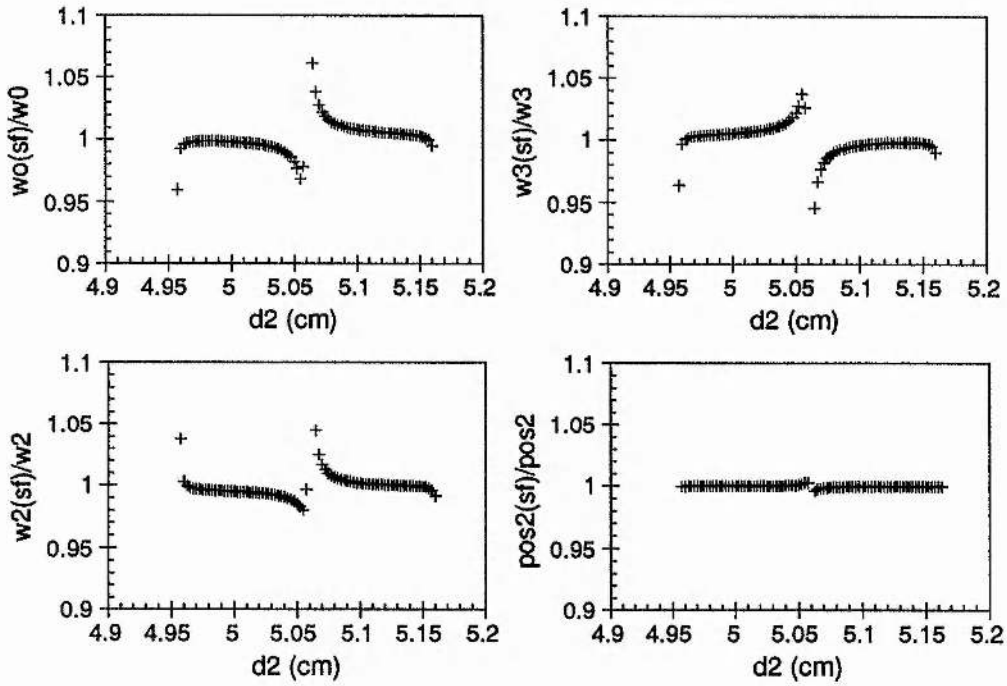

Figure 4.8. Beam waist sizes and locations when a 5 cm focal length lens in included at the centre of the tight focusing section.

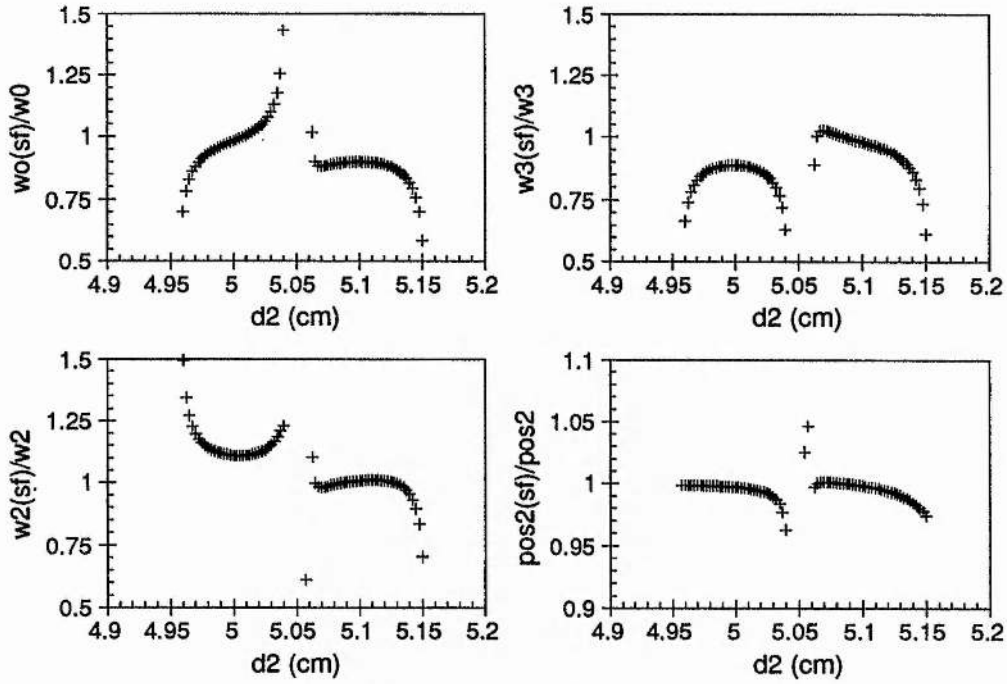

Figure 4.9. Beam waist sizes and locations when a 5 cm focal length lens in included asymmetrically in the tight focusing section. The lens is located towards mirror M3.

It should be stressed that this modelling was undertaken to give a basic, qualitative understanding of the effects of lensing within the resonator. The model did not take into account any intracavity elements such as the colour-centre crystal, prism sequences or birefringent filters. In particular, the effect of astigmatism introduced by off-axis spherical mirrors was not included. This effect is of importance since, even in an astigmatically compensated resonator design, the beam has different saggital and tangential dimensions within the focusing sections. The lack of circular symmetry in the beam would cause the intensity-dependent lens to have different powers in the two planes. This makes the insertion of an intracavity slit, rather than an aperture, more effective in discriminating between mode-locked and cw operation.

4.6 Group-velocity dispersion compensation of the self-mode-locked laser.

The interaction of self-phase modulation (SPM) and group-velocity dispersion (GVD) is fundamental to the generation of femtosecond duration pulses from self-mode-locked lasers. Knox[34] has measured the complete intracavity dispersion of a self-mode-locked Ti:Al_2O_3 laser by measuring the pulse repetition frequency of the laser as a function of the oscillation wavelength. He reported that mode locking could only be obtained for a certain region of anomalous GVD. Outwith this region, the mode locking became unstable with cw spikes appearing in the laser output. It is

therefore necessary to control the net GVD of self-mode-locked lasers for optimum stability and performance.

A prism sequence is an attractive means of adjusting the intracavity GVD of femtosecond lasers[35]: It has low insertion loss since the prisms are used at minimum deviation (chosen to be Brewster's angle). It can be operated independently from other cavity elements and, with an appropriate choice of prism material, can contribute positive or negative GVD to the laser cavity. If the laser is operated in a ring cavity geometry, a four prism sequence is required as shown in Figure 4.10. Whereas, in a linear arrangement, only two prisms are required as an end mirror can be placed in the plane of symmetry indicated by SS'. If the output is taken after the prism pair, it will be spectrally dispersed and an additional prism pair, external to the laser, will be required to recombine the output.

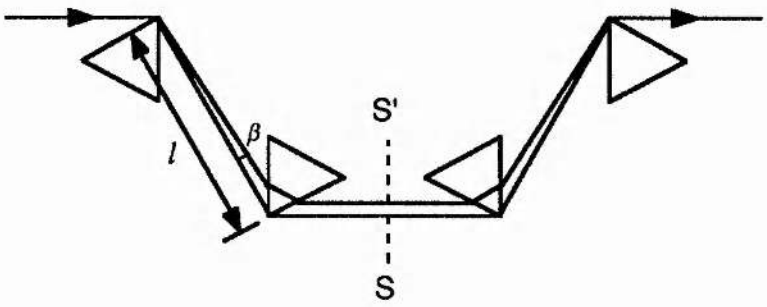

Figure 4.10. A four-prism sequence (adapted from Ref **35**)

There are two contributions to the GVD of a prism sequence: The GVD of the prism material itself and a geometrical contribution introduced by the wavelength dependence of the optical path length, P, between the prisms. Fork *et al.*[35]. showed that the geometrical contribution to the GVD from a prism pair is given by

$$\frac{d^2\phi}{d\omega^2} = \frac{\lambda^3}{2\pi c^2}\frac{d^2P}{d\lambda^2} \tag{4.11}$$

where $\frac{d^2P}{d\lambda^2}$ is the second derivative of the path length with respect to wavelength. This may be approximated to

$$\frac{d^2P}{d\lambda^2} = 2l\left\{\left[\frac{d^2n}{d\lambda^2} + \left(2n - \frac{1}{n^3}\right)\left(\frac{dn}{d\lambda}\right)^2\right]\sin\beta - 2\left(\frac{dn}{d\lambda}\right)^2\cos\beta\right\} \tag{4.12}$$

where l is the prism separation, n is the refractive index of the prism material and β is the angle between the two spectral components considered. In general β is of the order of the angular deviation of the ray bundle, which is small, and so cos β ~1 and l sin β may be approximated to twice the spot size (~ 3 mm in this case). Values for n, and its derivatives with respect to wavelength can be obtained from Sellmeier expansions for the prism material. Table 4.3 shows values for n, $\frac{dn}{d\lambda}$ and $\frac{d^2n}{d\lambda^2}$ for fused silica in the 1500 to 1600 nm wavelength range, calculated from the expansion given by Malitson[36]. Substituting in 4.11 gives (at 1575 nm)

$$\frac{d^2\phi}{d\omega^2}(\text{mm}\cdot\mu\text{m}^{-1}) = -170.6 - 4.04l\ (\text{mm}) \tag{4.13}$$

(For a four-prism sequence the geometrical GVD is, by symmetry, twice that for a pair of prisms.)

The GVD contribution from the prism material is simply

$$\frac{d^2\phi}{d\omega^2} = \frac{\lambda^3}{2\pi c^2}\frac{d^2n}{d\lambda^2}L \tag{4.14}$$

where L is the path length in the prisms. The GVD is ~ 31.0 fs^2 per 1 mm of silica.

Combining this with equation 4.13 gives the net GVD of the prism sequence

Wavelength (nm)	n	$\frac{dn}{d\lambda}$ (μm^{-1})	$\frac{d^2n}{d\lambda^2}$ (μm^{-2})
1500	1.44461	-0.01178	-0.00373
1525	1.44432	-0.01187	-0.00400
1550	1.44402	-0.01198	-0.00425
1575	1.44372	-0.01209	-0.00449
1600	1.44341	-0.01220	-0.00471

Table 4.3. Dispersion data for fused silica calculated from Ref. 36.

4.7 Experiment

The cavity configuration shown schematically in Figure 4.11 has been assessed. It was based upon the resonators modelled earlier in this chapter. A four-mirror cavity with arm lengths of 122 cm and 51 cm was first constructed. The

spacing of the -10 cm RoC mirrors around the NaCl:OH- colour-centre crystal was adjusted such that the laser operated in the centre of the stability region where the beam was collimated onto mirror M6. A focusing section comprising two -5 cm RoC mirrors and an 8.45 mm long rod of SF59 glass was inserted into the longer arm of the cavity. The SF59 glass was mounted on a translation stage with 25 mm travel such that its position relative to the beam waist could be adjusted. Although the geometry of the cryostat prevented full astigmatic compensation of the four-mirror cavity, the residual astigmatism could be removed by adjusting the angle of the mirrors positioned around the SF59 glass. A fused-silica prism pair was incorporated in the shorter arm of the cavity to ensure overall anomalous group-velocity dispersion and an adjustable slit was positioned near mirror M1. The slit was placed near this mirror as opposed to mirror M6 since the beam was not spectrally dispersed at this location.

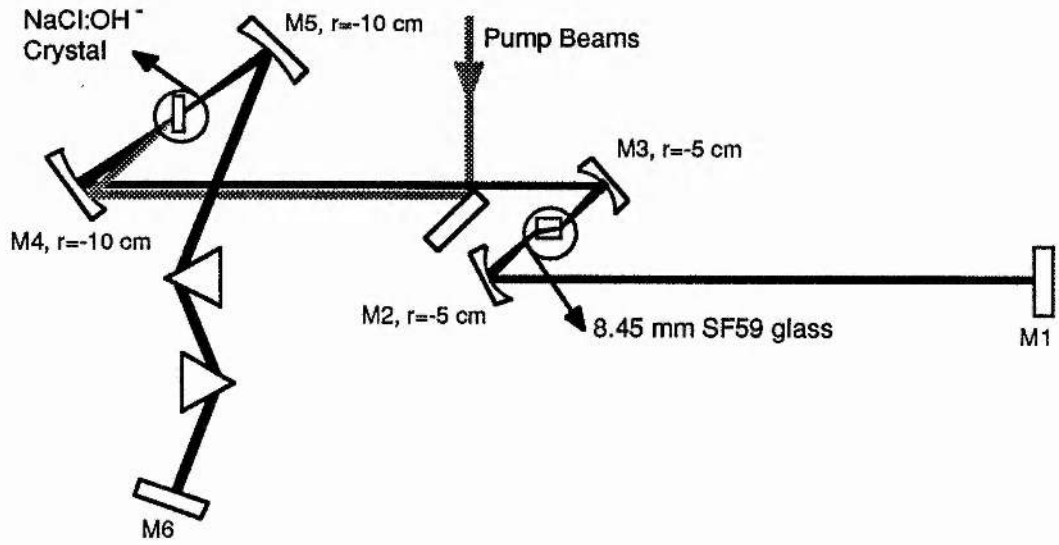

Figure 4.11. Schematic of the self-mode-locked laser cavity.

When the laser was aligned for maximum output power 300 mW output was obtained at 4.5 W pump. At first the laser was synchronously mode locked to provide intense pulses for initiation of the self-mode locking process. With no bandwidth restriction, the synchronously pumped laser produced noise bursts of approximately 10 ps duration.

Careful adjustment of the separation of the -5 cm RoC focusing mirrors and of the SF59 glass between them resulted in self-mode locking. The duration of the self-mode-locked pulses was 85 fs and associated intensity and interferometric autocorrelations of the pulses are reproduced in Figure 4.12.

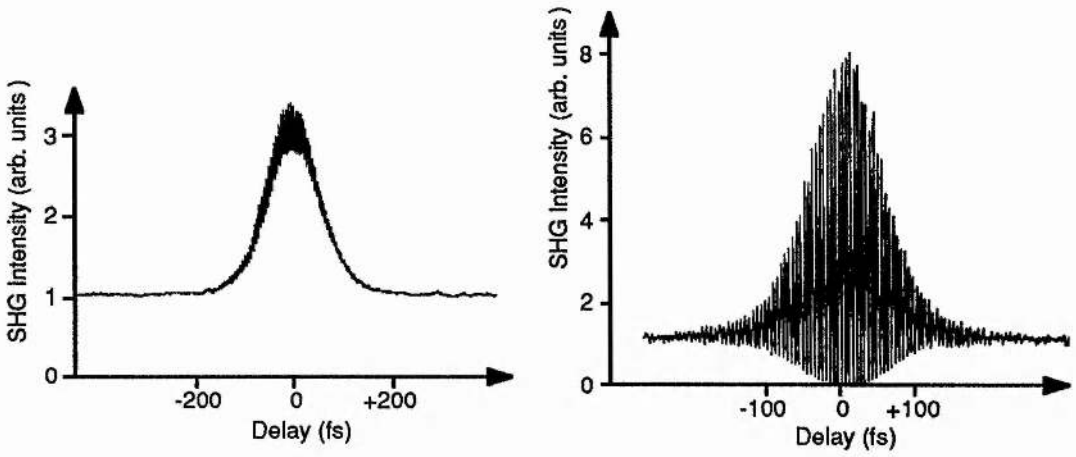

Figure 4.12. Autocorrelations of the self-mode-locked laser pulses when the mode locking was initiated by synchronous pumping.

When the laser cavity was aligned for self-mode locking, the output power of the laser dropped to less than 100 mW for synchronously mode-locked operation and rose to 140 mW when self-mode locking occurred. The transverse-mode profile of the laser was also observed to change from a mixture of TEM_{00} and TEM_{01} modes when synchronously pumped, to a predominantly TEM_{00} mode when self-mode locked. This implies that the synchronously pumped laser was operating at the end of a stability region where the effects of the self-focusing are greatest. Furthermore, the laser operated in the self-mode-locked state when the intracavity slit was removed. It was concluded that changes in the size and location of the beam waist in the colour-centre crystal were responsible for mode-locking: When the laser was operating in the synchronously pumped regime the effects of self-focusing were small. The resonator was near one extreme of a stability region and the beam waist in the NaCl:OH^- crystal was small, much smaller than the pump beam waist. The self-focusing caused an increase in the waist size in the colour-centre crystal, resulting in a greater overlap between the laser and pump beams. The laser field could then extract energy from the gain medium more efficiently.

The maximum average output power obtainable from the self-mode-locked laser was 140 mW when pumped by 4.5W from a Nd:YAG laser at 1064 nm. (60 mW of 532 nm radiation was used to reorient the active centres). The threshold for self-mode locking was measured to occur at ~60 mW average output power. The output coupling was 7% and so the peak intracavity power at threshold was 1.1 kW (assuming 10 ps duration noise bursts).

Examination of the output pulse train using a 300 MHz bandwidth germanium photodiode and an oscilloscope showed the self-mode locking to be unstable. This was attributed to the large gain modulation induced by the synchronous pumping. To

avoid this instability, the Nd:YAG laser was operated in continuous wave mode and the colour-centre laser was acousto-optically mode locked to provide an intense feature for the initiation of self-mode locking. The Brewster-angled acousto-optic mode-locker (Newport Electro-Optic Systems model N12041-2) was placed near mirror M1 It was driven by ~500 mW of RF power at 40.54 MHz which was obtained by amplifying the output from a Marconi model 2019 frequency synthesiser.

The pulse durations obtained from the acousto-optically mode-locked laser were typically around 100 ps. It was therefore necessary to reduce the output coupling to ~0.6 % to achieve sufficient intracavity peak powers to initiate self-mode locking.

Using this method of initiation, 95 fs duration pulses were obtained around 1575 nm. The average output power from the laser was 40 mW at 6 W pump power. The 4 mW of 532 nm light required for reorientation of the colour centres was obtained by frequency doubling 3 W of the cw 1064 nm pump beam.

A periodic amplitude modulation was observed on the output pulse train of the laser. This modulation arose from the beating of the mode-locked pulse train with the applied amplitude modulation as described in section 3.2.3. There are two possible approaches to eliminating this modulation. One is to actively control the length of the laser cavity so that the pulse repetition frequency of the laser is exactly twice the applied modulation frequency. An alternative method is to derive the signal applied to the acousto-optic modulator directly from a frequency component of the pulse train from the laser itself. In this scheme the modulation frequency follows that of the laser pulses. This latter technique was first used by Huggett[37] in 1968 to FM mode lock a HeNe laser and was termed regenerative mode-locking. More recently, the method was applied to initiate a self-mode-locked Ti:Al_2O_3 laser[26]. In this instance, the technique was termed regenerative initiation.

The regenerative initiation scheme

The regenerative initiation scheme employed was similar to that described by Spence *et al.* [Ref. **26**]. A schematic of the circuitry is presented as Figure 4.13. A portion of the laser output was focused onto a fast germanium photodiode (300 MHz bandwidth). The 162 MHz output from the photodiode, corresponding to the second harmonic of the laser pulse repetition frequency, was selected using a band-pass filter (4 MHz pass band) and was then amplified and power-limited. This signal was passed through a divide-by-4 frequency converter to obtain a 40.5 MHz signal at half the laser pulse repetition frequency. The output from the frequency-divider was then filtered, amplified to ~500 mW and applied to the acousto-optic modulator. In order to obtain a sufficient modulation depth to initiate and sustain mode locking, it was necessary to drive the acousto-optic modulator on resonance. This is in contrast to the

scheme described in Reference **26**, where a sufficient modulation could be obtained when the modulator was driven off-resonance.

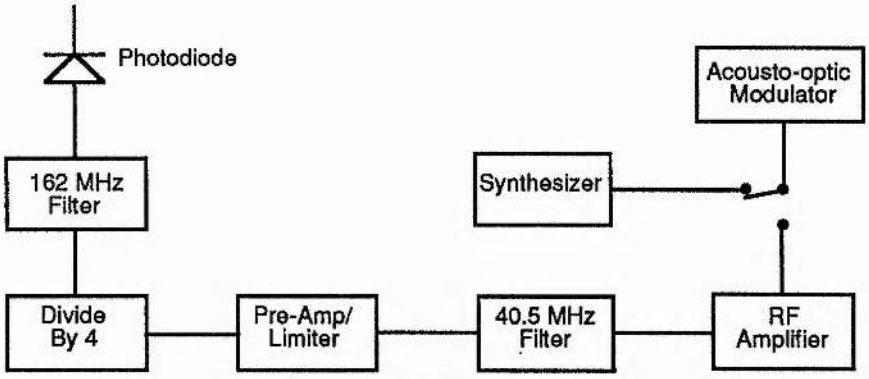

Figure 4.13. The regenerative initiation circuitry.

Intensity and interferometric autocorrelations, and a spectrum of the self-mode-locked pulses are reproduced as Figure 4.14. The pulse duration was measured to be 95 fs (assuming a $sech^2$ intensity profile). The spectral bandwidth of the pulses was 27 nm, resulting in a near-transform-limited duration-bandwidth product of 0.32. This is verified by the near ideal shape of the fringe-resolved autocorrelation.

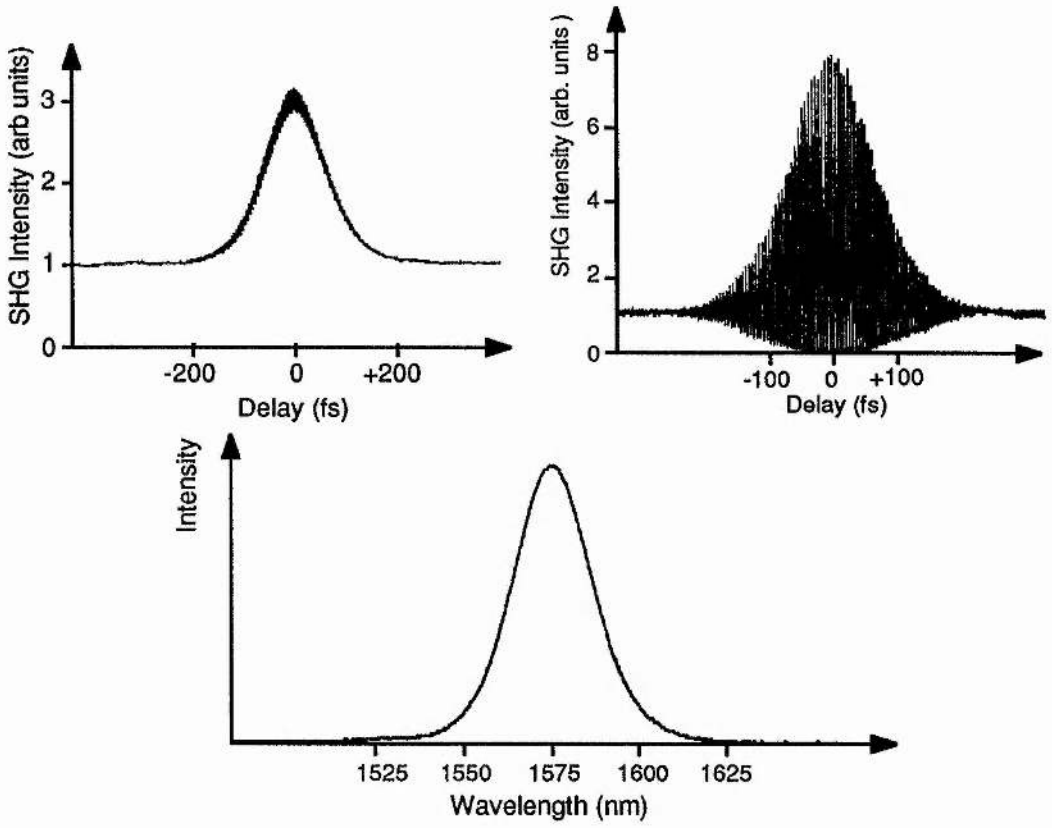

Figure 4.14. Autocorrelations and a spectrum of the regeneratively-initiated self-mode-locked laser.

Figure 4.15 shows intensity and interferometric autocorrelations of the pulses obtained from the opposite end of the laser. These pulses were 120 fs in duration and possessed considerable frequency chirp. This is indicated by the structure on the wings of the interferometric autocorrelation.

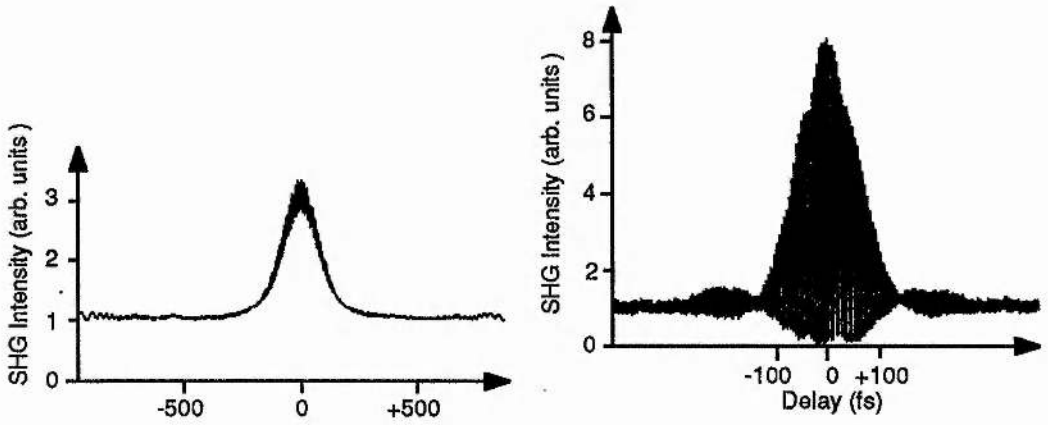

Figure 4.15. Autocorrelations of the pulses from the opposite end of the self-mode-locked laser.

The net GVD of the self-mode-locked laser cavity was calculated to be -1126 fs^2 at 1575 nm. The contributions to the GVD from the individual cavity components are tabulated in Table 4.4.

Cavity Element	Length (mm)	GVD (fs^2mm^{-1})	Total GVD (fs^2)
Acousto-optic modulator	8	-31	-248
Dewar windows	4	-31	-124
Prism material	30	-31	-930
Prism separation	106	-170 - 4.04 *l*	-599
SF59 glass	9.5	+91	+865
NaCl:OH⁻ crystal	2.5	-36[38]	-90
			Total = -1126

Table 4.4. Dispersion budget for the regeneratively-initiated self-mode-locked laser.

4.9 Summary

Self-mode locking of a NaCl:OH⁻ colour-centre laser has been demonstrated for the first time. The nonlinear effect of self-focusing was exploited in an intracavity

rod of Schott SF59 glass to achieve mode locking. A simple Gaussian beam analysis program was used to model the laser resonator so that the effects of the self focusing could be maximised. Pulses of 85 fs duration were obtained from the laser when synchronous pumping was used to initiate mode locking. However, the laser output was unstable so an alternative means of regenerative initiation using acousto-optic modulation was employed. In this configuration the laser produced stable, near-transform-limited pulses of 95 fs duration.

In view of its inherent simplicity, this mode-locking technique may become an alternative to coupled-cavity mode-locking described in Chapter 3 The self-mode-locking scheme is based on a single cavity and therefore does not require any interferometric stabilisation. Also, It should be easier to implement higher-order dispersion compensation to obtain shorter mode-locked pulse durations. One disadvantage of the self-mode-locking technique compared with coupled-cavity mode locking is the relatively low output powers from the self-mode-locked laser. This is due to the low output coupling which is used to obtain the high intracavity powers required to reach the threshold for mode locking. The output power could be increased by using an intracavity element which has a higher Kerr coefficient than the SF59 glass (such as rutile or ZnSe) and by optimising the design of the resonator to maximise the effect of the self focusing.

References

1. D. E. Spence, P. N. Kean and W. Sibbett, in *1990 Conference on Lasers and Electro-Optics*, Vol. 7 OSA Technical Digest Series (Optical Society of America, Washington D.C., 1990) Paper CPDP10.
2. D. E. Spence, P. N. Kean abd W. Sibbett,. Opt. Lett. **16,** 42 (1991).
3. Spectra-Physics Model 3900.
4. J. D. Kafka, M. L. Watts, D. J. Rouch, M. S. Keirstead, H. W. Scheiff and T. Baer, in *Technical Digest on Ultrafast Phenomena 1990* (Optical Society of America, Washington D.C., 1990) Paper PD8.
5. Y. Ishida, N. Sarukura and H. Nakano, in *Technical Digest on Ultrafast Phenomena 1990* (Optical Society of America, Washington D.C., 1990) Paper PD11.
6. J. Squier, F. Salin, C. Rouger, S. Coe and G. Morou , in *1990 Conference on Lasers and Electro-Optics*, Vol. 7 OSA Technical Digest Series (Optical Society of America, Washington D.C., 1990) Paper CPDP9.
7. N. Sarukura, Y. Ishida, N. Nakano and Y. Yamamoto, Appl. Phys. Lett. **56,** 814 (1990).
8. J. D. Kafka and T. Baer, in *1991 Conference on Lasers and Electro-Optics*, Vol. 10 OSA Technical Digest Series (Optical Society of America, Washington D.C., 1991) Paper JMA 2.
9. D. K. Negus, L. Spinelli, N. Goldblatt and G. Feugnet in Advanced Solid-State Lasers Topical Meeting Vol. 10 OSA Procedings Series (Optical Society of America, Washington, D.C. 1991) p 120.
10. F. Salin, J. Squier, and M. Pichet, Opt. Lett. **16,** 1674 (1991).
11. M. Pichet, Opt. Commun. **86,** 156 (1991).
12. G. P. A. Malcolm and A. I. Ferguson, Opt. Lett. **16,** 1967 (1991).
13. K. X. Liu, C. J. Flood, D. R. Walker and H. M. van Driel, Opt. Lett. **17,** 1361 (1992).
14. A. Miller, P. Li Kam Wa, B. H. T. Chai and E. W. Van Stryland, Opt. Lett. **17,** 195 (1992).
15. J. M. Evans,D. E Spence, B. H. T Chai and A. Miller, Opt. Lett. **17,** 1447 (1992).
16. P. Li KamWa, B. H. T. Chai, H. S. Wang and A. Miller, in *1992 Conference on Lasers and Electro-Optics*, Vol. 12 OSA Technical Digest Series (Optical Society of America, Washington D.C., 1992) Paper CTuP 1.
17. A. Seas, V. Petricevic and R. R. Alfano, in *1992 Conference on Lasers and Electro-Optics*, Vol. 12 OSA Technical Digest Series (Optical Society of America, Washington D.C., 1992) Paper CPD 10.
18. G. Gabetta D, Huang, J. Jacobson, M. Ramaswammy, H. A. Haus, E. P. Ippen and J. G. Fujimoto, in *1991 Conference on Lasers and Electro-Optics*, Vol. 10 OSA Technical Digest Series (Optical Society of America, Washington D.C., 1991) Paper PDP 8.
19. M. T. Asaki, C. P. Huang, D. G. Garvey, J. Zhou, H. C. Kapteyn and M. Murnane, Opt. Lett. **18,** 977 (1993).

20. A. E. Siegman, Lasers (University science booko Mill Valley, CA, 1986).
21. F. Salin, P. Grangier, G. Roger and A. Brun, Phys. Rev. Lett.**56,** 1132 (1986).
22. H.Avramopoulous, P. M. W. French, J. A. R. Williams, G. H. C. New and J. R. Taylor, IEEE J. Quantum Electron. **24,** 1884 (1988).
23. N. Sarukura, Y. Ishida, T. Yanagawa and N. Nakano, Appl. Phys. Lett. **57,** 229 (1990).
24. Clark Instrumentation mode locked Ti:saphire laser.
25. Ch. Spielman, F. Krausz, T. Brabec, E Wintner and A. J. Schmidt, Opt. Lett. **16,** 1180 (1991).
26. D. E. Spence, J. M. Evans, W. E. Sleat and W. Sibbett, Opt. Lett. **17,** 1762 (1991).
27. I. Thomazeau, J. Etchepare, G. Grillon and A. Migus, Opt. Lett. **10,** 223 (1985).
28. S. R. Friberg and P. W. Smith, IEEE J. Quantum Electron. **QE-23,** 2089 (1987).
29. D. W. Hall, M. A. Newhouse, N. F. Borreli, W. H. Dumbaugh and D. L.Weidman, Appl. Phys. Lett. **54,** 1293 (1989).
30. M. Sheik-Bahae, D. C. Hutchings, D. J. Hagan and E. W. Van Stryland, IEEE J. Quantum Electron. **27,** 1296. (1991).
31. B. S. Wherret, J. Opt. Soc. Amer. B **1,** 62 (1984).
32. Schott Glass Catalogue 1992.
33. G. P. Agrawal, Nonlinear Fiber Optics (Academic Press, Boston, 1989) chapter 2.
34. W. H. Knox, Opt. Lett. **17,** 514 (1992).
35. R. L. Fork, O. E. Martinez and J. P. Gordon, Opt. Lett **9,** 150 (1984).
36. I. H. Malitson, J. Opt. Soc. Am. **55,** 1205 (1965).
37. G. R. Huggett, Appl. Phys. Lett. **13,** 186 (1968).
38. Handbook of Optical Constants of Solids ed. E. D. Palik (Academic Press, Orlano,1985).

Chapter 5

Applications

In Chapters 2, 3 and 4, novel means for generating ultrashort pulses around 1.55 μm from a NaCl:OH^- colour-centre laser have been described. The main application for these sources is the evaluation of nonlinear optical phenomena, and the testing of devices utilising these phenomena, for optical-fibre-based telecommunications systems. Although there are other sources in this wavelength region, such as semiconductor diode lasers, erbium-doped fibre lasers and optical parametric oscillators, the versatility of colour-centre lasers cannot be rivalled at present. Colour-centre lasers are capable of producing pulses of nanojoule energies having durations from 200 ps to 100 fs. They can also easily be reconfigured to operate continuous-wave at output powers in excess of one watt.

During the course of this project, several nonlinear-optical experiments were performed and, in this Chapter, four experiments shall be described. The experiments fall into two categories. The first two sections describe experiments where both NaCl:OH^- and KCl:$Tl^0(1)$ colour-centre lasers were synchronously mode locked using one Nd:YAG pump laser to produce two synchronous pulse trains which were used to perform dual-wavelength experiments. Two nonlinear optical waveguide experiments, utilising the enhancement in the coefficient for nonlinear refraction around the two-photon bandgap in the AlGaAs semiconductor material system are described in sections 5.3 and 5.4. For the latter two experiments, the KCl:$Tl^0(1)$ colour-centre laser was used.

5.1 Synchronously-Pumped Raman Amplification

5.1.1 Introduction

When light is propagated down an optical fibre a small portion of the beam is converted into a signal at a longer wavelength. This occurs as the propagating photons excite molecular vibrations in the form of acoustic phonons in the silica matrix, reducing their energy and down-shifting their frequency (Stokes' shift). The process is termed spontaneous Raman scattering. For silica fibres, the Stokes' shift peaks at 440 cm^{-1} from the input signal and extends for several terahertz. If some power exists

at the Stokes' wavelength, either from spontaneous Raman scattering or from a second injected signal, the scattering can be stimulated and the Stokes' wave will rapidly increase in amplitude. This provides a convenient means for broadband signal amplification for optical fibre based communications systems, since the fibre itself acts as the amplifying medium.

The pump powers required for cw Raman amplification are excessive. For example, to compensate for the loss in 10 km of optical fibre, 70 mW of pump is necessary. This is around one order of magnitude greater than the pump powers required for erbium-doped fibre amplifiers[1]. In soliton systems where the mark to space ratio is typically 10:1, the average pump power could conceivably be reduced by pulsing the pump laser at the system bit rate and co-propagating it with the signal solitons. However, in this scheme, the group-velocity dispersion of the optical fibre can result in walk-off between the pump and signal pulses, reducing the interaction between the pulses and severely limiting the gain. In this section efficient pulsed Raman amplification is described. Synchronism between the signal and pump pulses along the entire fibre length was ensured by using a dispersion-shifted optical fibre with zero dispersion midway between the pump and signal wavelengths.

5.1.2 Experiment

The experimental configuration is illustrated in Figure 5.1. Pump and signal pulses were obtained from synchronously mode-locked KCl:Tl^0(1) and NaCl:OH^- lasers. Both colour-centre lasers were pumped by a single cw mode-locked Nd:YAG laser having a pulse repetition frequency of 82 MHz. This ensured that the pump and signal pulse trains were at exactly the same frequency.

The pulses from the two lasers were temporally overlapped by adjusting an optical delay line in the NaCl:OH^- laser beam and then coupled into 6.6 km of Corning Corguide dispersion-shifted optical fibre. At the output of the fibre, a monochromator was used to separate the pump and signal components and pulse duration measurements were performed using a synchroscan Photochron II streak camera having a temporal resolution of approximately 5 ps.

For the optical fibre used in these experiments, the zero group-velocity dispersion wavelength (λo) occurred at 1.56 μm. Pump pulses were obtained from the KCl:Tl^0(1) laser at 1.51 μm and were 30 ps in duration and the signal pulses, from the NaCl:OH^- laser at 1.61 μm, were approximately 10 ps duration. Gain measurements were performed by measuring the output signal power as a function of the input pump power and saturation effects were observed by varying the input signal power at a fixed pump power.

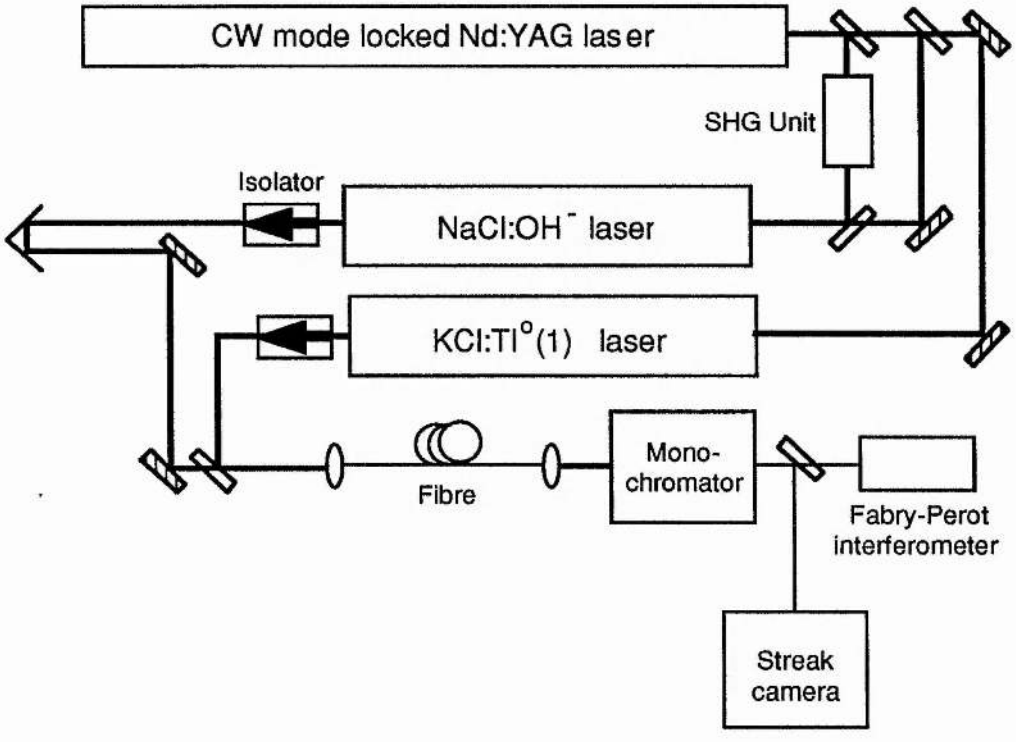

Figure 5.1. Schematic of the experimental arrangement for measuring synchronous Raman amplification.

5.1.3 Results and discussion

A graph of the gain versus the average pump power for mean signal powers of 28 μW (circles) and 19 μW (crosses) is shown in Figure 5.2. The departure from linearity for both signal powers is an indication of gain saturation. From the linear part of this graph the Raman gain coefficient g, could be calculated using the relation[2]

$$\frac{P_{si}}{P_{so}} = \exp\left(gI_{po}L_{eff}\right)$$

P_{si} and P_{so} are the input and output signal powers respectively, I_{po} is the effective input pump intensity and L_{eff} is the effective gain length. The effective gain length accounts for the fibre loss and is given by

$$L_{eff} = \frac{1-e^{-\alpha l}}{\alpha}$$

where l is the actual fibre length and α is the linear loss coefficient. Assuming a linear loss of $\alpha = 0.0461$ km^{-1} (0.2 dBkm^{-1}), the effective length of the fibre was calculated to be $L_{eff} = 5.69$ km. The effective input intensity I_{po} was calculated from

$$I_{po} = \frac{P_{ave}}{1.065 f_m \tau_p 2\pi\omega^2}$$

where ω is the mode-field radius of the fibre at the pump wavelength and τ_p, f_p and P_{ave} are the pump pulse duration, repetition rate and average power respectively. The factor of 1.065 accounts for the temporal profile of the pulses (assumed to be Gaussian).

From the experimental data, the Raman gain coefficient was calculated to be 5.7 x 10^{-12} cmW^{-1}, in close agreement with the value of 6.0 x 10^{-12} cmW^{-1} published by Stolen[2].

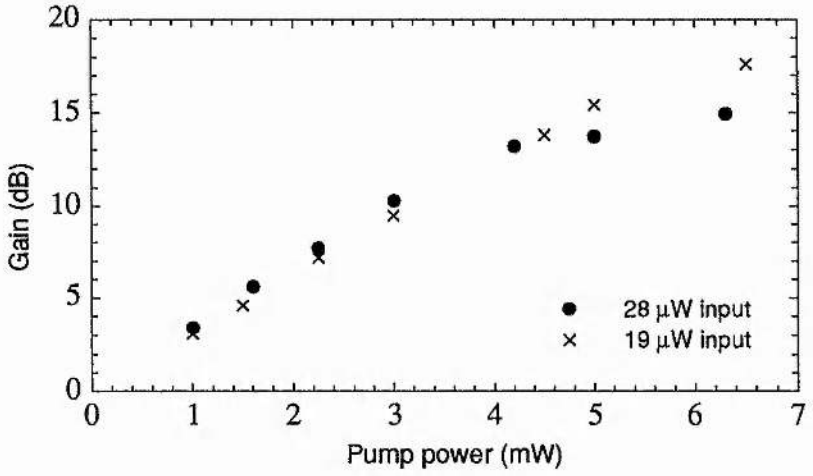

Figure 5.2. Graph of gain versus pump power for the synchronous Raman amplifier.

A graph of gain versus input signal peak power (for a fixed average pump power of 6 mW) is presented in Figure 5.3. From this graph gain saturation is clearly evident. Unfortunately, insufficient data were taken to obtain a value for the unsaturated gain. However, a minimum value can be estimated by assuming that a 3 dB compression of the gain occurs at 15.8 dB (3dB down from the maximum measured gain). This occurs at a peak input signal power of 9.8 dBm, indicating a 3 dB compression for output powers in excess of +25.8 dBm.

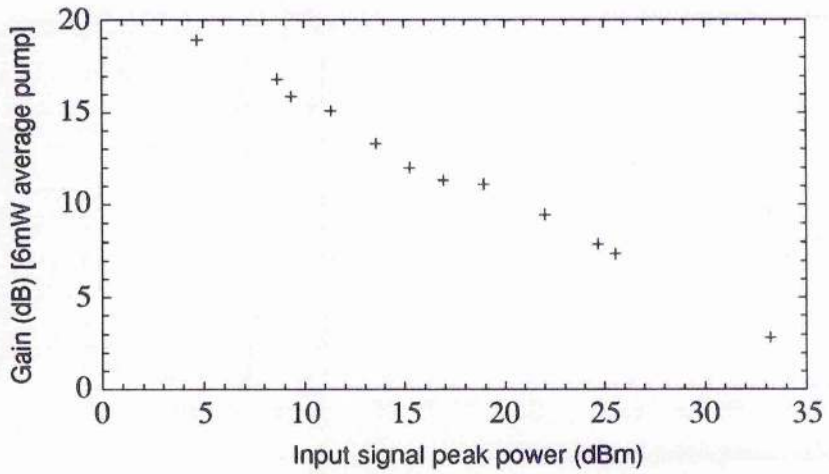

Figure 5.3 Graph of gain versus signal power for the synchronous Raman amplifier.

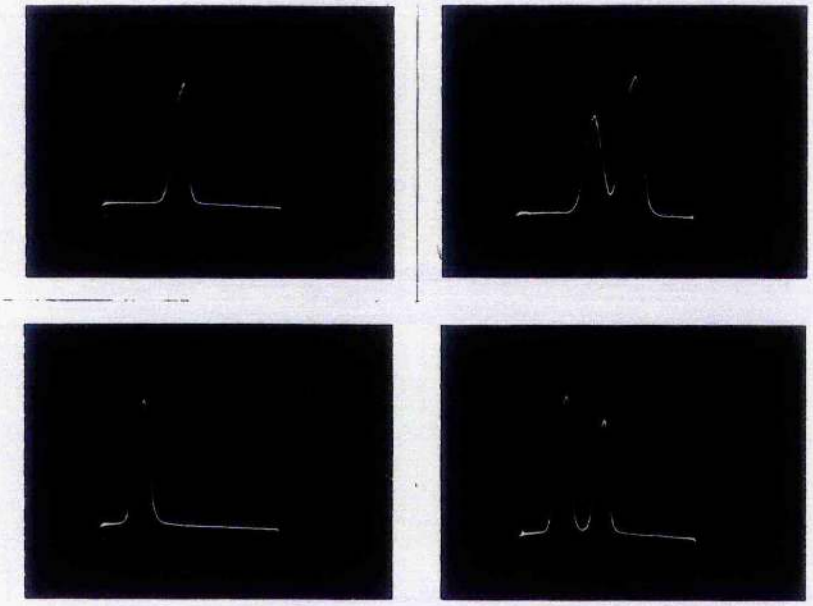

Figure 5.4. Streak traces of the input (left) and output (right) pulses for the amplifier. The top row shows the pump pulses, and the bottom row the signal pulses. The second pulse shown in each output streak trace is generated using a 100 ps Michelson delay line to provide a time calibration.

Streak traces of the input and output pulses are shown in Figure 5.4. After propagating through the fibre the pump pulse duration increased from 30 ps to 40 ps as a result of self-phase modulation and normal group-velocity dispersion, whereas, the duration of the signal pulse was unchanged. For a fibre group-velocity dispersion of 4.0 ps $nm^{-1}km^{-1}$ at a wavelength of 1.61 μm, and a launched peak power of 1 mW, the signal pulses would be expected to propagate as N = 1 solitons. However, in the presence of the Raman pump, the signal pulses will experience cross-phase

modulation from the pump pulses. This will effectively increase the nonlinearity of the optical fibre seen by the signal, reducing the power required for soliton formation.

5.1.4 Summary

Synchronous pumping of a Raman-fibre amplifier has been demonstrated. Using this technique, it was possible to obtain small-signal gains in excess of 15 dB for average pump power of 6 mW. A potential use for this amplifier would be for soliton-based communications schemes, however, cross-phase modulation from the pump pulse may limit its applicability.

5.2 Cross-Phase Modulation in a Semiconductor Optical Amplifier

5.2.1 Introduction

Travelling-wave semiconductor optical amplifiers provide an efficient and straightforward means of signal amplification for optical-fibre-based telecommunication systems. Semiconductor amplifiers fabricated in the InGaAsP quaternary material system, which exhibit gain spanning the 1.3-1.5 μm spectral region have been reported.[3] Such broadband devices are suitable for wavelength division multiplexed (WDM) communications networks or for amplifying pulses of picosecond durations.

Recently, the nonlinear properties of semiconductor optical amplifiers have attracted attention both to determine the limitations of the devices as amplifiers and also, to assess their potential for all optical switching. In particular, spectral broadening of pulses due to the nonlinear optical phenomenon of self-phase modulation has been studied[4]. The physical mechanism behind self-phase modulation (SPM) is gain or absorption saturation, which leads to relatively large intensity-dependent changes in the refractive index arising from carrier density fluctuations in the active region. For pulse durations less than a few tens of picoseconds (i.e. much shorter than the gain or absorption recovery time), the spectral broadening is asymmetric since only the leading edge of the pulse experiences a rapidly changing refractive index.

For pulse durations much greater than the spectral hole burning recovery time (approximately 0.1 ps), the gain of a semiconductor amplifier is effectively homogeneously broadened, and therefore, the gain at one wavelength will be affected by the presence of a signal at a second wavelength[5-7]. The reduction in gain induced by an energetic pulse could conceivably be used to shape a pulse at a different wavelength, provided that the two pulses have some temporal overlap. Furthermore, coupling between the pulses will occur through the refractive index changes that accompany gain saturation, resulting in frequency chirping. This interaction

corresponds to the phenomenon of cross-phase modulation (XPM) that has been extensively studied in optical fibres.[8] Here, the observation of spectral broadening and distortion due to XPM in a semiconductor optical amplifier is described.

To observe XPM, energetic pump pulses together with probe pulses were injected into the amplifier (in the same direction). The probe pulses were sufficiently weak that they did not significantly saturate the amplifier gain and experienced negligible spectral broadening from SPM. On the other hand, the pump pulses caused appreciable saturation of the gain and sustained significant SPM. The refractive index changes induced by the pump pulses were experienced by the co-propagating probe pulses and frequency chirp and thereby spectral broadening was induced solely through XPM.

5.2.2 Amplifier Characteristics.

The amplifier used for these experiments was an InGaAsP double-channel planar buried heterostructure (DCPBH) device, fabricated by BNR Europe Ltd. A cross section of the amplifier chip is shown as Figure 5.5. The active region cross section was 1.5 x 0.17 μm^2 which results in a confinement factor of ~ 0.39 (calculated from Reference **9**). The thin anti-meltback layer was grown above the active layer to prevent meltback of the active region during the growth of the cladding region. Reflections from the facets of the device were frustrated by depositing dielectric anti-reflection coatings on them. The coatings raised the oscillation threshold of the device to approximately 60 mA drive current. For efficient heat sinking, the amplifier was mounted p side down on a dual facet (DF) mount. This permitted access to both sides of the device using bulk optics.

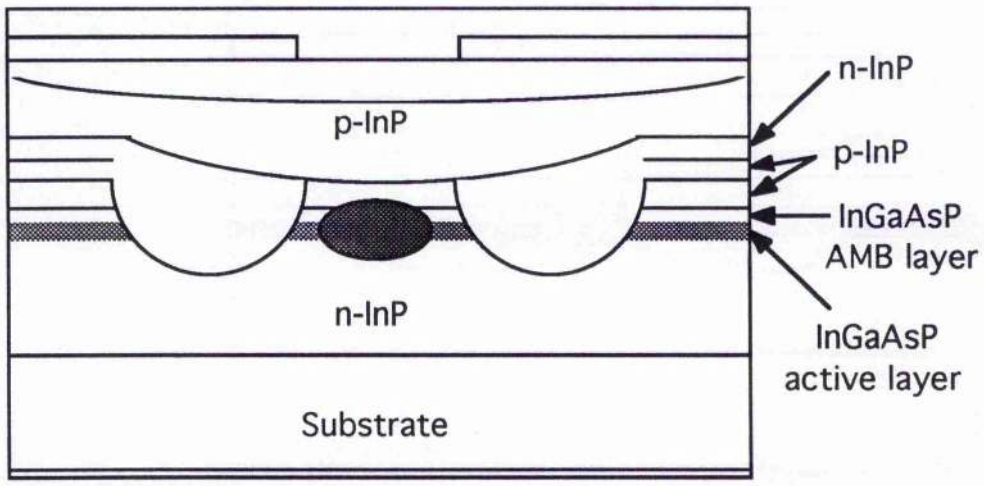

Figure 5.5. Cross section of the double-channel planar buried-heterostructure semiconductor optical amplifier. The shaded ellipse in the centre of the structure represents the optical mode.

5.2.3 Experiment

Independently tunable pulse trains were generated by synchronously mode-locked KCl:Tl^0(1) and NaCl:OH^- colour-centre lasers (see Fig. 5.6). Pulse synchronism between the two colour-centre lasers was assured by using a single CW mode-locked Nd:YAG laser to excite both lasers,. An adjustable optical delay in the NaCl:OH^- laser beam enabled the relative timing between the two pulse trains to be altered. Optical isolators were required to prevent the amplifier from using the output couplers of the colour-centre lasers in order to reach the threshold for laser oscillation, and also to avoid the degradation of mode locking by parasitic optical feedback. The two pulse trains were combined at a beamsplitter and then polarised to match the transverse electric (TE) mode of the amplifier. An antireflection-coated X 20 microscope objective was used to couple the pulses into the amplifier and a Melles-Griot diode collimating lens was used for output coupling. The pump and probe pulses transmitted by the amplifier were spatially filtered to remove the light not coupled into the waveguide, and then they were separated from each other by a monochromator which acted as a bandpass filter (bandwidth ~5 nm). The spectra of the pulses were monitored using a scanning Fabry-Perot interferometer.

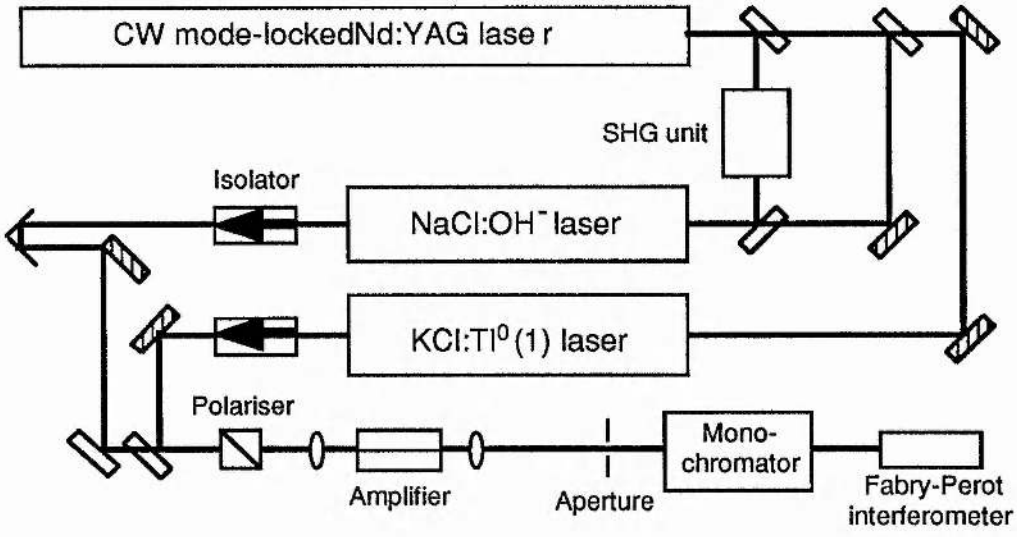

Figure 5.6. Experimental arrangement used to measure cross-phase modulation in an optical amplifier.

The mode-locked KCl:Tl^0(1) laser, which was operated at a centre wavelength of 1526 nm, generated probe pulses of approximately 40 ps duration (measured using second harmonic generation autocorrelation - Gaussian pulseshape assumed), while the mode-locked NaCl:OH^- laser was used to provide the pump pulses at a centre wavelength of 1506 nm. To simplify the analysis of the results, the NaCl:OH^- pulse duration, normally 5 ps, was increased to ~40 ps by bandwidth limitation and slight

cavity length detuning. The drive current supplied to the semiconductor amplifier was 40 mA, and the small-signal resonant gain of the amplifier at the probe pulse wavelength was approximately 16 dB. The gain ripple was ~1.3 dB, and so travelling-wave characteristics were assumed. The saturation energy E_{sat} was estimated to be approximately 6 pJ at the probe wavelength.

The pump pulse energy was set to approximately 10 pJ at the input facet. This was large enough to strongly saturate the gain, and consequently, only the leading portion of the pulse was amplified and spectrally broadened to longer wavelengths by SPM. The trailing portion of the pump pulse was transmitted unamplified and unchirped. A typical spectrum of the pump pulses transmitted by the amplifier is reproduced in Figure 5.7, together with an undistorted spectrum recorded in the small-signal regime.

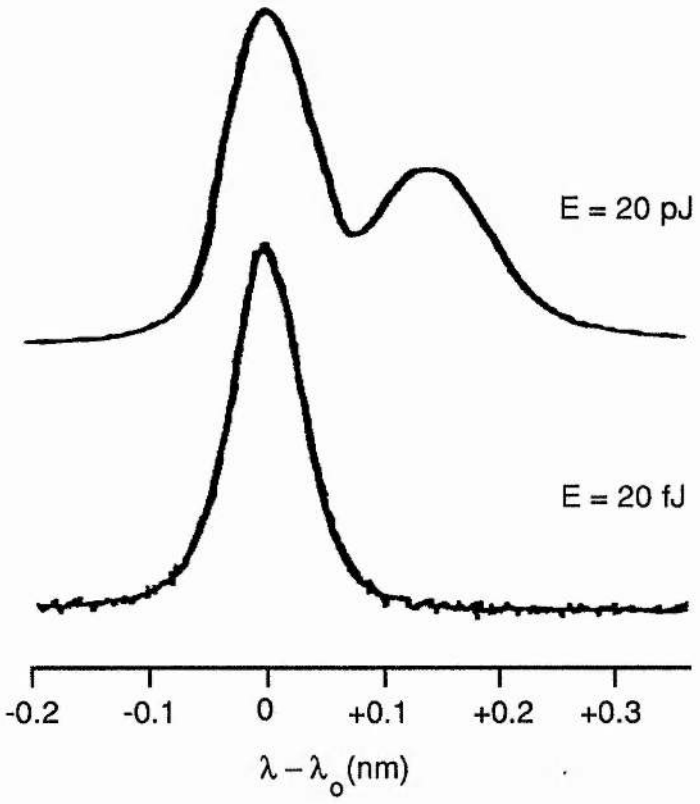

Figure 5.7. Spectra of the pump pulses before (bottom) and after (top) propagating through the amplifier.

The spectra of the probe pulses (input energy ~80 fJ) transmitted by the amplifier are shown in Figure 5.8. The spectra in Figs 5.8(a) to 5.8(e), distorted by XPM, are labelled by the time delay relative to the pump pulse, *i.e.* in Fig. 5.8(a), the probe pulse precedes the pump pulse. The point of zero delay was chosen somewhat arbitrarily as the position where the maximum spectral distortion was recorded and

does not necessarily imply complete overlap of pump and probe pulses. As discussed above, the probe pulse will only be noticeably chirped where it overlaps with the pump pulse, and so for the conditions of Figs 5.8(a) and 5.8(e) the frequency chirp on the probe pulse will be confined to the trailing and leading edges, respectively.

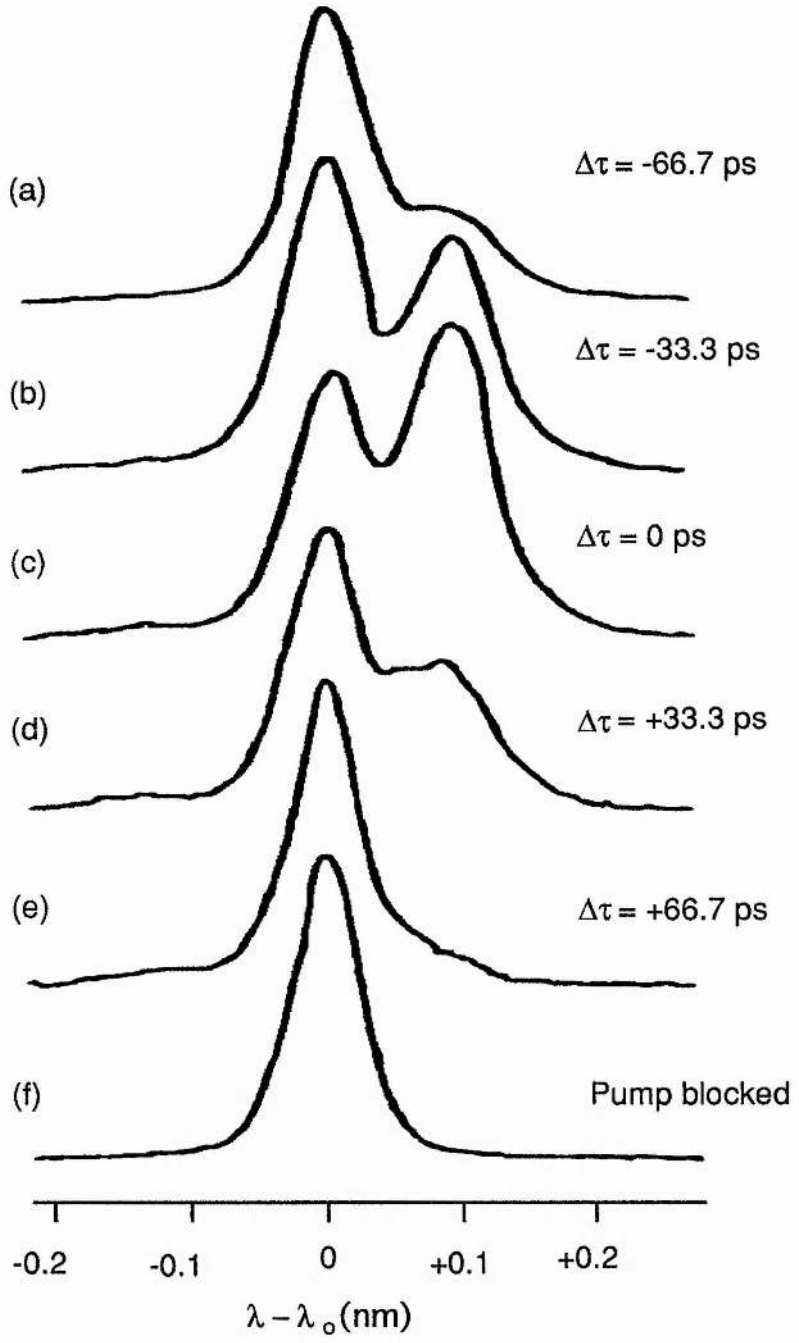

Figure 5.8. Progression of the transmitted probe pulse spectra for various pump pulse delays.

The pulse spectra are broadened asymmetrically to longer wavelengths when compared to the spectrum taken when the pump pulse train was blocked (Fig. 5.8(f)).

This asymmetry is not the result of any group-velocity mismatch and subsequent walk-off, which affects XPM in fibres. For the case described here, the pulses are much longer than the length of the nonlinear medium, and walk-off is negligible. Instead, the spectral asymmetry is attributed to the long recovery time of the refractive index change compared to the pulse durations, as discussed in the context of SPM in amplifiers.

5.2.4 Summary

Observations of cross-phase modulation in a semiconductor optical amplifier have been reported and the temporal detuning characteristics have been briefly described. Even with pump pulse energies as low as ~1 pJ, XPM should still be observable. For an amplifier with a higher small signal gain than that used here, the spectral distortion would be more dramatic and would appear at even lower pump pulse energies.

5.3 Ultrafast All-Optical Switching in an Asymmetric AlGaAs Mach-Zehnder Interferometer

5.3.1 Introduction

The asymmetric Mach-Zehnder interferometer (AMZI) device is illustrated in Figure 5.9. The nonlinear performance of the device is similar to that of the nonlinear Sagnac interferometer described in Chapter 2. The input light is split at the Y junction, propagates down the two arms of the interferometer and is recombined at the output Y junction. If the light in each arm of the interferometer is in phase, the resultant waveguide mode, after the Y junction, will be guided and will propagate along the output waveguide. However, if the two fields are out of phase, the resultant field will couple into radiation modes in the substrate and will not be guided at the output of the Y junction. As with the nonlinear Sagnac interferometer, the intensities in the two arms of the interferometer have to be different such that a differential phase shift can accumulate between the two propagating fields through self-phase modulation. This is achieved by utilising an asymmetric Y-junction geometry.

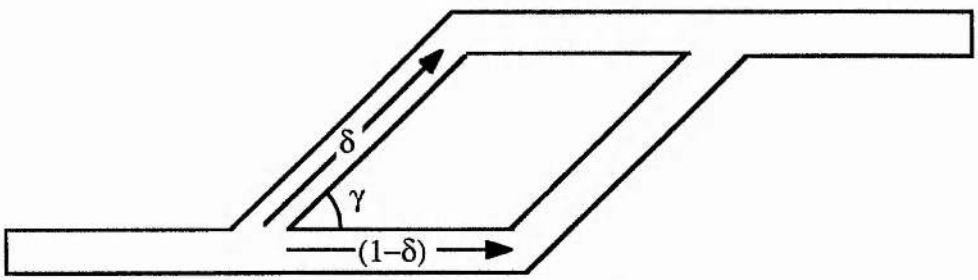

Figure 5.9. Schematic of the asymmetric Mach-Zehnder interferometer.

The device is based upon the, more familiar, integrated electro-optic Mach-Zehnder interferometer[10]. For these devices, the split ratio of the Y junction is 0.5 and the differential phase change is produced by applying an electric field across one arm of the interferometer. In this case, the switching speed of the devices is determined by the electronics used to apply the electric field, and is restricted to several tens of gigahertz. In the all-optical version of the integrated Mach-Zehnder interferometer, however, the phase change is produced by the light itself via the intensity-dependent refractive index. The speed of the all-optical device is therefore limited by the time constant of the optical Kerr effect, which is of the order of a few femtoseconds (*i.e.* a bandwidth of ~200 terahertz).

According to a model of the dispersion of the non-resonant refractive nonlinearity in semiconductors,[11,12] there is a local enhancement of the nonlinear refractive index coefficient around the two-photon bandedge. Operating with a photon energy slightly less than one half the bandgap energy therefore results in an increased nonlinearity with minimal loss due to two-photon absorption. The device was designed to operate in this region of enhanced nonlinearity at wavelengths around 1.55 μm. All-optical switching utilising the enhanced nonlinearity at half the band-gap energy has been observed for a directional coupler[13]. The advantage of the Mach-Zehnder design is that the phase change required for switching is reduced by a factor of two.[14]

5.3.2 Fabrication of the device

The material structure of the wafer used to construct the AMZI device is the same as that described in Reference **13**. A schematic of the wafer cross section is presented as Figure 5.10. The GaAlAs epitaxial layers were grown by MBE, and consisted of a 1.5 μm thick $Ga_{0.82}Al_{0.18}As$ guiding region, a 1.5 μm thick $Ga_{0.75}Al_{0.25}As$ upper cladding layer and a 4 μm thick $Ga_{0.75}$ $Al_{0.25}As$ layer as a lower cladding. The epitaxial layers were grown on a semi-insulating (SI) GaAs substrate.

The mask pattern consisted of straight waveguides to measure the linear propagation losses (α) and AMZIs with Y-junction angles varying from 0.5^{o} to 4^{o}. The patterned samples were etched in Plasmaetch RIE80 reactive ion etching equipment using $SiCl_4$ gas. The rib width and height for a single-mode waveguide were 3 μm and 1.6 μm respectively. A scanning electron micrograph of the asymmetric Y-junction is displayed as Figure 5.11. The device was fabricated at the Department of Electrical and Electronic Engineering at Glasgow University.

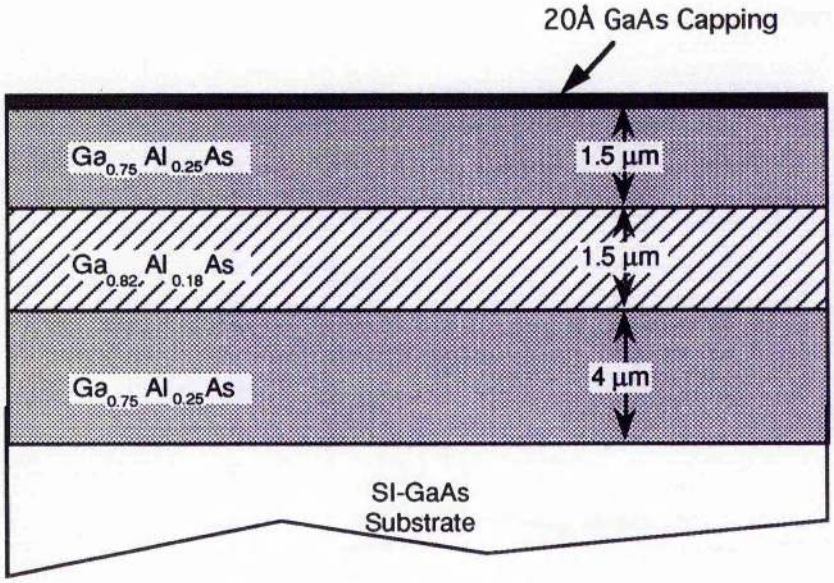

Figure 5.10. Cross-section of the asymmetric Mach-Zehnder device wafer.

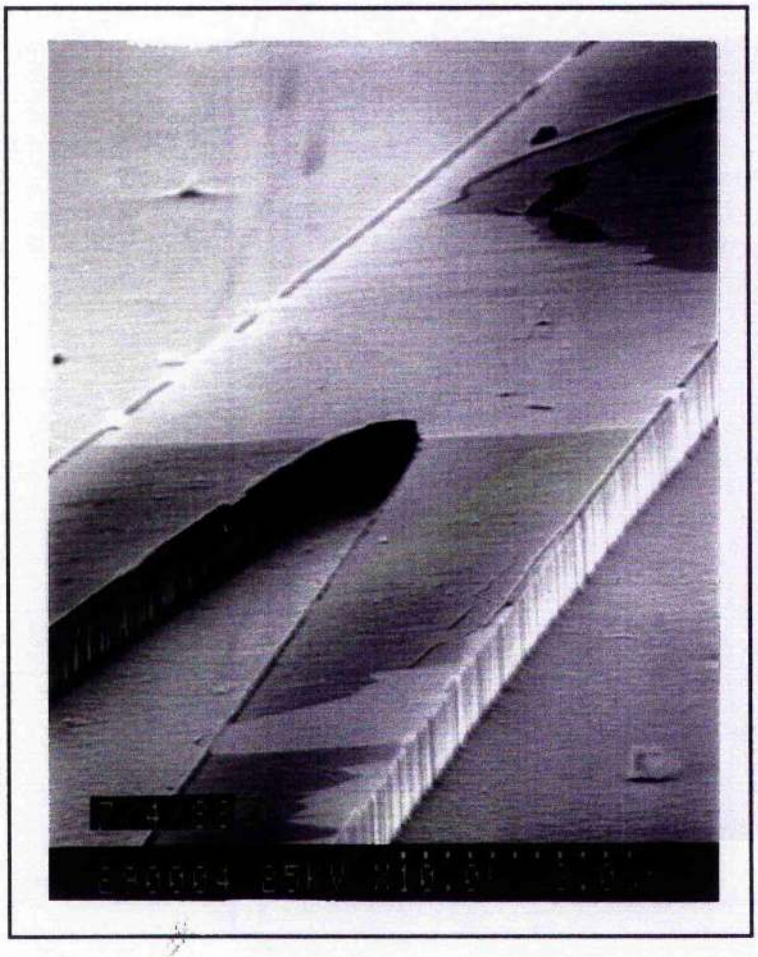

Figure 5.11. Scanning electron micrograph of one of the Mach-Zehnder Y-junctions.

5.3.3 Experiment

The linear propagation losses were measured in a straight waveguide using the Fabry-Perot technique[15] and a value for the linear loss α = 1.7 +/- 0.15 cm^{-1} was deduced. The split ratio between the two arms of the AMZI was measured after cleaving the AMZI into two Y junctions. This was achieved by directly observing the power of the light output from each arm of the Y junction[16].

Ultrashort pulses having a duration of 330 fs (FWHM) were generated using a coupled-cavity mode-locked KCl:Tl^0(1) colour-centre laser. The centre wavelength of the pulses was 1520 nm and the pulse repetition rate was 82 MHz. When the coupled-cavity section of the laser was blocked, the synchronously mode-locked laser produced pulses of approximately 30 ps duration with no change to the average output power. Pulses, of up to 63 mW average power, were coupled into the waveguide sample using an anti-reflection coated X 20 microscope objective lens. A X 40 microscope objective lens was used for output coupling. The near-field and far-field mode profiles of the waveguides were examined using a CCD camera. The power of the pulses coupled into the device was varied using a motor-controlled attenuator wheel. The polarisation of the incident beam was set to either transverse electric (TE) or transverse magnetic (TM) using a zero-order half-wave plate. To separate the guided mode from light travelling over the sample or through the substrate and cladding regions the output from the device was spatially filtered by focusing it through a < 0.5 mm diameter aperture positioned ~1.5 m from the output facet. The filtered light was then measured using a calibrated germanium detector.

5.3.4 Results and Discussion

The intensity-dependent refractive change in the straight waveguide was determined by measuring the spectral broadening of the transmitted pulses caused by self-phase modulation (SPM). This was carried out for both TE and TM polarisations and the data showed that the spectral broadening via SPM was polarisation independent in the AlGaAs waveguides. From these measurements the corresponding nonlinear refractive index coefficient was calculated to be n_2 = (5.4 +/- 0.5) x 10^{-14} cm^2W^{-1}.

A figure of merit given by[14]

$$T = \frac{\beta\lambda}{n_2}$$

where β is the two-photon absorption coefficient and λ is the free-space wavelength of light used to characterise the suitability of a material for all-optical switching. For the GaAlAs waveguides, a value of β = 0.14 $cmGW^{-1}$ can be deduced from the

transmission measurements of the 330 fs pulses presented in Figure 5.12. A figure of merit of $T = 0.38$ at $\lambda = 1.52$ μm was calculated which satisfies the criterion for an all-optical switch since $T<<2$.

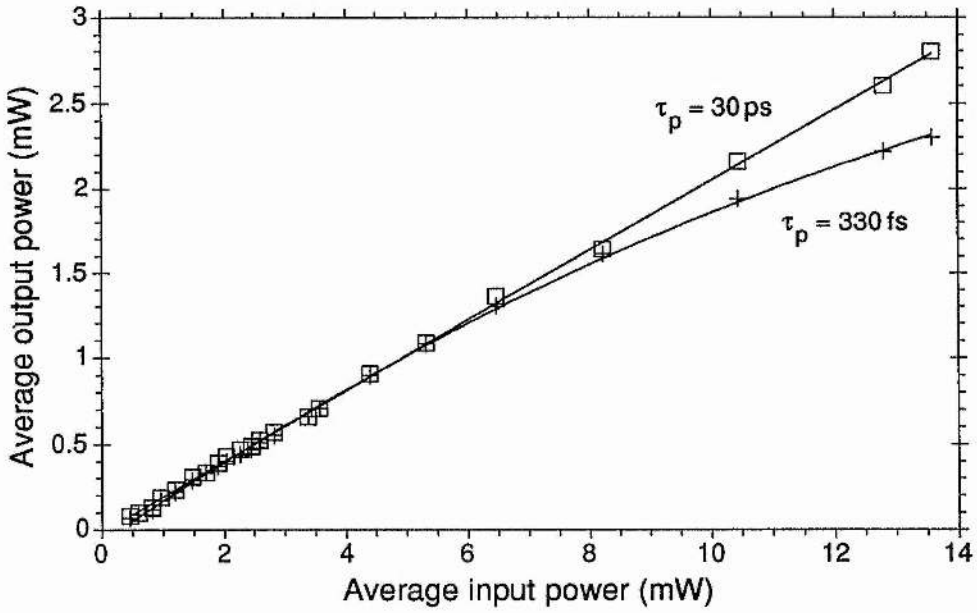

Figure 5.12. Graph of output power versus average input power for a straight waveguide. The decrease in the transmission for 330 fs pulses is a result of multi-photon absorption.

A single beam experiment was used to characterise the AMZI as an all-optical switch. The transmission of the AMZI was monitored as a function of the input light intensity. Figure 5.13 shows a plot of the normalised transmission as a function of the average input power (*i.e.* the estimated input power in the device after taking account of the coupling and reflection losses). The full angle of the AMZI Y-junction was $\gamma = 3^{o}$ and the length of the interferometer arms was L=0.5 cm. The split ratio between the two arms δ:(1-δ) was 0.18:0.82. The squares denote the normalised transmission of the device for an input pulse duration of 30 ps and the crosses denote data for a pulse duration of 330 fs. As the peak power was increased by a factor of 100 (for the 330 fs duration pulses), a switching of more than 80 % in the normalised transmission of the AMZI was achieved at an average power of 8.5 mW (*i.e.* a peak intensity of 3.92 GWcm^{-2}). From continuous-wave theory, the output response of the device is given by[17]

$$T = 4\delta(1-\delta)\cos^2\left(\frac{\Delta\varphi}{2} + \theta\right)$$

where the angle θ takes account of any built in phase difference in the device caused by slight differences in the optical path arising from fabrication inaccuracies and $\Delta\varphi$ is the relative phase difference resulting from the intensity dependent change in the refractive index and is given by

$$\Delta\varphi = \pm\frac{2\pi n_2 I_{in} l(1-2\delta)}{\lambda_o}$$

where λ_o is the free-spacewavelength and I_{in} is the peak input intensity.

From the results obtained from the AMZI the nonlinear refractive index coefficient n_2 was estimated to be 5.8 x 10-14 cm^2W^{-1}. This value agrees well with that obtained from the SPM measurements carried out on the straight waveguides. Full switching was not achieved since the temporal profile of the input pulses were $sech^2$ and not square: different parts of the two recombined pulses (at the output Y junction of the AMZI) have different relative phases, the centre of the pulse experiences destructive interference (owing to a π radians relative phase difference caused by the SPM) whereas the low power wings of the recombined pulses remain in phase and propagate along the output waveguide (similar pulse break up has been observed for the nonlinear directional coupler[13]).

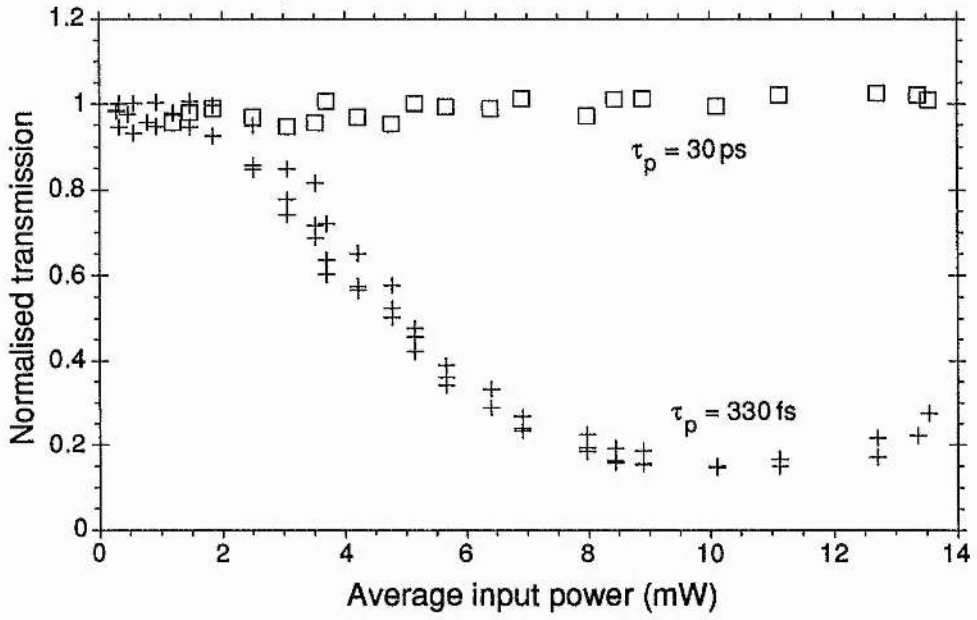

Figure 5.13. Graph of the normalised transmission of the Mach-Zehnder interferometer. Switching is clearly evident for the 330 fs duration pulses.

5.3.5 Summary

All-optical switching in the 1.5 μm spectral region was demonstrated in a passive Mach-Zehnder interferometer. The device was fabricated in the AlGaAs material system. The bandgap energy of the waveguides was designed such that the local enhancement in the nonlinear refractive index could be utilised. to reduce the power required for switching. A switching fraction of 80% was measured for pulses having peak powers of 320 W.

5.4 Coupled-Cavity Mode Locking using Passive Semiconductor Waveguides

5.4.1 Introduction

Ultrafast all-optical switching has been demonstrated using AlGaAs based semiconductor waveguide structures at photon energies corresponding to approximately half the bandgap energy.[13,18]At these wavelengths, nonlinear phase shifts in excess of 2π radians have been directly observed in straight guides[19], due mainly to the minimal competition from nonlinear absorption, but also with the assistance of a localised enhancement in the nonlinear refractive index related to two-photon transitions (real or virtual, depending on wavelength).[12] Nonlinear index coefficients of $n_2 \approx +1 \times 10^{-13}$ cm^2W^{-1} have been estimated for this material which is more than 100 times stronger than that observed for fused-silica-based optical fibres. This large nonlinearity, together with their potential for inducing nonlinear phase shifts of the order of π radians, make these semiconductor guides attractive and compact replacements for optical fibres in coupled-cavity mode-locked lasers.[20] In this section, the mode locking of a coupled-cavity KCl:Tl^0(1) colour-centre laser is described where a passive AlGaAs waveguide was incorporated in the control cavity.

In previous experiments where a near travelling-wave semiconductor optical amplifier was used as a nonlinear element in a coupled-cavity laser[20,21], considerable care had to be taken to minimise parasitic reflections from the facets. The anti-reflection coatings on the device were found to be inadequate, and a complex approach involving a ring cavity geometry containing two optical isolators was necessary to obtain stable mode-locked operation[21].

5.4.2 Experiment

The coupled-cavity laser was constructed in the conventional Fabry-Perot configuration as shown in Figure 5.14, with mirrors M0 to M1 forming the master cavity and M1 to M2 the control cavity. The KCl:Tl^0(1) colour-centre crystal was pumped at average powers of up to 2 W by an acousto-optically mode-locked

Nd:YAG laser operating at 1064 nm. The useful output from the colour-centre laser was obtained by inserting a 50/50 beamsplitter (BS) in the control cavity as illustrated in Figure 5.14. In the experiments described here, the passive AlGaAs waveguides were fabricated at an angle to the cleaved facets, such that light entered and exited the guide at Brewster's angle thus reducing parasitic reflections from the facets and rendering anti-reflection coatings unnecessary.

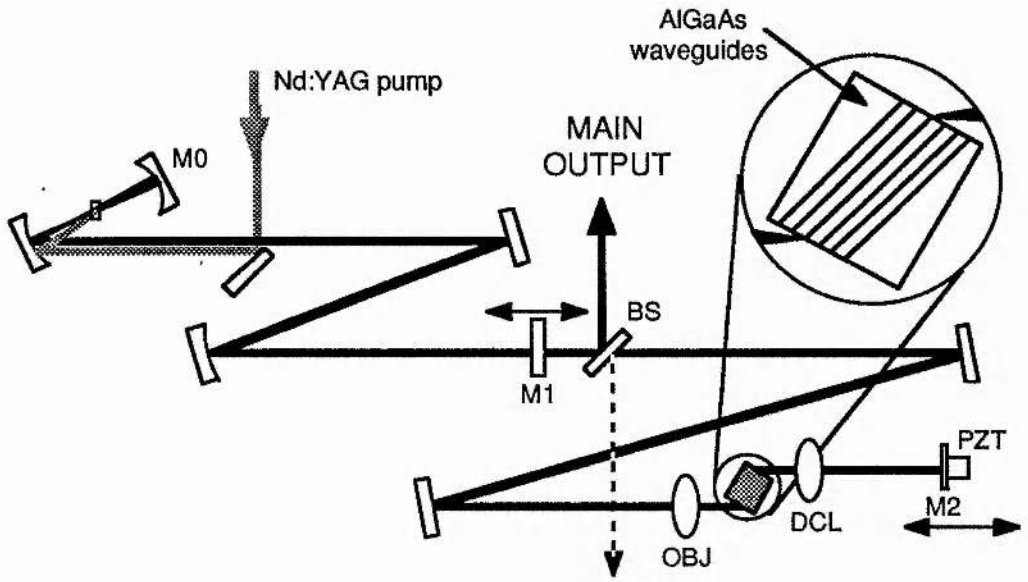

Figure 5.14. Schematic of the coupled-cavity mode-locked laser incorporating a passive waveguide in the control cavity.

The waveguides were grown in AlGaAs onto a GaAs substrate using molecular beam epitaxy at the Department of Electrical and Electronic Engineering at Glasgow University. The composition of the waveguide is the same as that of the integrated Mach-Zehnder interferometer described in the previous section. A 1.5 μm thick $Al_{0.18}Ga_{0.82}As$ guiding layer was sandwiched between buffer and upper cladding layers, both having 24% Al composition. Twelve parallel guiding ribs with widths varying from 3.0 to 5.5 μm were revealed in a 1.5 μm thick upper cladding layer to a height of approximately 1.3 μm using reactive ion etching. Using an estimate for the modal refractive index, the Brewster's angle was calculated to be 73.3 deg for these waveguides. The substrate (see inset of Fig. 5.14) had dimensions (l x w) = 4.15 x 5.35 mm^2, and the waveguides were 4.33 mm long. This relatively large substrate presented at the Brewster angle required coupling lenses with working distances greater than 2 mm, and hence light was coupled into the waveguides using a X 10 microscope objective (OBJ). The exit beam was collected using a Melles-Griot diode collimating lens (DCL) having a numerical aperture of 0.276 and this beam was focussed onto the highly reflecting mirror M2 and retroreflected.

The throughput of the guide was typically 15% for the initial pass, and the effective reflection coefficient for the combined waveguide and mirror M2 was estimated to be just less than 2%. (Typically, we would have an equivalent reflection coefficient of around 50% when using an optical fibre in the control cavity). The poor efficiency is primarily related to modal mismatches caused by the Brewster-angling of the substrate, and by the use of long-working-distance lenses, although the linear loss of the guide also contributes. The parasitic reflectivity of the device as seen by the master cavity (mirror M2 blocked) was approximately a factor of 500 smaller, and so this did not prevent mode locking. The most stable mode-locking condition was observed when the transmission of the common mirror M1 was increased to 22%, which resulted in average output powers of around 50-70 mW in the main output (see Fig. 5.14).

As is normal with coupled-cavity lasers, the optical path lengths of the master and control cavities were required to be matched to within a fraction of a wavelength. This was achieved using stabilisation electronics to control the position of mirror M2, which was mounted on a piezo-electric translator (PZT)[22]. Normally the error signal would be derived by monitoring the average output power, but the low level of feedback in the laser described here was insufficient to induce significant interferometric fluctuations of the power levels in either of the two output beams. Long term stabilisation was achieved, however, by deriving an error signal from the second-harmonic of the main output power. By contrast, this latter, more complicated approach was not required in the previous experiments where the semiconductor optical amplifier was employed, even though the feedback level was less. The active waveguide[21] differs in that it suffered from significant nonlinear attenuation, which in turn, caused a large modulation of the output power of the secondary output as the laser switched alternately from mode-locked to continuous operation with changes in the length of the control cavity.

The colour-centre laser was mode-locked by synchronous pumping in order to initiate the coupled-cavity mode locking. Self-starting of the mode locking was not observed during these experiments. as result of the ultrafast recovery time of the nonlinearity of the AlGaAs waveguides. With the active waveguide[21], start-up from mode-beating was possible since it relied on self-phase modulation (SPM) primarily associated with the much stronger resonant nonlinearity arising from carrier density changes.

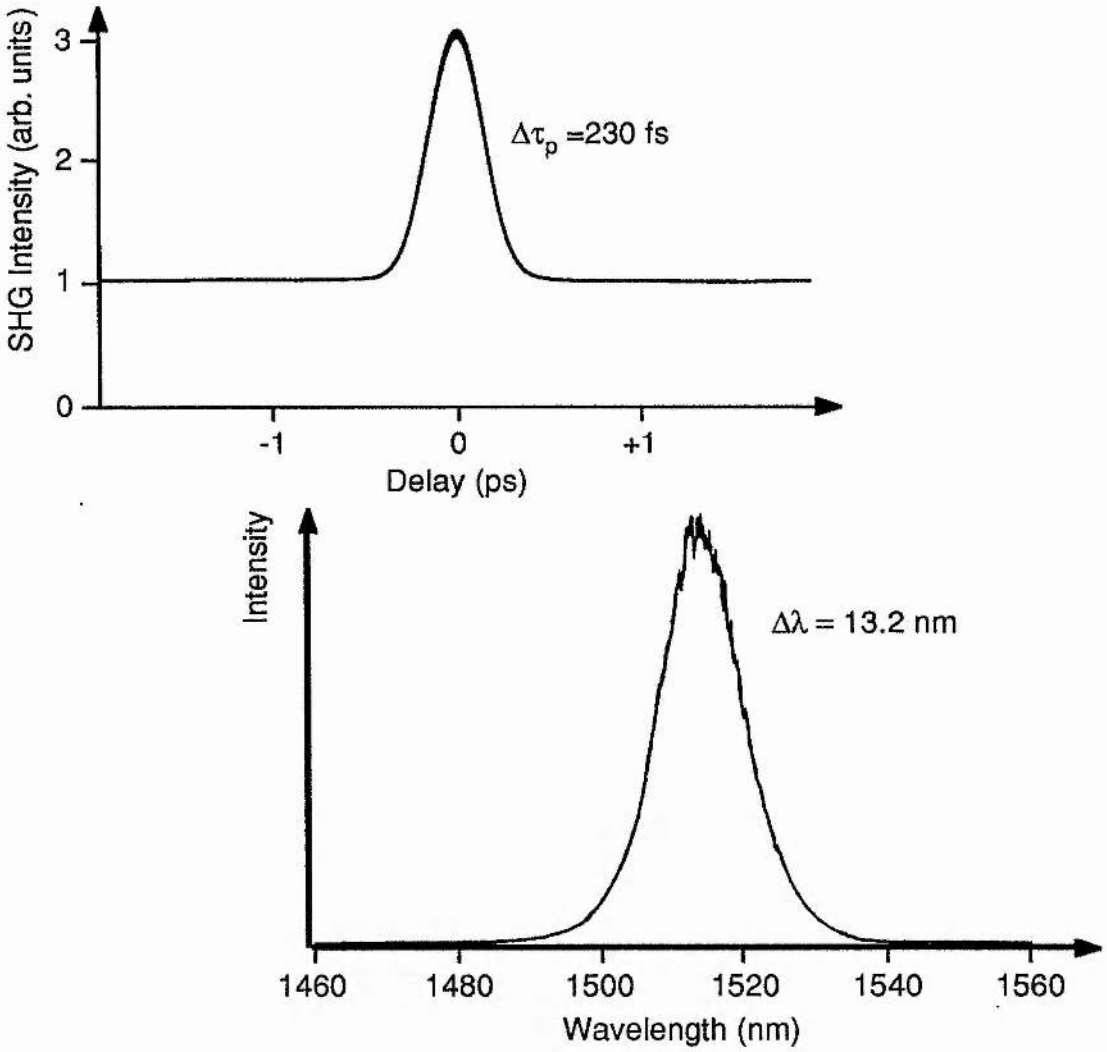

Figure 5.15. Intensity autocorrelation and spectrum for the coupled-cavity mode-locked laser.

Figure 5.15 shows an intensity autocorrelation of the pulses obtained from the laser. The pulse duration was 230 fs (assuming a sech^2 intensity profile). The spectrum for these pulses (shown in Figure 5.15) had a bandwidth of 13.2 nm which results in a calculated duration-bandwidth product of 0.39. This relatively large value indicates that the pulses were frequency-chirped. This was confirmed by the slight increase in the wings of the interferometric autocorrelation which is reproduced as Figure 5.16.

An intensity autocorrelation and a spectrum for the pulses returning from the control cavity, measured at the subsidiary output (shown by the dashed line in Fig. 5.14) are reproduced in Figure 5.16. The temporal (120%) and spectral (30%) broadening of the return pulses is consistent with the combined action of SPM and normal group-velocity dispersion (GVD) in the semiconductor waveguide. From this spectral broadening, the peak nonlinear phase shift in the steady state was estimated

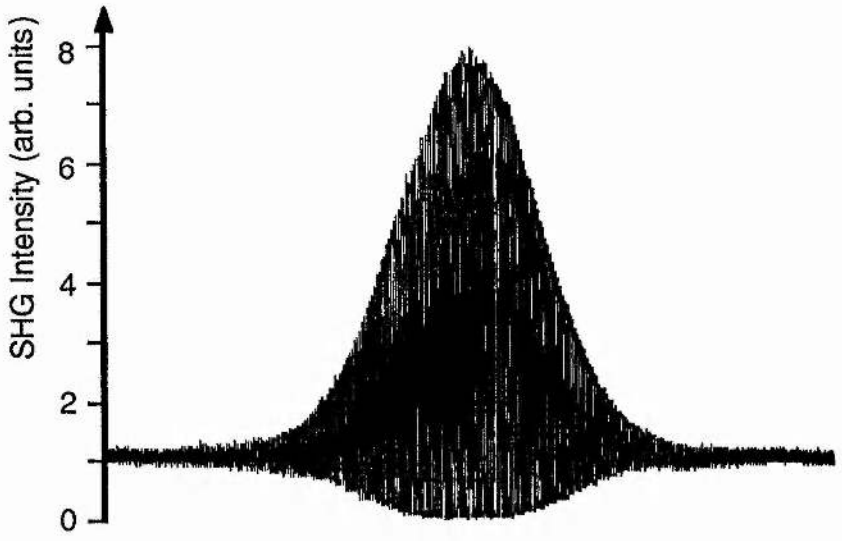

Figure 5.16. Interferometric autocorrelation of the coupled cavity mode-locked laser pulses,

to be between $\pi/2$ and π radians. Temporal broadening arising from nonlinear absorption was expected to be minimal at this value of phase shift, especially given that the laser operated at wavelengths longer than the two-photon band edge (1504 nm). This was confirmed by the insignificant modulation (~2%) in the feedback power measured at the subsidiary output when switching from continuous to mode-locked operation.

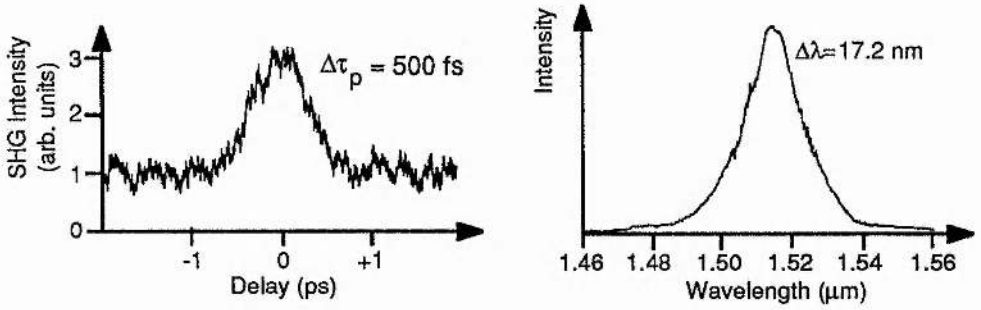

Figure 5.16. Autocorrelation and spectrum of the pulses returning from the passive waveguide.

Unfortunately the low intensity level of the control signal fed back into the main cavity prevented the use of bandwidth limiting and tuning elements. Unstable operation resulted when a thin (0.8-mm-thick) quartz plate was inserted in the cavity, probably because of insufficient nonlinear phase shift at the steady state. It is anticipated that considerable improvements in the laser performance will be possible once the overall throughput is increased by using alternative substrate geometries. For example, a reduction in the rib angle from 16.7 deg to 10 or even 7 deg (relative to the facet normal) may be possible without significantly compromising the parasitic reflectivity caused by external and internal reflections[23], while allowing better

coupling at the input facet. Furthermore, by using curved guides such that the guiding rib meets the exit facet at normal incidence, the chip itself will become the retroreflector. The expected increase in efficiency will make shorter guides feasible, thus minimising the effects of GVD in the guide, and will result in the generation of sub-200 fs pulses. Moreover, by using a nonlinear Michelson cavity configuration, the laser could be made considerably more compact. Finally, further gains in efficiency may be obtained by using multiple-quantum-well waveguides, where a factor of two enhancement in the nonlinearity has been observed[24].

5.4.3 Summary

A coupled-cavity mode-locked colour-centre laser using passive semiconductor waveguides at wavelengths in the vicinity of the half-bandgap has been described. Pulse durations of less than 300 fs were recorded and the performance of the laser is limited mainly by the poor coupling efficiencies associated with the waveguide design. Changes to this design, together with the use of a nonlinear Michelson cavity configuration, will allow shorter pulses and greater stability.

References

1. S. T. Davey, D. L. Williams, D. M. Spiritand B. J. Ainslie,Electron. Lett. **26,** 1149 (1990).
2. R. H. Stolen and E. P. Ippen, Appl, Phys. Lett. **22,** 276 (1973).
3. M. Bagley, R. Wyatt, D. J. Elton, H. J. Wickes, P. C. Spurdens, C. P. Seltzer, D. M. Cooper and W. J. Devlin, Electron. Lett. **26,** 269 (1990).
4. G. P. Agrawal and N. A. Olson, IEEE J. Quantum Electron. **QE-25,** 2297 (1989).
5. R. M. Jopson, K. L. Hall, G. Eisenstein, G. Raybon and M. S. Whalen, Electron. Lett. **23,** 510 (1987).
6. T. Mukai, K. Inoue and T Saitoh, Appl. Phys. Lett. **51,** 381 (1987).
7. M. P. Kesler and E. P. Ippen, Electron. Lett. **24,** 1102 (1988).
8. G. P Agrawal, *Nonlinear Fibre Optics* (Academic Press, Boston, 1989), chapter 7.
9. D. Botez, IEEE J. Quantum Electron. **QE-17,** 178 (1981).
10. J. E. Zuker, I. Bar-Joseph, B. I. Miller and U. Koren, IEEE Photonics Technol. Lett. **2,** 32 (1990)
11. K. W. Delong and G. I Stegeman, Appl. Phys. Lett. **57,** 2063 (1990).
12. M. Sheik-Bahae, D. C. Hutchings, D. J. Hagan, and E. W Van Stryland, IEEE J. Quantum Electron. **QE-27,** 1296 (1991).
13. J. S. Aitchison, A. H. Kean, C. N. Ironside, A. Villeneuve and G. I. Stegeman, Electron. Lett. **27,** 1709 (1991).
14. G. I. Stegeman and E. M Wright, Opt & Quantum Electron. **22,** 95 (1990).
15. R. G. Walker, Electron. Lett. **21,** 581 (1985).
16. K. Al-Hemyari, G. F. Doughty, C. D. W. Wilkinson, A. H. Kean and C. R. Stanley, J. Lightwave Technol. **11,** 272 (1993).
17. K. Al-Hemyari, C. N. Ironside, and J. S. Aitchison, IEEE J. Quantum Electron. **28,** 1090 (1992)
18. K. Al-Hemyari, J. S. Aitchison, C. N. Ironside, G. T. Kennedy, R. S. Grant and W. Sibbett, Electron. Lett. **28,** 1090 (1992).
19. S. T. Ho, C. E. Soccolich, M. N. Islam, W.S. Hobson, A. F. J. Levi and R. E. Slusher, Appl. Phys. Lett. **59,** 2558 (1991).
20. P. N. Kean, X. Zhu, D. W. Crust, R. S. Grant, N. Langford and W. Sibbett, Opt. Lett. **14,** 39 (1989).
21. R. S. Grant, P. N. Kean, D. Burns and W. Sibbett, Opt. Lett. **16** 384 (1991).
22. F. M. Mitsche and L. F. Mollenauer, IEEE J. Quantum Electron. **QE-22,** 2242 (1986).
23. D. Marcuse, J. Lightwave Technol. **7,** 336 (1989).
24. H. K. Tsang, R. S. Grant, R. V. Penty, I. H. White, J. B. D. Soole, E. Colas, H. P. LeBlanc, N. C. Andredakis, M. S. Kim and W. Sibbett, Electron. Lett. **27,** 1994 (1991).

Chapter 6

General Conclusions

The work reported in this thesis has been concerned with the generation and nonlinear propagation of ultrashort laser pulses using a NaCl:OH^- colour-centre laser. Two active mode-locking techniques were examined: mode locking by synchronous pumping using a mode-locked Nd:YAG laser, and mode locking by acousto-optic loss modulation. For both schemes, the performance of the laser was found to be qualitatively similar to actively mode-locked dye lasers. When actively mode locked by loss modulation, the laser produced pulses having durations as short as 80 ps. However, the long gain window permitted the formation of satellite pulses at high pump powers. To maintain a single output pulse at elevated pump powers, it was necessary to positively detune the cavity length which caused an increase in the pulse duration. The shorter gain window provided by synchronous pumping with 80 ps duration Nd:YAG laser pulses enabled the production of 8 ps duration pulses from the NaCl:OH^- laser. Output powers in excess of one watt were obtained at this pulse duration and the laser was tunable from 1470 nm to 1670 nm. These characteristics represent a significant improvement, both in terms of pulse duration and output power, over the KCl:Tl^0(1) colour-centre laser.

Soliton compression of the synchronously mode-locked laser pulses was investigated as a straightforward means of generating pulses of sub-picosecond durations. Pulses of 250 fs duration were simply obtained by propagating the 8 ps pulses down a length of standard telecommunications optical fibre. Unfortunately, 70% of the launched power was uncompressed and remained as a broad background pedestal. A novel pulse compressor was constructed from a nonlinear fibre-loop mirror. The pulses were compressed as they traversed the loop, and the intensity-dependent transmission of the loop mirror efficiently separated the pedestal from the compressed pulse. Using this device, the pulses from the synchronously-mode-locked laser were compressed to 300 fs.

There remains some scope for optimisation of the pulse compressor. By compressing the laser pulses in a single length of optical fibre, and using a nonlinear loop mirror with a low normal dispersion to separate the compressed pulse from its pedestal, greater compression factors may be achieved. Although the quality of the

output from a pulse compression system will never be of the same high quality as that obtained directly from a mode-locked laser, it provides an extremely simple means of generating sub-picosecond duration pulses.

In Chapter 2, the technique of coupled-cavity mode locking, using nonlinear Fabry-Perot and Michelson cavities, was described in detail. A sawtooth amplitude modulation whose period could be adjusted by changing the length of the colour-centre laser cavities, was observed on the output of the laser. It was established that the modulation was caused by the beating of the passively mode-locked NaCl:OH^- laser pulse train with the gain modulation imposed by the mode-locked Nd:YAG pump laser. An electronic stabilisation scheme was implemented to match the length of the colour-centre laser to the Nd:YAG laser and, by using this circuitry, the modulation of the laser output was completely eliminated. In the amplitude-stabilised format, the laser produced transform limited pulses of 110 fs duration.

An alternative approach to eliminate the amplitude modulation would be to operate the pump laser cw and employ the regenerative initiation scheme described in Chapter 4. Provided sufficient amplitude modulation can be achieved to start the coupled-cavity mode-locking process, this all-electronic method may be more stable than the frequency referencing scheme, since it does not require physical adjustment of the cavity length.

The phase noise of the frequency-referenced coupled-cavity mode-locked laser was measured by analysing the radio-frequency power spectrum of the mode-locked pulse train. It was found that the timing jitter of the colour-centre laser closely followed that of the Nd:YAG pump laser. By replacing the frequency synthesiser for the pump laser mode locker with a low noise crystal oscillator, the timing jitter of both lasers was substantially reduced from 125 ps to less than 2 ps in the 50 - 500 Hz frequency range. These phase noise values are still around one order of magnitude greater than the values achieved for a coupled-cavity mode-locked KCl:$Tl^0(1)$ colour centre laser, and further work to reduce the timing jitter could be carried out.

The highlight of this thesis is the demonstration of self-mode locking of the NaCl:OH^- laser, which is described in Chapter 4. In this technique, the ultrafast nonlinear effect of self-focusing is converted into amplitude modulation to obtain mode locking. For the NaCl:OH^- laser, the relatively low nonlinearity of the 2 mm thick gain medium, combined with the moderate intracavity powers, resulted in insufficient self-focusing to cause self-mode locking. It was therefore necessary to include a rod of high-nonlinearity lead-silicate glass in a focusing section within the laser cavity. Self-mode locking was initiated by both synchronous pumping and active loss modulation and it was observed that initiation by loss modulation resulted in a more stable output from the laser. A modulation of the output power occurred as a result of the beating between the applied loss modulation and the mode-locked pulse

train. To overcome this, the acousto-optic modulator was driven regeneratively from the laser output, ensuring identical modulation and pulse-repetition frequencies. When optimally configured, the laser produced near-transform-limited pulses having a duration of 95 fs.

There remains considerable opportunity for further development of the self-mode-locked laser. Replacing the nonlinear SF59 glass by semiconductor materials such as ZnSe and CdS, which have substantially larger nonlinearities, will result in a lower threshold for self-mode locking. This will enable greater output powers to be obtained from the laser. Optimisation of the cavity design, using a more sophisticated analysis of the laser resonator may also result in greater output powers and an increase to the stability of the mode-locked pulse train. Furthermore, by choosing appropriate prism materials to minimise the third order dispersion of the laser cavity, it may be possible to achieve shorter pulse durations. If these measures are successfully implemented, the self-mode-locked laser will certainly become an attractive alternative to the, considerably more complex, coupled-cavity mode-locked NaCl:OH^- laser.

In Chapter 5, several experiments on optically-nonlinear waveguides were reported. Synchronous Raman amplification was investigated as a means of reducing the pump power required for Raman amplification of solitons in long-distance telecommunications systems. In the experiment pump and signal pulses, generated from the colour-centre lasers, were synchronously propagated through an optical fibre. The wavelengths of the two pulse trains were adjusted to be symmetric about the minimum dispersion wavelength of the optical fibre to avoid a reduction in gain due to walk-away of the pump and signal pulses. Signal gains of 15 dB were measured for average pump powers of only 6 mW which is comparable to the performance of erbium-doped fibre amplifiers.

The effect of cross-phase modulation was observed in a semiconductor amplifier by copropagating synchronously mode-locked pulses from the NaCl:OH^- and KCl:Tl^0(1) lasers through a InGaAsP amplifier. Significant spectral broadening was sustained by the low-energy pulses from the KCl:Tl^0(1) laser as a result of refractive index changes caused the gain saturation induced by the energetic pulses from the NaCl:OH^- laser. This effect may be a detrimental source of cross-talk in wavelength-division multiplex telecommunication systems.

A coupled-cavity mode-locked KCl:Tl^0(1) laser was used to demonstrate ultrafast all-optical switching in an integrated Mach-Zehnder interferometer. The interferometer was constructed from the AlGaAs material system such that the nonresonant enhancement of the Kerr effect around the two-photon bandedge reduced the power requirement for switching. For 330 fs duration pulses, switching was observed for a peak power of 320 W with minimal loss due to multi-photon

absorption. Although this power greatly exceeds the powers that can currently be obtained from mode-locked diode lasers, optimisation of the interferometer design may result in a considerable reduction of the power required for switching.

The enhanced nonlinearity around the two photon bandedge in GaAlAs was also used to coupled-cavity mode-lock the KCl:Tl^0(1) colour-centre laser. Parasitic feedback from the waveguide facets was avoided by etching the waveguides at Brewster's angle to the cleaved facets. Pulses of 300 fs were obtained from the laser. Unfortunately, the low-level of feed back from the nonlinear cavity prevented tuning of the laser and an optimisation of the waveguide geometry is being carried out to increase the power being fed back into the main laser cavity. With suitable bandgap engineering, it should be possible to apply this mode-locking technique to a variety of gain media.

These experiments illustrate the usefulness of mode-locked colour-centre lasers at 1.5 μm, However, the requirement for cryogenic cooling of the laser crystal is certainly a drawback. In the longer term, research into more robust gain media such as erbium-doped waveguides and Cr:YAG may yield an alternative, room-temperature, mode-locked source at 1.5 μm. Until this occurs colour centre lasers, especially the NaCl:OH^- colour-centre laser, will remain in widespread laboratory use.

Appendix 1

Computer Programs

Nonlinear-Loop Mirror Program (Chapter 2)

```
program Loopmirror (input, output);
{*    GT Kennedy 1991    *}

 uses
  SANE;
 const
  pi = 3.1415927;
  n2 = 3.2e-20;
  nopoints = 301;
  min = -150; { min, max = +/- (nopoints - 1) /2 }
  max = 150;
  area = 78e-12;
 type
  datarray = array[1..5, min..max] of real;
 var
  ein, eout, lambda, tfwhm, length, sratio, start, finish, t, dtau, po, total, intensity,
  totalout, %noise, noise, norm : real;
  j : integer;
  ran0_1, s : extended;
  Screen : rect;
  f : text;
  shape, textname : string;
  outdata : datarray;

{*****************************************************}

 procedure Readdata (var pulseshape : string;
    var e, wavelength, duration, looplength, aratio, noise : real);
 begin
  repeat
   begin
    write('enter pulseshape (gaussian or sech2) ');
    readln(pulseshape)
   end;
  until (pulseshape = 'gaussian') or (pulseshape = 'sech2');
  write('enter pulse energy (pJ) ');
  readln(e);
  e := e * 1e-12;
  write('enter pulse duration (fwhm (ps)) ');
  readln(duration);
  duration := duration * 1e-12;
  write('enter wavelength (nm) ');
```

```
 readln(wavelength);
 wavelength := wavelength * 1e-9;
 write('enter splitting ratio (0-0.5) ');
 readln(aratio);
 write('enter loop length (m)');
 readln(looplength);
{write('enter noise level (%) ');}
{readln(noise);}
 writeln
end;


procedure Writedata (var data : datarray);
 var
  i : integer;
begin
 for i := min to max do
  begin
{writeln(data[1, i] : 20, ' ', data[2, i] : 18, ' ', data[3, i] : 18, ' ', data[4, i] :
   18,data[5,i]:18);}
   writeln(f, data[1, i] : 20, chr(9), data[2, i] : 18, chr(9), data[3, i] : 18, chr(9),
   data[4, i] : 18, chr(9), data[5, i] : 18, chr(9));
  end;
end;


function Pnought (pulseshape : string;
   duration, energy : real) : real;
begin
 if pulseshape = 'gaussian' then
  Pnought := (1.665 * energy) / (sqrt(pi) * duration)
 else
  Pnought := (1.763 * energy) / (2 * duration)
end;


function Power (pulseshape : string;
   duration, io, time : real) : real;
begin
 if pulseshape = 'gaussian' then
  Power := io * exp(-1 * sqr((1.665 * time) / duration))
 else
  Power := io * sqr(1 / (0.5 * (exp(1.763 * time / duration) + exp(-1 * (1.763 * time /
  duration)))))
end;


function Transmission (i, looplength, wavelength, aratio : real) : real;
begin
 Transmission := i * (1 - 2 * aratio * (1 - aratio) * (1 + cos((1 - 2 * aratio) * i * 2 * pi
 * n2 * looplength / wavelength)))
end;


procedure autocorrelate (var oppulse : datarray);
 var
  sep, i, j, k, l, m, n, r, s, nmin, nmax : integer;
  insum, outsum, a, inbackground, outbackground : real;
```

```
begin
 outbackground := 0;
 inbackground := 0;
 for i := min to max do
  begin
   inbackground := inbackground + sqr(oppulse[2, i]);
   outbackground := outbackground + sqr(oppulse[3, i]);
  end;
 for sep := 0 to max do
  begin
   outsum := 0;
   insum := 0;
   nmin := min + sep;
   k := sep;
   for j := max downto nmin do
    begin
    m := max - k;
    outsum := outsum + (oppulse[3, j] * oppulse[3, m]);
    insum := insum + (oppulse[2, j] * oppulse[2, m]);
    k := k + 1;
    end;
   s := -1 * sep;
   oppulse[4, sep] := 1 + 2 * (insum / inbackground);
   oppulse[5, sep] := 1 + 2 * (outsum / outbackground);
   oppulse[4, s] := 1 + 2 * (insum / inbackground);
   oppulse[5, s] := 1 + 2 * (outsum / outbackground);
  end;
end;

{************************************************}

begin
 HideAll;
 Screen.top := 40;
 Screen.left := 0;
 Screen.bottom := 345;
 Screen.right := 510;
 SetTextRect(screen);
 ShowText;

 Readdata(shape, ein, lambda, tfwhm, length, sratio, %noise);
 textname := newfilename('name for new text file ? ');
 if textname <> '' then
  rewrite(f, textname);

 start := -5 * tfwhm;
 finish := 5 * tfwhm;
 total := 0;
 dtau := (finish - start) / nopoints;
 po := Pnought(shape, tfwhm, ein);
{s := 12;  }
                                {seed for random number generator}
 for j := min to max do
  begin
   t := j * dtau;
{ran0_1 := RandomX(s) / (scalb(31, 1) - 1);}
{noise := ran0_1 * po * %noise / 100;}
{Intensity := (Power(shape, tfwhm, po, t) + noise) / area;}
```

```
  Intensity := Power(shape, tfwhm, po, t) / area;
  eout := Transmission(Intensity, length, lambda, sratio);
  total := total + eout;
  outdata[1, j] := t;
  outdata[2, j] := Intensity;
  outdata[3, j] := eout;
 end;
norm := outdata[2, 0];
for j := min to max do
 begin
  outdata[2, j] := outdata[2, j] / norm;  {normalise o/p}
  outdata[3, j] := outdata[3, j] / norm;
 end;

Autocorrelate(outdata);
Writedata(outdata);
close(f);
totalout := total * Dtau * area;
Writeln('total energy switched = ', totalout)
end.
```

Six-Mirror Cavity With Kerr Lens (Chapter 4)

```
program SelfFocussing (input, output);
(*   GT Kennedy1992     *)
 uses
  SANE;
 const
  pi = 3.141592654;
 var
  RealPart, ComplexPart, WaveFrontRadius : extended;
  RealQ1, ComplexQ1 : extended;
  Wo, W1, W2, W3, Wavelength : extended;
  Element, N : integer;
  pos1, pos2, dtotal, d1, d22, dk1, dk2, d3, d4, d5, f1, f2, f3, f4, fk, pk : extended;
  A, B, C, D, A2, B2, C2, D2 : extended;
  Screen : rect;
  f : text;
  textname : string;
 procedure FindElement;
 begin
  case Element of
   1 :
    begin
     A := 1;
     B := d1;
     C := 0;
     D := 1;
    end;
   2 :
    begin
     A := 1;
     B := 0;
     C := -1 / f1;
     D := 1;
    end;
   3 :
    begin
     A := 1;
     B := dk1;
     C := 0;
     D := 1;
    end;
   4 :
    begin
     A := 1;
     B := 0;
     C := -1 * pk;
     D := 1;
    end;
   5 :
    begin
     A := 1;
     B := dk2;
     C := 0;
     D := 1;
    end;
   6 :
```

```
 begin
  A := 1;
  B := 0;
  C := -1 / f2;
  D := 1;
 end;
7 :
 begin
  A := 1;
  B := d3;
  C := 0;
  D := 1;
 end;
8 :
 begin
  A := 1;
  B := 0;
  C := -1 / f3;
  D := 1;
 end;
9 :
 begin
  A := 1;
  B := d4;
  C := 0;
  D := 1;
 end;
10 :
 begin
  A := 1;
  B := 0;
  C := -1 / f4;
  D := 1;
 end;
11 :
 begin
  A := 1;
  B := d5;
  C := 0;
  D := 1;
 end;
12 :
 begin
  A := 1;
  B := d5;
  C := 0;
  D := 1;
 end;
13 :
 begin
  A := 1;
  B := 0;
  C := -1 / f4;
  D := 1;
 end;
14 :
 begin
  A := 1;
```

```
  B := d4;
  C := 0;
  D := 1;
 end;
15 :
 begin
  A := 1;
  B := 0;
  C := -1 / f3;
  D := 1;
 end;
16 :
 begin
  A := 1;
  B := d3;
  C := 0;
  D := 1;
 end;
17 :
 begin
  A := 1;
  B := 0;
  C := -1 / f2;
  D := 1;
 end;
18 :
 begin
  A := 1;
  B := dk2;
  C := 0;
  D := 1;
 end;
19 :
 begin
  A := 1;
  B := 0;
  C := -1 * pk;
  D := 1;
 end;
20 :
 begin
  A := 1;
  B := dk1;
  C := 0;
  D := 1;
 end;
21 :
 begin
  A := 1;
  B := 0;
  C := -1 / f1;
  D := 1;
 end;
22 :
 begin
  A := 1;
  B := d1;
  C := 0;
```

```
    D := 1;
   end;
  end;
 end; (*    FindElement    *)
 procedure Multiply;
  var
   A3, B3, C3, D3 : extended;
 begin
  A3 := A * A2 + B * C2;
  B3 := A * B2 + B * D2;
  C3 := C * A2 + D * C2;
  D3 := C * B2 + D * D2;
  A2 := A3;
  B2 := B3;
  C2 := C3;
  D2 := D3;
 end; (*  Multiply  *)

 procedure Invert (var RealPart, ComplexPart : extended);
(*     performs  1/Q -> Q or Q -> 1/Q where Q = x + iy       *)
  var
   RealQ1, ComplexQ1 : extended;
 begin
  RealQ1 := RealPart / (sqr(RealPart) + sqr(ComplexPart));
  ComplexQ1 := -1 * ComplexPart / (sqr(RealPart) + sqr(ComplexPart));
  RealPart := RealQ1;
  ComplexPart := ComplexQ1;
 end;(*    InvertQ     *)
 procedure TransformQ;
  var
   Denominator, RealQ2, ComplexQ2 : extended;
 begin
  Denominator := (sqr(C * RealPart + D) + sqr(C * ComplexPart));
  RealQ2 := ((A * RealPart + B) * (C * RealPart + D) + (A * ComplexPart * C *
  ComplexPart)) / Denominator;
  ComplexQ2 := ((A * ComplexPart * (C * RealPart + D)) - (C * ComplexPart * (A *
  RealPart + B))) / Denominator;
  RealPart := RealQ2;
  ComplexPart := ComplexQ2;
 end;(*  TransformQ    *)
begin (*       main program    body     *)
 HideAll;
 Screen.top := 20;
 Screen.left := 0;
 Screen.bottom := 342;
 Screen.right := 512;
 SetTextRect(Screen);
 ShowText;
 textname := newfilename('name for new text file ? ');
 if textname <> '' then
  rewrite(f, textname);
 Wavelength := 1.56e-4;
 dtotal := 181;
 f1 := 2.5;
 f2 := 2.5;
 f3 := 5;
 f4 := 5;
 write('enter distance d3 (cm) > ');
```

```
readln(d3);
write('enter power Kerr lens (such that 1/pk = fcm) > ');
readln(pk);
d4 := 10.1;
d5 := 48;
writeln(f, 'd2', chr(9), 'wo', chr(9), 'w1', chr(9), 'pos1', chr(9), 'w2', chr(9), 'pos2',
chr(9), 'w3', chr(9));
for N := 1960 to 2200 do
 begin
  d22 := N / 400;
  write('d2:', d22 : 5 : 3, ' ');
  d1 := dtotal - d22 - d3 - d4 - d5;
  dk1 := 0.45 * d22;
  dk2 := d22 - dk1;

  A2 := 1;
  B2 := 0;
  C2 := 0;
  D2 := 1;
  for Element := 1 to 22 do
   begin
    FindElement;
    Multiply;
   end;
  if abs((D2 + A2) / 2) < 1 then
   begin
    Wo := sqrt(abs((Wavelength * B2) / (pi * sqrt(1 - sqr((D2 + A2) / 2)))));
    write(' W0: ', Wo * 10000 : 2 : 2);

    A2 := 1;
    B2 := 0;
    C2 := 0;
    D2 := 1;
    for element := 12 to 22 do
    begin
    FindElement;
    Multiply;
    end;
    for element := 1 to 11 do
    begin
    FindElement;
    Multiply;
    end;
    W3 := sqrt(abs((Wavelength * B2) / (pi * sqrt(1 - sqr((D2 + A2) / 2)))));
    write('  W3: ', w3 * 10000 : 2 : 2);

    A2 := 1;
    B2 := 0;
    C2 := 0;
    D2 := 1;
    for Element := 3 to 22 do
    begin
    FindElement;
    Multiply;
    end;
    for Element := 1 to 2 do
    begin
    FindElement;
```

```
    Multiply;
    end;
    RealPart := (D2 - A2) / (2 * B2);
    ComplexPart := -1 * abs(sqrt(abs(1 - sqr((D2 + A2) / 2))) / B2);
    Invert(RealPart, ComplexPart);
    pos1 := -1 * Realpart;
    write('  Pos1: ', pos1 : 3 : 3);
    W1 := sqrt(abs((ComplexPart * Wavelength) / pi));
    write(' W1: ', W1 * 10000 : 2 : 2);

    A2 := 1;
    B2 := 0;
    C2 := 0;
    D2 := 1;
    for Element := 9 to 22 do
    begin
    FindElement;
    Multiply;
    end;
    for Element := 1 to 8 do
    begin
    FindElement;
    Multiply;
    end;
    RealPart := (D2 - A2) / (2 * B2);
    ComplexPart := -1 * abs(sqrt(abs(1 - sqr((D2 + A2) / 2))) / B2);
    Invert(RealPart, ComplexPart);
    pos2 := -1 * Realpart;
    write('  Pos2: ', pos2 : 3 : 3);
    W2 := sqrt(abs((ComplexPart * Wavelength) / pi));
    writeln(' W2:', W2 * 10000 : 2 : 2);
    writeln(f, d22 : 6 : 6, chr(9), wo * 10000 : 8 : 8, chr(9), w1 * 10000 : 8 : 8,
    chr(9), pos1 : 6 : 6, chr(9), w2 * 10000 : 8 : 8, chr(9), pos2 : 6 : 6, chr(9), w3 *
    10000 : 8 : 8, chr(9));

   end
  else
   writeln('unstable');
 end;
close(f)
end.
```

Appendix 2

Dispersion of the Kerr Coefficient

Sheik-Bahae *et al.*[1] evaluated the contributions to the dispersion of the Kerr coefficient $G_2\left(\frac{\hbar\omega}{E_g}\right)$ below the bandedge for four effects: two photon absorption (TPA), Raman, the linear Stark effect (LSE) and the quadratic Stark effect (QSE). These are listed below together with a term to account for the divergence of these functions as the optical frequency approaches zero.

Effect	Contribution to $G_2(x)$
QSE	$\frac{1}{2^{10}x^5}\left[(1-x)^{-\frac{1}{2}}-(1+x)^{-\frac{1}{2}}-\frac{x}{2}(1-x)^{-\frac{3}{2}}-\frac{x}{2}(1+x)^{-\frac{3}{2}}\right]$
LSE	$\frac{1}{(2x)^6}\left[2-(1-x)^{\frac{3}{2}}-(1+x)^{\frac{3}{2}}\right]$
Raman	$\frac{1}{(2x)^6}\left[-\frac{3}{8}x^2(1+x)^{-\frac{1}{2}}+3x(1+x)^{\frac{1}{2}}-2(1+x)^{\frac{3}{2}}+2(1+2x)^{\frac{3}{2}}\right]$
TPA	$\frac{1}{(2x)^6}\left[-\frac{3}{8}x^2(1-x)^{-\frac{1}{2}}+3x(1-x)^{\frac{1}{2}}-2(1-x)^{\frac{3}{2}}+2\theta(1-2x)(1-2x)^{\frac{3}{2}}\right]$
Divergent term	$\frac{1}{(2x)^6}\left[-2-\frac{35}{8}x^2+\frac{x}{8}(3x-1)(1-x)^{-\frac{1}{2}}-3x(1-x)^{\frac{1}{2}}+(1-x)^{\frac{3}{2}}+\frac{x}{8}(3x+1)(1+x)^{-\frac{1}{2}}+3x(1+x)^{\frac{1}{2}}+(1+x)^{\frac{3}{2}}\right]$

1. M. Sheik-Bahae, D. C. Hutchings, D. J. Hagan and E. Van Stryland, IEEE J. Quantum Electron. **27**, 1296 (1991).

Appendix 3

List of Publications

Journal Publications

High speed synchronously pumped Raman fibre amplification,
K. C. Byron, D. Burns, R. S. Grant, G. T. Kennedy, C. I. Johnston and W. Sibbett,
Electron. Lett. **27,** 597 (1991).

Cross-phase modulation in a semiconductor optical amplifier,
R. S. Grant, G. T. Kennedy and W. Sibbett,
Electron. Lett. **27,** 801 (1991).

Ultrafast all-optical switching in GaAlAs integrated interferometer in 1.55 μm spectral region,
K. Al-hemyari, J. S. Aitchison, C. N. Ironside, G. T. Kennedy, R. S. Grant and W. Sibbett
Electron. Lett. **28,** 1090 (1992).

Amplitude noise reduction of a coupled-cavity mode-locked NaCl:OH^- colour centre laser by active synchronisation,
G. T. Kennedy, R. S. Grant and W. Sibbett,
Opt. Lett. **18,** 208 (1993).

Carrier lifetimes in MBE and MOCVD InGaAs quantum wells,
J. E. Erlich, D. T. Neilson, A. C. Walker, G. T. Kennedy, R. S. Grant, W. Sibbett and M. Hopkinson,
Semicond. Sci. Tech. **8,** 307 (1993).

All-optical modulation with ultrafast recovery at low pump energies in passive InGaAs/InGaAsP multiquantum well waveguides,
H. K. Tsang, P. A. Snow, I. E. Day, I. H. White, R. S. Grant, Z. Su, G. T. Kennedy and W. Sibbett,
Appl. Phys. Lett. **62,** 1451 (1993).

Ultrafast nonlinear refraction in an active MQW waveguide,
M. A. Fisher, H. Wickes, G. T. Kennedy, R. S. Grant and W. Sibbett,
Electron. Lett. **29,** 1185 (1993).

Coupled-cavity mode locking using passive semiconductor waveguides,
R. S. Grant, G. T. Kennedy, W. Sibbett and J. S. Aitchison,
To be published Opt. Lett. **18,** 1st October (1993).

Self-mode-locked NaCl:OH^- color-center laser,
G. T. Kennedy, R. S. Grant and W. Sibbett,
Accepted for publication in Optics Letters August 1993.

Nonlinear switching in InGaAsP laser amplifier directional couplers biased at transparency,
D. A. O. Davies, M. A. Fisher, D. J. Elton, S. D. Perrin, M. J. Adams, G. T. Kennedy, R. S. Grant, P. D. Roberts and W. Sibbett,
Accepted for publication in Electronics Letters August 1993.

Optical bistability in an InGaAs/InP multiple quantum well waveguide Fabry-Perot cavity,
J. E. Ehrlich, D. T. Neilson, A. C. Walker,G. T. Kennedy, R. S. Grant, W. Sibbett and M. Hopkinson,
Accepted for publication in Applied Physics Letters July 1993.

Sub-milliwatt optical bistability in a coated InGaAs/InP multiple quantum well waveguide Fabry-Perot cavity,
D. T. Neilson, J. E. Ehrlich, P. Meredith, A. C. Walker, G. T. Kennedy, R. S. Grant, P. D. Roberts, W. Sibbett and M. Hopkinson,
Accepted for publication in Electronics Letters, July 1993.

Conference Publications

Soliton compression and pedestal suppression using a nonlinear fibre loop mirror,
G. T. Kennedy, D. Burns, R. S. Grant, W. Sibbett and K. C. Byron,
Paper PD10, European Quantum Electronics Conference, Edinburgh, August 1991.

Nonlinear optical properyies of a GaAS/GaAlAs integrated asymmetric Mach-Zehnder interferometer,
C. N. Ironside, K. Al-Hemyari, J. S. Aitchison, G. T. Kennedy, R. S Grant and W. Sibbett,
OSA Topical Meeting on Integrated Photonics, Houston, April 1992.

Time-domain evidence for spectrl hole burning in an InGaAsP optical amplifier,
R. S. Grant, G. T. Kennedy and W. Sibbett,
Paper CTu49, Conference on Lasers and Electro-Optics, Anaheim, May 1992.

Amplitude stabilisation of a coupled-cavity mode-locked NaCl:OH⁻ color-center laser,
G. T. Kennedy, R. S. Grant and W. Sibbett,
Paper CTu60, Conference on Lasers and Electro-Optics, Anaheim, May 1992.

Ultrafast switching in AlGaAs waveguide devices,
J. S. Aitchison, K. Al-Hemyari, C. N. Ironside, A. Villeneuve, G. I. Stegeman, G. T. Kennedy, R. S. Grant and W. Sibbett,
Paper ThO3 (invited), OSA Annual Meeting, Albuquerque, September 1992.

Low-loss ultrafast all-optical switching in a GaAlAs integrate interferometer at half the bandgap,
K. Al-Hemyari, J. S. Aitchison, C. N. Ironside, G. T. Kennedy, R. S. Grant and W. Sibbett,
Paper ThO5 , OSA Annual Meeting, Albuquerque, September 1992.

Ultrafast nonlinear refraction in an active MQW waveguide,
M. A. Fisher, H. Wickes, G. T. Kennedy, R. S. Grant and W. Sibbett,
Paper PWA2, OSA Topical Meeting on Photonics in Switching, Palm Springs, March 1993.

All-optical switching in AlGaAs waveguides at 1.55 μm,
J. S. Aitchison, K. Al-Hemyari, C. N. Ironside, A. Villeneuve, G. I. Stegeman, G. T. Kennedy, R. S Grant and W. Sibbett,
Invited paper, European Conference on Integrated Optics, Neuchatel, April 1993.

Self-mode locking of a NaCl:OH- color-centre laser,
G. T. Kennedy, R. S. Grant, J. M. Evans and W. Sibbett,
Paper CThS82, Conference on Lasers and Electro-Optics, Baltimore, May 1993.

Self-mode locking of a NaCl:OH⁻ colour-centre laser,
G. T. Kennedy, R. S. Grant and W. Sibbett,
Paper , Eleventh National Quantum Electronice Conference (QE 11), Belfast, August 1993.

Coupled-cavity mode locking using passive AlGaAs waveguides,
Z. Su, R. S. Grant, G. T. Kennedy, J. S. Aitchison and W. Sibbett,
Paper , Eleventh National Quantum Electronice Conference (QE 11), Belfast, August 1993.

Mode-locking usng the half-bandgap nonlinearity in passive AlGaAs waveguides,
Z. Su, R. S. Grant, G. T. Kennedy, W. Sibbett and J. S. Aitchison,
Paper MA3 ,OSA Topical Meeting on Nonlinear Guided-Wave Phenomena, Cambridge, September 1993.

Low-loss ultrafast all-optical switching in a GaAlAs integrated interferometer at the 1.55 μm spectral region without multiphoton absorption,

K. Al-hemyari, J. S. Aitchison, C. N. Ironside, G. T. Kennedy and W. Sibbett,

Paper MA5, OSA Topical Meeting on Nonlinear Guided-Wave Phenomena, Cambridge, September 1993.

Optically-induced electronic nonlinearities and passive optical bistability in InGaAs/InP QW waveguides at 1.5 μm,

D. T. Neilson, J. E. Ehrlich, A. C. Walker, G. T. Kennedy, R. S. Grant, W. Sibbett, M. Hopkinson and M Pate,

Paper TuC3 ,OSA Topical Meeting on Nonlinear Guided-Wave Phenomena, Cambridge, September 1993.

High speed low power switching of a polarisation rotation gate using AlGaAs MQW waveguides,

P. A. Snow, I. E. Day, I. H. White, R. V. Penty, G. T. Kennedy and W. Sibbett,

Paper TuC5, OSA Topical Meeting on Nonlinear Guided-Wave Phenomena, Cambridge, September 1993.

Femtosecond pulse generation using passive AlGaAs waveguides at half the bandgap

Z. Su, R. S. Grant, G. T. Kennedy, J. S. Aitchison and W. Sibbett,

Paper UPF3, European QuantumElectronics Conference, Firenze, September 1993.

Acknowledgements

I would like to thank my supervisor, Professor Wilson Sibbett for encouragement, support and cheerful optimism throughout this project. I am indebted to my CASE supervisor Dr Kevin Byron for providing the fibre-loop devices (Chapter2).

I am also grateful to:

Robert Grant for help in the laboratory,
Dave Burns for many late-night discussions,
Jonny Evans for help with self-mode-locking the NaCl:OH^- laser,
Bill Sleat for his electronic expertise,
all the other members of the 'W Squad',
and The boys of 172 South St.: Gordon, Jason, Neil and Jonny.

I am especially grateful to Lisa Bethel for proof reading this thesis, and sorting out my dangling modifier.

Thanks are due to all the members of the technical staff of the Physics Department, in particular:

Bob Mitchell for his cryogenic skills,
Andy Barman for providing a constant supply of liquid nitrogen,
Reg Gavine for instruction in the student workshop,
Jimmy Lindsay and other members of the Mechanical Workshop for constructing numerous mounts.

Finally I am grateful to the Science and Engineering Research Council for financial support.